IMPACT OF SUBSURFACE METHANE TRANSPORT ON SHALLOW MARINE SEDIMENT GEOCHEMISTRY

A Dissertation

by

Sajjad Abdullajintakam

MS, University of Delhi, 2012
BS, University of Delhi, 2010

Submitted in Partial Fulfillment of the Requirements for the Degree of

DOCTOR OF PHILOSOPHY

in

COASTAL AND MARINE SYSTEM SCIENCE

Texas A&M University-Corpus Christi
Corpus Christi, Texas

August 2020

August 2020

IMPACT OF SUBSURFACE METHANE TRANSPORT ON SHALLOW MARINE SEDIMENT GEOCHEMISTRY

A Dissertation

by

SAJJAD ABDULLAJINTAKAM

This dissertation meets the standards for scope and quality of
Texas A&M University-Corpus Christi and is hereby approved.

Richard B Coffin, Ph.D.
Chair

Hussain AN Abdulla, Ph.D.
Co-Chair

Brandi K Reese, Ph.D.
Committee Member

Timothy W Lyons, Ph.D.
Committee Member

Thomas H Naehr, Ph.D.
Committee Member

Pamela Brouillard, Ph.D.
Graduate Faculty Representative

August 2020

ABSTRACT

Marine sediments host a vast amount of methane, a potent greenhouse gas, in the subsurface. Transport of this subsurface methane towards the seafloor creates unique biogeochemical interactions which result in important consequences for the chemical and biological composition of the oceans at present and over the Earth's geological history. This dissertation studied the impact of subsurface methane venting to shallow marine sediment geochemistry with a goal to quantify the role of methane induced biogeochemical processes in marine carbon cycling and to recognize geochemical proxies that will enable better reconstruction of these processes from the geological record. Key results suggest the following: (i) Globally, diffusive methane charged sediments are significantly contributing to the oceanic dissolved inorganic carbon (DIC) pool (comparable to ~20% global riverine DIC flux to oceans) and sedimentary carbonate accumulation (comparable to ~15% of carbonate accumulation on continental shelves), primarily due to microbially induced carbon-sulfur (C-S) coupling. (ii) C-S coupling induced by methane seeps and crude oil seeps can be distinguished from the sediment records using a combined stable carbon ($\delta^{13}C$) and sulfur ($\delta^{34}S$) analysis of authigenic carbonate and sulfide mineral phases formed in seep settings. (iii) Molecular fossil records of methane metabolizing archaea in the sediment column involve unique isomer patterns of Isoprenoid Glycerol dialkyl glycerol tetraether (GDGT) lipids, which can serve as an important proxy to study paleo-methane flux records. These results will substantially contribute to our existing coastal and geological carbon models as well as enhance our existing inventory of geochemical proxies to characterize the methane venting systems in the geological past.

DEDICATION

This dissertation is dedicated to three beloved people for the support and love they offered in every step of my life: My parents Mr. Basheer Abdullajintakam and Mrs. Samzad Beegum and my late grandmother Aminabi KP.

ACKNOWLEDGEMENTS

The support from many people had helped me in this effort. I would start with Dr. Richard Coffin for being a highly supportive mentor. I am thankful for the backing you offered during many crucial times, creative freedom you encouraged, and the scientific passion you shared. You have inspired me as a scientist and an individual. Dr. Hussain Abdulla, thank you for training and guiding me in my biomarker project. I am indebted to the time, effort, and lab resources you offered during this project. Dr. Tim Lyons, your mentorship was a vital factor in developing this dissertation to the current format. Your willingness to support and collaborate at a critical time significantly helped me to channel the first two projects in this dissertation. Dr. Thomas Naehr, thank you for introducing me to the fascinating science of methane seeps and giving an opportunity to join the CMSS and TAMUCC family. I would like to thank Joshua Avalos (TAMUCC), Dr. David McGee (MIT), Jerry Dickens (Rice University), Steve Bates (UCR), Dr. Brandi Reese (TAMUCC), and Dr. Pamela Brouillard (Graduate Faculty Representative for this dissertation) for their support during the different stages of my dissertation.

I would also like to acknowledge a supportive bunch of people at TAMUCC: Dr. Xinping Hu, Dr. Dorina Murgulet, and Mrs. Alessandra Garcia from CMSS for their timely administrative assistance; Dr. Jennifer Smith-Engle, Dr. Val Murgulet, and Dr. Tania Anders from TAMUCC Geology for their help with teaching assignment allotments for the semesters. The Graduate Assistantship from CMSS and College of Graduate Studies (CGS) were important support factors during my Ph.D. Scholarship and support from CGS, AAPG, GSA, GCAGS,

A&WMA, and CCGS is duly acknowledged here. Friends from the CMSS program and TAMUCC, thank you for the making my stay an enjoyable experience. Dr. Mohd. Rafeeq (Malabar Christian College, Calicut) is remembered here for introducing me to the world of Geology. I would like to express my gratitude to my teachers at Department of Geology, University of Delhi, for nurturing the geologist in me. Dr. Divakar Naidu (National Institute of Oceanography, Goa) is acknowledged for the support after my masters, which eventually lead my way to joining the doctoral program at TAMUCC. As a budding scientist, you have inspired me in my career goals.

I am indebted to my family and friends for the love and support they have offered. My late grandma, who has been my greatest friend at home is fondly remembered here for the care and love she offered. My mom and dad, thank you for leading by example a life of integrity, love, and respect. My wonderful siblings – Shabna and Shahir for holding our family together while I was chasing my academic goals far away from home. I feel very lucky to be blessed with some incredible friends; Vaseem, Shamna, Pankaj, Tushar, Tarini, Nihad, Nihsan, Anees, Noyal, Tanya, Sai, Osman, Farha, Falu, Ismail, Shraddha, Vipin, Hongming, and many more – you all made my life eventful and merrier while I was chasing the long roads. I want to end this note by thanking my wife, partner, and soulmate – Nasla. Your presence, love, and, friendship, makes me complete.

TABLE OF CONTENTS

CONTENTS PAGE

ABSTRACT v

DEDICATION vi

ACKNOWLEDGEMENTS vii

TABLE OF CONTENTS ix

LIST OF FIGURES xiii

LIST OF TABLES xix

CHAPTER I: IMPORTANCE OF SUBSURFACE METHANE RESERVOIR TO SHALLOW MARINE SEDIMENT GEOCHEMISTRY 1

1.1 Introduction 1

1.2 Marine Methane and Climate Dynamics: A Geological Overview 1

1.3 Marine Methane Reservoirs: Present-Day Setting 3

1.3.1 Biogenic Methane 4

1.3.2 Thermogenic Methane 6

1.3.3 Abiotic Methane 7

1.3.4 Aerobic Methane Production 8

1.3.5 Continental Margins as Important Marine Methane Reservoir 9

1.4 Methane Transport to Shallow Sediments 12

1.5 The Fate of Methane Entering the Shallow Sediments 14

1.5.1 Biochemistry of AOM 15

1.5.2 Anaerobic Oxidation of non-methane hydrocarbon.....18

1.5.3 Aerobic Methanotrophy (AeM) 19

1.6 Recognizing the Methane Seepage Records from Sediment Records..... 21

CHAPTER II: DISSOLVED INORGANIC CARBON PUMP IN METHANE-CHARGED SHALLOW MARINE SEDIMENTS: STATE OF THE ART AND NEW MODEL PERSPECTIVES 25

2.1 Abstract..... 25

2.2 Introduction..... 26

2.3 Sulfate-Methane Transition Zones and Associated Carbon Cycling 27

2.3.1 DIC Sources at SMTZ.....29

2.4. Calculations..... 33

2.4.1 Estimations of Parameter Values 34

2.4.2 DIC production via AOM and OSR.....37

2.4.3 Total DIC through the SMTZ 39

2.4.4 Global Estimate..... 39

2.5. Synthesis 41

2.5.1 Importance of Methane Derived Authigenic Carbonate Precipitation.....43

2.5.2 Importance of DIC Outflux to the Water Column: Implication to C-S-Fe dynamics 45

2.6 Conclusion..... 49

2.7 Supplementary Documents 50

CHAPTER 3: CARBON-SULFUR COUPLING AND TEMPORAL PATTERNS FOR CHAPOPOTE ASPHALT SEEPS IN THE SOUTHERN GULF OF MEXICO BASED ON CARBONATE GEOCHEMISTRY 51

3.1 Abstract 51

3.2 Introduction 52

3.3 Study Area 55

3.4 Methods 58

3.5 Results 61

3.6 Discussion 68

3.6.1 C-S Isotope Systematics of the AOM and AONM settings 73

3.6.2 Implications for the sedimentary record 82

3.8 Conclusions 85

3.9 Acknowledgment 86

3.10 Supplementary documents 86

CHAPTER 4: UNIQUE ISOMER PATTERNS OF ARCHAEAL BIOMARKER LIPIDS AT METHANE FLUX SETTINGS: IMPLICATIONS TO GDGT BASED PALEOCEANOGRAPHIC PROXIES 87

4.1 Abstract 87

4.2 Introduction 88

4.3 Study Sites 92

4.4 Methods 96

4.5 Results and Discussions 97

4.6 Identification of different GDGTs Isomers: 100

4.7 Detection of GDGT Isomers Unique to ANME: Implications to MI 111

4.8 Conclusion 114

4.9 Supplementary documents 115

CHAPTER 5: SUMMARY AND FUTURE WORKS 116

REFERENCES 121

LIST OF FIGURES

FIGURES PAGE

Figure 1.1: Simplified graphical representation of methanogenic processes in marine sediments..5

Figure 1.2: Maturation stages in hydrocarbon generation, from Alexander et al., (2011). Diagenesis, Catagenesis, and Metagenesis occurs at a temperature range of <50°C, 50-150°C, and >150°C, respectively. The latter two results in thermogenic methane production and the former in biogenic methane production 7

Figure 1.3: Biogenic methanogenesis and subsequent transport to shallow system (Dean et al., 2018) 11

Figure 1.4: Global seep distribution adopted from Torres and Bohrmann (2016).....13

Figure 1.5: Schematic profile is SMTZ and the most accepted syntrophic model for AOM via direct interspecies electron transfer between ANME and SRB (Crémière et al., 2020) 18

Figure 1.6: Carbon fluxes associated with marine methane seeps (Boetius and Wenzhöfer, 2013) 20

Figure 2.1: A simplified representation of DIC cycling at diffusion-controlled marine settings. Figure 2.4 provides DIC flux estimates. Refer to section 3 for descriptions of flux parameters. 29

Figure 2.2: Schematic concentration (based on measured and modeled) profiles for CH_4, SO_4^{2-}, and DIC, at diffusive methane flux setting. Arrows indicate flux direction. SRZ indicates the sulfate reduction zone with dominant organoclastic sulfate reduction (OSR). The DIC concentration at the SMTZ is the result of AOM, OSR, deep-DIC input, and authigenic carbonate precipitation. Modified based on data from Snyder et al., (2007, Japan Sea), Malinverno and Pohlman (2011, IODP Site U1325, Cascadia Margin), Chatterjee et al., (2011

ODP Site 1244, Hydrate Ridge), and Wehrmann et al., (2011, IODP Site 1345, Bering Sea)…..32

Figure 2.3: Plots for SO_4^{2-}: DIC ratio for AOM and OSR. Black slopes indicate AOM (1:1) and OSR (1:2). The blue slope indicates SO_4^{2-}: DIC plot calculated from 740 diffusion-controlled marine methane flux sites globally by Egger et al (2018), with SO_4^{2-} flux data from 509 sites. CH_4 concentrations were adjusted using a 1:1.4 flux ratio for CH_4 : SO_4^{2-} and the combined effect of AOM and OSR results in a SO_4^{2-}: DIC ratio ~ 1:1.3 38

Figure 2.4: Sources and sinks of DIC through the SMTZ in methane-charged shallow sediments. The numbers in bold indicate flux values in Tmol yr^{-1}. Numbers in the parentheses indicate the flux values with an extended range of parameters considered in Table 2.1. Size of the arrows indicates relative DIC flux contribution.....42

Figure 2.5: Global trend of TA/DIC ratio above the seafloor for oxygen-limited coastal setting. A) Global distribution of TA/DIC at 100-250m bathymetry within 20m above the seabed. B) Global distribution of TA/DIC at different oxygen concentrations. It can be noticed that the minimum TA/DIC ratio is about 1, under oxygen-limited condition in the shallow bathymetry settings. Data Resource: GLODAPv2 (Key et al., 2015; Lauvset et al., 2016; Olsen et al., 2016) 47

Figure 3.1: Study Area. The orange star represents the primary study site, Chapopote Knolls, with significant asphalt seeps. Red dots with an arrow indicate the locations (GC 415 and GC 185) for carbonates samples from northern GoM analyzed in this study. The green dots indicate locations from published literature where we used to compare the C-S isotope results.....58

Figure 3.2: Petrographic observations on Chapopote Seep Carbonates. A) Multiple cement types. A fracture event postdating cement formation can be seen. B) Acicular aragonite cement forming radial-fibrous fabric. C) Large clast cemented by microcrystalline aragonite. D) Zoomed view of the box marked in 2C. Microsparitic filling of spaces between clasts and cement lining the clasts is incomplete, leaving significant pore space. Aragonite cement fills pore spaces, creating a peloidal texture in the left half of the picture. E) Peloidal texture indicative of microbial activity and early diagenetic cementation. F) Abundant pyrite formation is indicative of extensive sulfate reduction. Clots of residual hydrocarbons (dark brown) can be seen around the pore spaces adjacent to cemented structures as well as coating on the aragonite cements. All images are in plane-polarized light, and blue color indicates pore spaces. These observations are indicative of authigenic carbonate formation in a dynamic hydrocarbon seep setting 64

Figure 3.3: Indicators for pervasive autoendolithic activity at Chapopote Seeps (A-E). Arrows mark sites of potential mineralization induced by autoendolithic activity. Figure F is a schematic representation for relative locations and microbe-rock interactions of endolithic organisms adapted from Marlow et al., 2015. Circles represents endoliths and gray shading represents autoendolithic carbonate precipitation 71

Figure. 3.4: $\delta^{13}C_{carbonate}$ vs. $\delta^{34}S_{pyrite}$ from GoM seep carbonates with dominant endmembers contributing to the C-S coupling and associated DIC and sulfide sourcing. Refer to section 3.5.1 for details 74

Figure 3.5: $\delta^{13}C_{carbonate}$ vs. $\delta^{34}S_{pyrite}$ values sorted by carbonate mineralogy. HMC = High Magnesium Calcite and LMC = Low Magnesium Calcite 78

Figure 3.6: A plot of $\delta^{13}C_{CAS}$ vs. CAS concentration of seep carbonates from GoM. Chapopote samples (blue dots) showed distinctly depleted $\delta^{13}C_{CAS}$ and CAS concentration. The Chapopote

samples with $\delta^{13}C_{CAS}$ ~ +21‰ are control samples from a non-seep site adjacent to the seep site. It is also noteworthy that a bivalve shell (cross marked) with low pyrite content (0.07 wt%) and high CAS concentration (510 ppm) showed a $\delta^{34}S_{CAS}$ value (+19‰) very close to that of modern seawater.....80

Figure 4.1: Core structures of the most common isoprenoidal GDGTs with mass-to-charge ratios (m/z).....92

Figure 4.2: Study Area. A) Site 1230, ODP Leg 201, Peru Margin. B) Site U1427, IODP Leg 346, Japan Sea taken from cruise reports ODP Leg 204 and IODP Leg 346 95

Figure 4.3: SMTZ depth for Sites 1230 and U1427 taken from cruise reports ODP Leg 204 and IODP Leg 346 96

Figure 4.4: Bulk GDGT distribution. It can be seen that Peru margin samples (orange bars) gave relatively high GDGT distributions than Japan Margin (blue bar). GDGT-0 and Cren were the dominant compounds in both sites.....99

Figure 4.5: GDGT distribution at SMTZ intervals compared to average GDGT distribution throughout the sediment core. Relatively higher contribution of GDGTs 1 and 2 has a higher concentration than overall average GDGT distribution at the SMTZ.....100

Figure 4.6: a) UPLC chromatogram of GDGT-0 b) isotope pattern of GDGT-0 c) depth profile of GDGT-0 d) CID fragmentation spectrum of m/z 1302 e) Fragmentation structures that for the major fragments of GDGT-0.....105

Figure 4.7: a) UPLC chromatogram of GDGT-1 highlighting the different detected isomers b) isotope pattern of GDGT-1 c) depth profile of GDGT-1 isomer III d) CID fragmentation spectrum of m/z 1300 for GDGT-1 isomer III e) fragmentation structures for the major detected

fragments of GDGT-1-III isomer.....106
Figure 4.8: a) UPLC chromatogram of GDGT-2 highlighting the different detected isomers b) isotope pattern of GDGT-2 c) depth profile of GDGT-2 isomer III d) CID fragmentation spectrum of m/z 1298 for GDGT-2 isomer III e) fragmentation structures for the major detected fragments of GDGT-2-III isomer.....107
Figure 4.9: a) UPLC chromatogram of GDGT-3 highlighting the different detected isomers b) isotope pattern of GDGT-3 c) depth profile of GDGT-3 isomer III d) CID fragmentation spectrum of m/z 1296 for GDGT-3 isomer III e) Fragmentation structures for the major detected fragment of GDGT-1-III isomer.....108
Figure 4.10: a) UPLC chromatogram of Crenarchaeol highlighting the different detected isomers b) isotope pattern of Cren c) depth profile of Cren and iso-Cren isomers d) CID fragmentation spectrum of m/z 1292 for Cren main isomer e) Fragmentation structures for the major detected fragment of Cren main isomer.....109
Figure 4.11: Depth profiles of All GDGTs and their isomers in this study. A) GDGT-1, B) GDGT-2, C) GDGT-3, D) GDGT-0, Cren and Cren'. Note the distinct peaks for GDGT 1a, 2a, and 3a at the SMTZ and almost absence of it above and below the SMTZ, indicative of methanotrophic archaeal sourcing.....110
Figure 4.12: A comparison of MI values obtained from the traditional approach and the improved resolution approach used in this study. A) MI values from the traditional HPLC method using single-column separation. B) high-resolution method approach in this study using two silica column HPLC. MI values considered all the GDGT isomers in this case. C) MI values using only the specific Isomers that showed characteristic variation with regards to SMTZ (GDGT1a, 2a, and 3a). It can be seen that our method enables significant noise reduction by

identifying the isomers sourcing from ANME with that of non-Non ANME origin 112

Figure 4.13: A and B) Characteristic GDGT isomers with SMTZ peaks C) MI values using all the GDGT compounds and only the characteristic isomers with SMTZ peaking. The peak at depth 20.9 mbsf indicates a paleo SMTZ front. Note the isomer patterns identify the SMTZ zone from a false-positive peak (grey peak) below the SMTZ 113

Figure 5.1: Generalized representation of marine methane cycle acting as an intermediate in the global carbon cycle 118

LIST OF TABLES

TABLES PAGE

Table 2.1: Parameters controlling the DIC fluxes at SMTZ, with their average and extended range considered in carbon flux calculation.....37

Table 2.2: Global estimate of diffusive CH_4 and SO_4^{2-} flux based on 1:1.4 ratio, and average SMTZ depth compiled from 740 sites (Egger et al., 2018) 40

Table 2.3: Average values for parameters in Table 2, for a global CH4 flux of 3.8 Tmol yr-1 and SO42- flux of 5.3 Tmol yr-1. AOM and OSR consumes 70% and 30% of SO42- entering the SMTZ respectively, F(DIC-deep)= 50% of CH4 flux, Fcarb = 20%, FSOC = 5% and F(DIC-out)= 75% of the Total(DIC). All flux values are in Tmol yr-1 40

Table 2.4: Range of DIC flux values (in in Tmol yr-1) based on variable ranges of DIC flux parameters in Table 2.1 41

Table 3.1: $\delta^{13}C_{carbonate,}$ $\delta^{18}O_{carbonate}$, $\delta^{34}S_{pyrite}$, and pyrite content from studied samples. An extended database, which includes a compilation of published literature data from multiple seep sites in GoM, is provided in the supplementary datasheet.....65

Table 3.2: U-Th data from Chapopote Samples 67

CHAPTER I: IMPORTANCE OF SUBSURFACE METHANE RESERVOIR TO SHALLOW MARINE SEDIMENT GEOCHEMISTRY

1.1 Introduction

Methane (CH_4) is an important greenhouse with a significant role in the evolution of Earth's carbon cycle and the ongoing climate change. Compared to Carbon dioxide (CO_2), It has higher global warming potential in terms of cumulative forcing by a factor of at least 84 over 20 years and 28 over a 100-year time frame (Myhre et al., 2013; Etminan et al., 2016). At present, methane is the second most abundant greenhouse gas after CO_2 and the most abundant hydrocarbon present in the atmosphere accounting for 14% of global greenhouse gas emissions (Stocker et al., 2014). Subsurface marine methane reservoirs constitute a large exchangeable carbon pool significant for the climate system (Dickens, 2011) and the continental margins are characterized by numerous sites with methane transport from subsurface towards the seafloor. At present-day setting, microbially driven anaerobic oxidation consumes >80% of this methane transport and effectively prevent the direct impact of this large methane pool with climate system. This chapter provides an overview on the importance of subsurface methane reservoir to shallow sediment chemistry and their relevance to our understanding of geological evolution of Earth's carbon cycle.

1.2 Marine Methane and Climate Dynamics: A Geological Overview

Methane emission from geosphere is considered to have an important role in the early history of life and the evolution of carbon cycling through Earth's history. The early Archaean Earth is suggested to have low solar luminosity (faint young Sun), which is hostile for life (Sagan and

Mullen, 1972). An important hypothesis regarding the evolution of a habitable warm climate during this early Earth is the greenhouse effect of methane entering from the geosphere (Kasting et al., 1983; Pavlov et al., 2000; Ozaki et al., 2018). Massive volcanism and oceanic crust formation that followed has been suggested to deplete the Nickel availability for methanogens (Konhauser et al., 2009), which in turn aided in the drawdown of atmospheric methane, oxygen buildup, and Paleoproterozoic glaciation around 2.4 billion years ago (Kasting, 2005). The oxygenation of Earth's atmosphere via cyanobacterial photosynthesis is also suggested to have contributed to the Paleoproterozoic glaciation by the inhibitory effect of oxygen on anaerobic processes including methanogenesis as well as by the breakdown of the atmospheric methane by the oxygen (Kopp et al., 2005; Guo et al., 2009). There are also hypotheses that the Neoproterozoic glaciation (Jiang et al., 2003; Ganqing et al., 2006), end-Permian mass extinction (Krull and Retallack, 2000; Heydari and Hassanzadeh, 2003), Jurassic ocean anoxia event (Hesselbo et al., 2000), Paleocene-Eocene Thermal Maximum (Dickens et al., 1995; Zeebe et al., 2016) is connected to oceanic methane release to water column and atmosphere. Kennett et al., (2003) proposed that oceanic hydrate dissociation (clathrate gun hypothesis) as a plausible cause for the Late Quaternary atmospheric methane fluctuation since 400 ka. However, this hypothesis is widely disputed based on foraminiferal (Stott et al., 2002) and ice core studies (Sowers, 2006). The potential methane sourcing is instead suggested to be from wetlands (Bock et al., 2010). Ice core records for the past 800kyr shows atmospheric methane concentration varied between 300 to 800 ppb during the late Pleistocene glacial-interglacial cycles, at least until the past 5000 years (Ruddiman, 2003; Ruddiman and Raymo, 2003; Loulergue et al., 2008). These variations generally followed the temperature pattern in the late Pleistocene with a higher concentration during interglacial and a lower concentration during the glacial period and are in tune with the

Milankovitch cycle based on Earth's orbit (Dean et al., 2018). Anthropogenic land use and agriculture from 5000 years onwards initiated the increase of atmospheric methane concentration above the 800 ppb level and the industrial revolution from the 18th century onwards further spiked it to the modern high atmospheric methane levels (Ruddiman, 2003). 20% of postindustrial global warming is attributed to methane gas, with around 250% increase in atmospheric methane concentration since 1750, from ~720 ppb to 1800 ppb (Houghton et al., 2001; Ferretti et al., 2005; Dlugokencky et al., 2011).

1.3 Marine Methane Reservoirs: Present-Day Setting

Methane sourcing in marine sediments can be classified broadly as biogenic, thermogenic, and abiotic. Biogenic methane implies formation via microbial processes (methanogenesis) by methanogenic archaea, while thermogenic methane implies formation via thermal degradation of organic matter at deep depths with higher temperatures (Rice and Hotel, 1990; Whiticar, 1999). About 80% of marine methane reservoir is estimated to be sourced from methanogenic archaea (Kvenvolden and Rogers, 2005; Orcutt et al., 2011). Thermogenic sources are an important component of methane in natural gas (Dean et al., 2018). Abiotic methane forms via geochemical reactions that do not require the presence of organic matter (Hunt, 1996; Etiope, 2017) and is considered to make a relatively minor contribution to the global marine methane pool (Reeburgh, 2003). However, the abiotic methane sources are considered to have played an important role in the early Earth's history and evolution of carbon cycle.

1.3.1 Biogenic Methane

An estimated ~55 Gt C yr^{-1} is fixed by the phytoplankton (Watson et al., 1996). A minor portion of this organic matter, about 2-3 Gt C yr^{-1}, reaches the sediment floor after escaping the remineralization in the water column (Sarmiento and Gruber, 2006). More than 90% of this organic matter reaching the sediments undergo remineralization via sedimentary diagenesis. Here, the organic carbon pool undergoes remineralization (degradation) in the top sediments using different terminal electron acceptors (TEAs) like O_2, NO_3^-, Mn(IV), Fe(III) and SO_4^{2-} by the microbial communities. Microbial methane production (methanogenesis) is the final step in organic matter degradation (Claypool and Kaplan, 1974).

Methanogens are obligate anaerobes comprising seven Orders of class Euryarchaeota: *Methanococcales, Methanobacteriales, Methanosarcinales, Methanomicrobiales, Methanopyrales, Methanocellales, and Methanomassiliicoccales* (Thauer, 1998; Sakai et al., 2008; Borrel et al., 2013). The recent discovery of two novel phyla Bathyarchaeota (Evans et al., 2015) and Verstraetearchaeota (Vanwonterghem et al., 2016) has for the first time suggested methanogens outside the Euryarchaeota. There are three known methanogenic pathways

i) Hydrogenotrophic methanogenesis

ii) Acetotrophic/acetoclastic methanogenesis

iii) Methylotrophic methanogenesis

The hydrogenotrophic pathway is more energetically favorable and can be represented as:

$$CO_2 + 4\,H_2 \rightarrow CH_4 + 2H_2O \qquad (1)$$

This autotrophic pathway is the most abundant and energetically favored pathway in the marine settings (Liu and Whitman, 2008). The acetoclastic pathway involves disproportionation of an acetate molecule to CH_4 and CO_2.

$$CH_3COOH \rightarrow CH_4 + CO_2 \qquad (2)$$

Methylotrophic methanogens use methylated substrates like methanol, methylamines, methyl sulfides, etc. (e.g., Eq. 3)

$$4CH_3OH + H_2 \rightarrow 3CH_4 + CO_2 + 2H_2O \qquad (3)$$

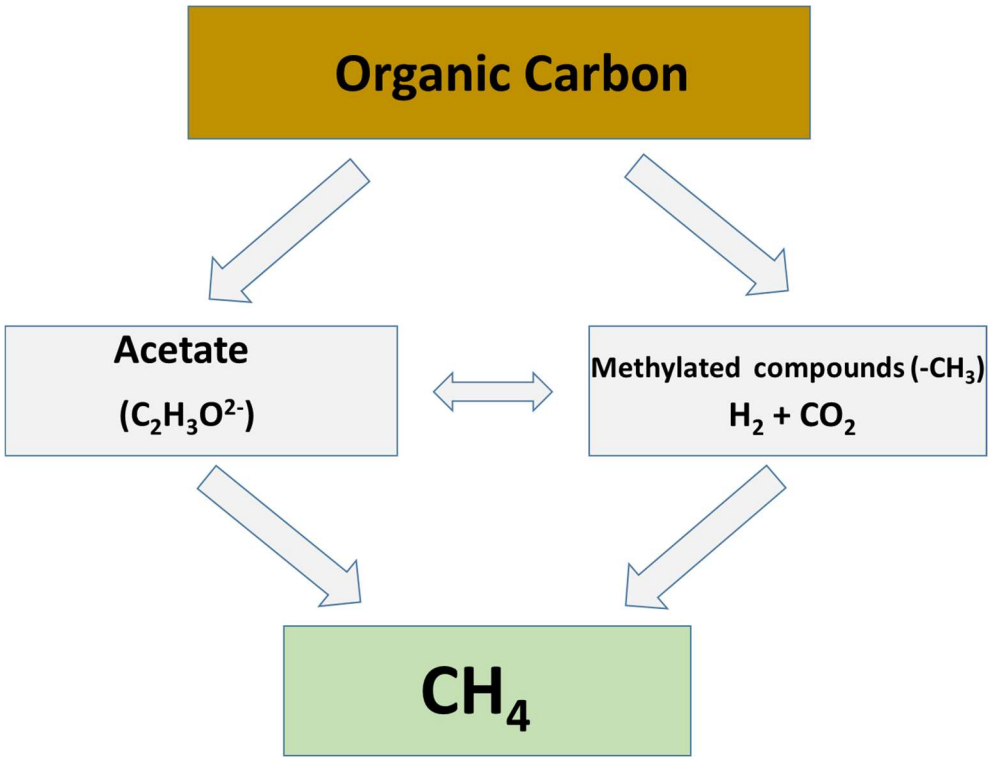

Figure 1.1: Simplified graphical representation of methanogenic processes in marine sediments

All the three pathways have the same final step where methyl-coenzyme M (CH_3-S-CoM) and coenzyme B (Co B) producing heterodisulphide (CoM-S-S-CoB) catalyzed by Methyl-coenzyme M reductase (Mcr) (Sikora et al., 2017; Timmers et al., 2017).

$$CH_3 - S - CoM + H - S - CoB \xrightarrow{Mcr} CoM - -S - CoB + CH_4 \quad (4)$$

1.3.2 Thermogenic Methane

Roughly 0.13 to 0.3 Gt yr^{-1} organic carbon, around 0.6%, of surface productivity, escapes all the remineralization and undergo sedimentary burial (Burdige, 2007; Wallmann et al., 2012). Organic matter that escapes the biogenic methanogenesis is mostly devoid of labile components and instead mainly consists of kerogen (c.f. Mahlstedt, 2018). This residual organic carbon then enters Catagenesis and Metagenesis phases at further depths (>2.5km) at a higher temperature up to 250°C. Thermal degradation and cracking of this organic matter that are millions of years old in deep sediments would result in the production of thermogenic methane (and other hydrocarbons) (Tissot and Welte, 1984).

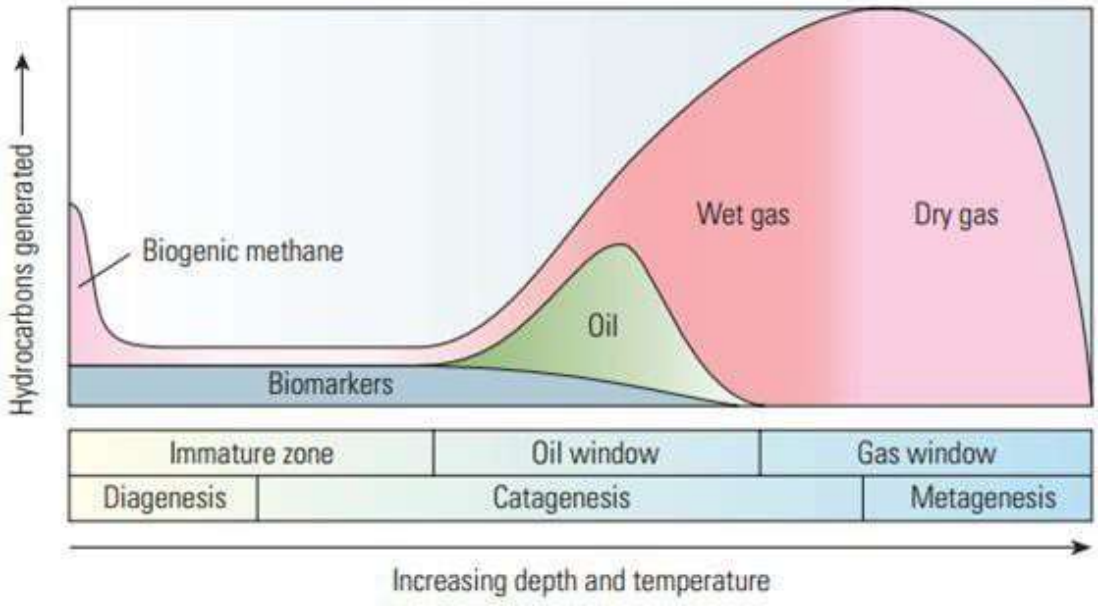

Figure 1.2: Maturation stages in hydrocarbon generation, from Alexander et al., (2011). Diagenesis, Catagenesis, and Metagenesis occurs at a temperature range of <50°C, 50-150°C, and >150°C, respectively. The latter two results in thermogenic methane production and the former in biogenic methane production.

1.3.3 Abiotic Methane

Abiotic Methane can be produced in the subsurface via chemical reactions without the necessity of organic compounds. Three primary abiotic sources have been identified (Etiope and Sherwood Lollar, 2013):

(i) Magmatic

(ii) Late magmatic

(iii) Gas-water-rock interactions

Fischer-Tropsch Type (FTT) Sabatier reaction is considered as a key process for abiogenic methane production in Earth and could be contributing to the marine methane pool from depth

(Horita and Berndt, 1999; Foustoukos and Seyfried, 2004). FTT reactions involve CO_2 and H_2 reaction under the presence of a metal catalyst. On a marine methane perspective, these reactions are particularly prone in sites of hydrothermally derived serpentinization at mid-ocean ridges and subduction zones (Schrenk et al., 2013). These reactions can be summarized as:

$$Olivine + Water + CO_2 \rightarrow Serpentine + Magnetite + CH_4 (5)$$

The H_2 is sourced from the hydration of olivine-rich minerals like peridotite (serpentinization). CO_2 could be sourced from meteoric water, limestone, or mantle. The metals like iron, nickel, cobalt or chromium could serve as the catalyst in these settings (McCollom and Seewald, 2007; McCollom, 2013). A wide range of temperature is known to support this reaction (Etiope and Whiticar, 2019).

1.3.4 Aerobic Methane Production

Methane concentrations in the water column of open oceans are generally quite low, in the range of few nanomoles. However, the methane concentration profile in the surface water column generally shows a trend of maximum concentration at the base of mixed layer. This mixed layer maximum of methane is a phenomenon also known as oceanic methane paradox where surface waters of world oceans are supersaturated with respect to atmospheric concentration (Lamontagne et al., 1973; Reeburgh, 2007; Naqvi et al., 2010). Multiple explanations exist for a plausible reasoning to this phenomenon. For example, Microbial methanogenesis within the anaerobic micro-niches of suspended particles that that accumulate at the pycnocline with maximum concentration (Holmes, 2000); methanogenesis under anoxic microenvironments within the guts of digestive tracts of organisms and immediately after defecation (Karl and Tilbrook, 1994; Stawiarski et al., 2019); supply from sediment sources, especially hydrocarbon

seeps (c.f. Naqvi et al., 2010; Lapham et al., 2017); later supply from supply from marshlands/estuaries in coastal waters (e.g., Bange, 2006) etc. However, recent studies provide strong support for aerobic methanogenesis as the potential explanation to this methane surplus in the surface water.

Recently, two aerobic pathways were also shown for microbial methane production in the water column. First is methylotrophic methanogenesis by bacteria using methyl-rich organic sulfur compounds such as DMSP (dimethylsulfoniopropionate) and/or dimethylsulfide (DMS) that are biosynthesized by phytoplankton (Damm et al., 2010; Florez-Leiva et al., 2013). The second method involves decomposition of methylphosphonate (MPn) under phosphate stressed conditions (Karl et al., 2008). Mpn was recently found to be an important component dissolved organic matter in surface water, providing a strong support to of this mechanism (Repeta et al., 2016). Weber et al., (2019) found positive relationship to phytoplankton growth (which can be linked to DOM) and a negative relationship to phosphate concentration to explain the observed surface methane disequilibrium at global scale, further supporting the Mpn degradation pathway.

1.3.5 Continental Margins as Important Marine Methane Reservoir

Continental margins are important zones of methane production due to high rates of organic carbon loading and low oxygen availability in the sediments. The result is favorable conditions for methane production at relatively shallow depths via microbial methanogenesis and at greater depths through the thermal breakdown of organic matter. Due to rapid sedimentation over millions of years, the organic carbon pool of continental margin sediments is estimated to be around 200,000 Gt C at depths of 1–4 km below the seafloor (Burdige, 2007; Lipp et al., 2008). This enormous organic carbon pool feeds subsurface microbial and thermogenic methane

production. Estimates of microbial methanogenesis range from 10–300 Tg CH_4 yr^{-1} (Hinrichs and Boetius, 2002; Wallmann et al., 2012). A range of 60–80 Tg CH_4 yr^{-1} can be taken as an average (Reeburgh, 1993; Egger et al., 2018). Under favorable pressure-temperature settings, the methane formed in at depth would form gas hydrate structures (Kvenvolden, 2002; You et al., 2019).

Due to their large abundance, methane hydrates are of particular interest for their role in carbon cycling, oceanic slope stability, and as a future energy resource (Kvenvolden, 1988; Milkov, 2004; Boswell and Collett, 2011; Boswell et al., 2014). Methane hydrates are crystalline cage-like structures where CH_4 is surrounded by water molecules. The methane-to-water ratio of these hydrate structures ranges from 1:5.75 to 1:17 under a narrow range of stability conditions at low temperatures (<25°C) and high pressures ~5 (Mpa) (Sloan Jr and Koh, 2007). The amount of methane in gas hydrates probably exceeds the reserves of conventional oil and gas (Kvenvolden, 1988; Collett and Kuuskraa, 1998). The current estimate of the amount of methane hydrates stored in oceanic sediments ranges from 500 Gt to 55000 Gt C (Kvenvolden, 1988; Milkov, 2004; Klauda and Sandler, 2005; Archer et al., 2009; Boswell and Collett, 2011; Dickens, 2011; Wallmann et al., 2012; Yamamoto et al., 2014; Kretschmer et al., 2015). Over the last decade, confidence in the estimates has improved, and those values have moved toward the lower end of this range due to better sediment characterization through dedicated drilling expeditions. A recent review by Ruppel and Kessler (2017) adopted an estimate of ~1800 Gt C for global methane hydrate reservoirs.

In addition to the hydrate phase, an equally significant amount of methane carbon exists as the microbial gas (Milkov, 2011). It is important to note that significant gaps exist in quantifying the total marine methane reservoir. This dissertation, however, emphasize that there is a significant methane carbon pool in the subsurface regardless and that it can interact with shallow sediments and the water column to support important methane-powered carbon cycling.

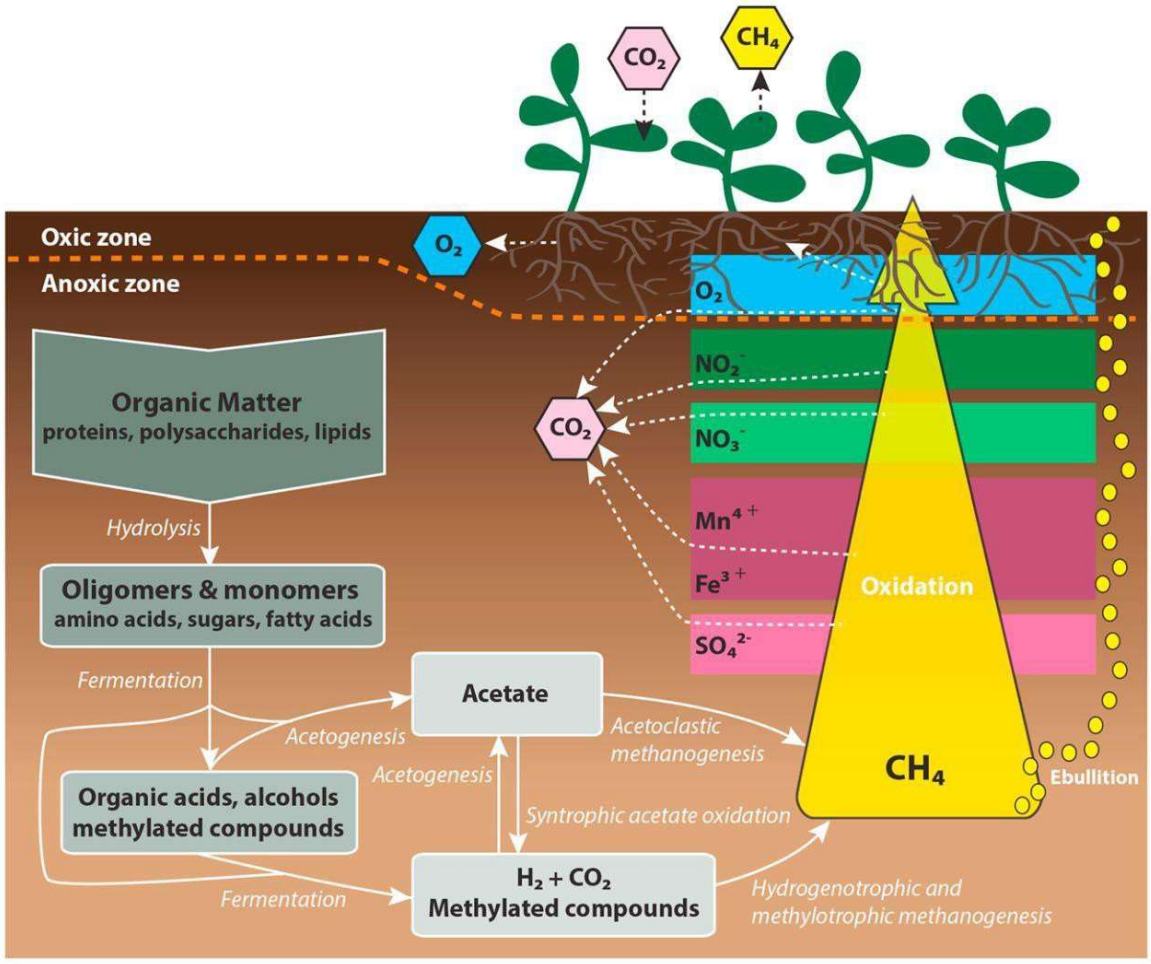

Figure 1.3: Biogenic methanogenesis and subsequent transport to shallow system (Dean et al., 2018)

1.4 Methane Transport to Shallow Sediments

The methane formed in gaseous or dissolved form at depth would migrate toward the seafloor and can be trapped in reservoirs, form gas hydrate structures under favorable pressure-temperature settings, oxidize in shallow sediments and the water column, or escape to the atmosphere (Barnes and Goldberg, 1976; Hovland et al., 1993; Judd et al., 2002). Continental margins are hydro-geologically active zones (Saffer and Tobin, 2011). Active and passive ocean margins are characterized by geological processes that facilitate the exchange of fluids containing bioactive reductants—including sulfide, methane, and hydrogen—from depth (from tens of meters to several kilometers) to the seafloor by fluid and gas advection (Suess, 2010). Marine sediments contain pore fluids of an estimated volume equivalent to ~6% of total seawater (LaRowe et al., 2017). These pore fluids act as an important medium to transport methane from the subsurface toward the seafloor channeled by tectonic and/or sedimentary processes. Plate tectonics, dehydration reactions of hydrous minerals, gas generation, groundwater discharge, salt-tectonics, as well as higher burial pressure and temperature at depth causing dewatering in hydrous minerals, porosity reduction are common causes resulting in upward flux of solutions (Torres and Bohrmann, 2016). Globally, fault permeability is suggested as the most important factor that dictates the distribution and spatiotemporal variability of submarine seep systems (Talukder, 2012). A recent study by Phrampus et al., (2020) finds equal likelihood of encountering fluid expulsion between passive and active margins. This study suggests that globally, lateral compaction on active margins and predominantly vertical compaction on passive margins are equally important in facilitating focused fluid flow sites like cold seeps.

Seepage of methane towards the seafloor, in turn, creates a characteristic chemosynthetic ecosystem based on benthic microbe-mineral interactions and highly interconnected carbon cycling coupled with other elements such as sulfur, iron, calcium, and trace metals (Suess, 2010). Cold seeps are characterized by the release of methane and other reduced compounds typically with associated chemosynthetic ecosystems. They are distinguishable from hydrothermal vents, which release hot, chemically diverse fluids to the seafloor. Cold seeps, by contrast, produce almost no temperature anomalies compared with ambient seawater (Levin et al., 2016). Overall, methane seeps on continental margins are sites of unique geosphere-biosphere coupling that affects marine ecology, ocean chemistry, and atmospheric composition over wide spatial and temporal scales and plays a significant role in the chemical and biological composition of the oceans, as well as the global carbon cycle (Judd and Hovland, 2009; Boetius and Wenzhöfer, 2013; Levin et al., 2016; Suess, 2018)

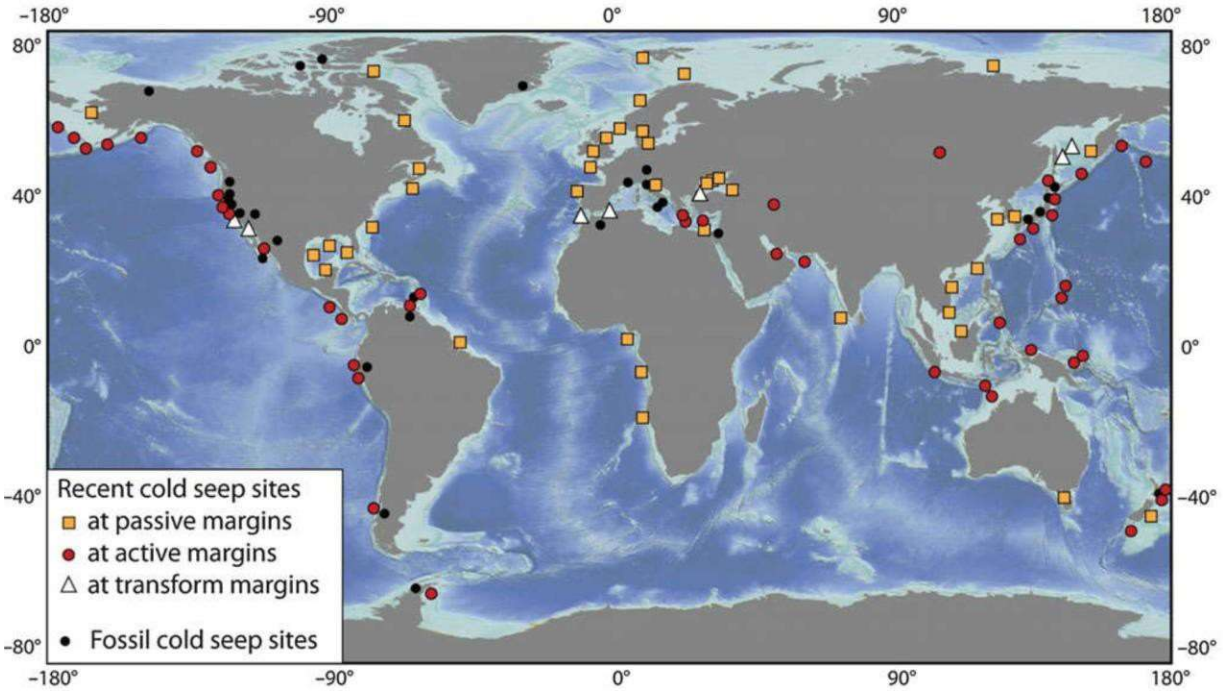

Figure 1.4: Global seep distribution adopted from Torres and Bohrmann (2016).

1.5 The Fate of Methane Entering the Shallow Sediments

Transport of methane from deep to shallow sediment zones with active diagenesis supports an array of biogeochemical processes that effectively convert a large amount of methane carbon to inorganic and subsequent organic carbon pools. These processes primarily involve Anaerobic Oxidation of Methane (AOM) in shallow sediment depths (and in anoxic water columns) (Eq. 5) as well as Aerobic oxidation of Methane (AeM) in oxygenated water columns (Eq. 6).

$$CH_4 + SO_4^{2-} \rightarrow HCO_3^- + HS^- + H_2O \quad (5)$$

$$CH_4 + 2CO_2 \rightarrow CO_2 + 2H_20 \quad (6)$$

It is estimated that roughly 45–300 Tg CH_4 yr^{-1} enter the shallow sediments from deep methanogenic zones, and >90% undergoes AOM (Hinrichs and Boetius, 2002; Orcutt et al., 2011). The remaining <~10% enters the water column (mainly in advective settings) where the majority undergoes AeM, leaving behind a small amount of marine methane to enter the atmosphere where it can have a direct impact on the climate system (Boetius and Wenzhöfer, 2013; Ruppel and Kessler, 2017). The current estimate of the contribution of offshore methane seepage to the atmosphere is in the range of 5–25 Tg CH_4 yr^{-1} (Bange et al., 1994; Kvenvolden et al., 2001; Wuebbles and Hayhoe, 2002; Etiope, 2012; Saunois et al., 2016), with the most recent estimate suggesting a range of 6-12 Tg CH_4 yr^{-1} (Weber et al., 2019). Microbial methane cycling in the ocean sediments is thus one of the most important greenhouse gas emission controls on Earth.

1.5.1 Biochemistry of AOM

Microbial consortia involved in AOM coupled to sulfate reduction are represented by three phylogenic clusters of Euryarchaeota: ANME-1 (with subgroups a and b), ANME-2 (with subgroups: a, b, c, and d), and ANME-3, their SRB partners: Desulfosarcina–Desulfococcus branch (DSS) and Desulfobulbus spp. (DBB) belonging to Deltaproteobacteria class (Niemann and Elvert, 2008; Knittel and Boetius, 2009; Cui et al., 2015). ANME-1 clade is dominant in many AOM systems (Rossel et al., 2008). ANME-1 and -2 are usually reported to be associated with distinct SRB of the DSS clusters (Boetius et al., 2000; Orphan et al., 2002) whereas ANME-3 is associated with DBB species and are mostly restricted to mud volcanoes (Niemann et al., 2006). More recently, ANME-3 clades have been reported to occur in coastal sediments with high methane fluxes and high rates of sediment accumulation (Gautam, 2018). ANME-2 are phylogenetically affiliated with the order Methanosarcinales, ANME-3 are closely related to the genera Methanococcoides and Methanolobus. ANME-1 are not directly affiliated with any of the major orders of methanogens (Rossel et al., 2008).

While most of the reported ANME clades have been suggested to perform SD-AOM, ANME 2d clusters have not been found in consortia with SRBs. Instead, they are suggested to perform nitrate driven AOM in consortium with nitrate reducing or anammox bacteria (Haroon et al., 2013). ANME-1 and -2 are usually reported to be associated with distinct DSS clusters (Boetius et al., 2000; Orphan et al., 2002) whereas ANME-3 is associated with DBB cluster (Niemann et al., 2006). ANME 2 and 3 forms stronger and structured consortia with SRB partners (Orphan et al., 2002; Niemann et al., 2006) whereas ANME 1 is loosely associated with their SRB symbionts (Knittel et al., 2005) and are also reported to occur sometimes as monospecific

aggregates or as single cells without a clear bacterial partner (Orphan et al., 2002). The lifestyle of ANME-1 clades is suggested to be capable to shift from methanotrophic to methanogenic lifestyle (Treude et al., 2007; Lloyd et al., 2011) potentially linked to varying seepage intensities (Feng et al., 2014). Rare putative partnerships of ANME 2c with certain bacterial species from Alpha and Beta-proteobacteria has been also suggested (Knittel and Boetius, 2009).

ANME groups are remarkably related to different methanogenic archaea (orders Methanosarcinales and Methanomicrobiales) in terms of phylogenetics, lipid structures, cell shapes, presence of methyl coenzyme M reductase (MCR), the terminal enzyme of methanogenesis enzyme), and their evolutionary path (Orphan et al., 2002; Niemann and Elvert, 2008; Cui et al., 2015). Analysis of intact polar lipids (IPL), which are derived from living cells, indicated that ANME-1 clade is dominant in diffusive AOM systems (Rossel et al., 2008). In general, ANME-1/DSS consortia are often prevalent at lower methane flux setting whereas ANME-2/DSS and ANME-3/DBB are suggestive of being adapted to diagenetic setting with higher methane flux and relatively higher sulfate supply (Blumenberg et al., 2004; Elvert et al., 2005; Nauhaus et al., 2005; Pape et al., 2005; Stadnitskaia et al., 2008; Rossel et al., 2011).

No members of the ANME groups or of their electron donor partner has been cultivated yet, and the details of the biochemical process are not understood in detail. Multiple mechanisms have been proposed for the transfer of reducing equivalents from ANMEs to their bacterial partners. Along with the reverse methanogenesis pathway of interspecies H_2 transfer from Archaea to SRB, Sulfate induced AOM is proposed to occur or via electron transfer as interspecies transfer of other syntrophic intermediate compounds like acetate (Valentine and Reeburgh, 2000;

Nauhaus et al., 2005) or the compound methanethiol (Moran et al., 2008), with higher thermodynamic energy yields than from H_2 transfer. ANME-2 clades are further reported to have an unusual strategy to perform both AOM and sulfate reduction single-handedly to produce a zero-sulfur (S^0) which is subsequently disproportioned by SRB partners (Milucka et al., 2012). The leading model of metabolic interaction to date is the recently proposed mechanism via direct interspecies electron transfer between ANME and SRB (McGlynn et al., 2015; Wegener et al., 2015, Fig. 1.5). Apart from sulfate, nitrate (Raghoebarsing et al., 2006; Haroon et al., 2013), nitrite (Ettwig et al., 2010), iron, and manganese (Beal et al., 2009; Wankel et al., 2012; Riedinger et al., 2014; Ettwig et al., 2016) have been linked to AOM as electron acceptors. Their impacts on the SMTZ are limited as a function of their low concentrations relative to sulfate's but require additional study. Detailed reviews of the biochemistry of AOM and the physiology of the ANMEs are provided by Timmers et al. (2017) and Evans et al. (2019). AOM produces DIC sourced from methane with depleted $\delta^{13}C$ values [average range -70‰ to -25‰ VPBD (Whiticar, 1999)].

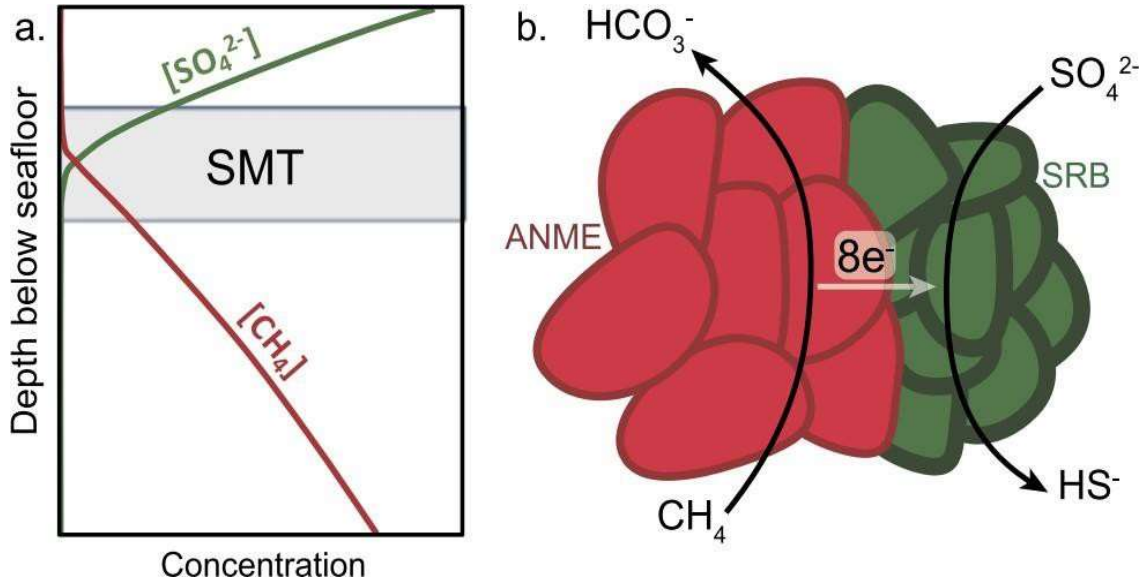

Figure 1.5: Schematic profile is SMTZ and the most accepted syntrophic model for AOM via direct interspecies electron transfer between ANME and SRB (Crémière et al., 2020)

1.5.2 Anaerobic Oxidation of non-methane hydrocarbon

Methane seeps in hydrocarbon-rich basins like the Gulf of Mexico, the Guyamas Basin, and the Gulf of California are often characterized by the seepage of co-existing non-methane hydrocarbons (e.g. n-alkanes, cycloalkanes, and branched-chain alkanes). Natural hydrocarbon seeps are estimated to account for ~47% of all crude oil entering the marine environment, with an estimate of 180 million tons of petroleum annually (National Research Council, 2003; Kvenvolden and Cooper, 2003). A large fraction of the hydrocarbon seep would be consumed anaerobically by the subsurface microbial consortium (Widdel et al., 2010) which effectively reduces the petroleum entering the water column to current estimates. Anaerobic hydrocarbon oxidation coupled with sulfate reduction is a well-known process in the subsurface (Teske, 2018), and, hence can co-consume sulfate along with the ANMEs at seepage system with mixed

hydrocarbon pools. The magnitude and variability of biogeochemical processes involving complicated C-S coupling are loosely constrained at many seep sites with methane and non-methane hydrocarbon seeps. Studies of organic biomarkers in sediments from the Gulf of Mexico (Pancost et al., 2005), observed disparities between measured rates of sulfate reduction and methane oxidation (Joye et al., 2004), and carbon isotopic data from authigenic carbonates (Formolo et al., 2004) suggest that AOM may not be the only process responsible for the DIC production at many seep sites. Rather, it seems likely that the oxidation of non-methane hydrocarbons provides a significant source of metabolic energy and DIC pools at these locations (Naehr et al., 2009; Smrzka et al., 2019).

1.5.3 Aerobic Methanotrophy (AeM)

A large share of the methane entering the shallow sediment (<90%) is sequestered below the seafloor, primarily via C-S coupling at the SMTZ. However, a relatively minor part of the contemporaneous methane fluxes from the deep sediments enter the bottom-water, mainly in the advective setting. Modeling studies have shown that fluid advection rates up to 50 cm $year^{-1}$ is completely (~99%) consumed within the shallow sediments (Luff and Wallmann, 2003). 0.02 Gt of C is considered to enter the oceanic water annually from the advective system (Boetius and Wenzhöfer, 2013). Methane entering the water column could reach the atmosphere depending upon the water depth, especially at very shallow (<100m) water depths (McGinnis et al., 2006). Otherwise, the methane dissolves into the water column and would undergo aerobic oxidation and/or transportation and dilution (Valentine et al., 2001). AeM by methanotrophic bacteria, consumes the water column oxygen and produces CO_2 (Hanson and Hanson, 1996; Yamamoto et al., 2014, Eq. 6)

The CO_2 produced during AeM can reduce the water column pH and could contribute to ocean acidification and oxygen depletion (Yamamoto et al., 2014). A modeling study by Boudreau et al (2015) suggested that the potential dissociation of gas hydrate stability zones in future warming could enhance the ongoing ocean acidification due to anthropogenic warming.

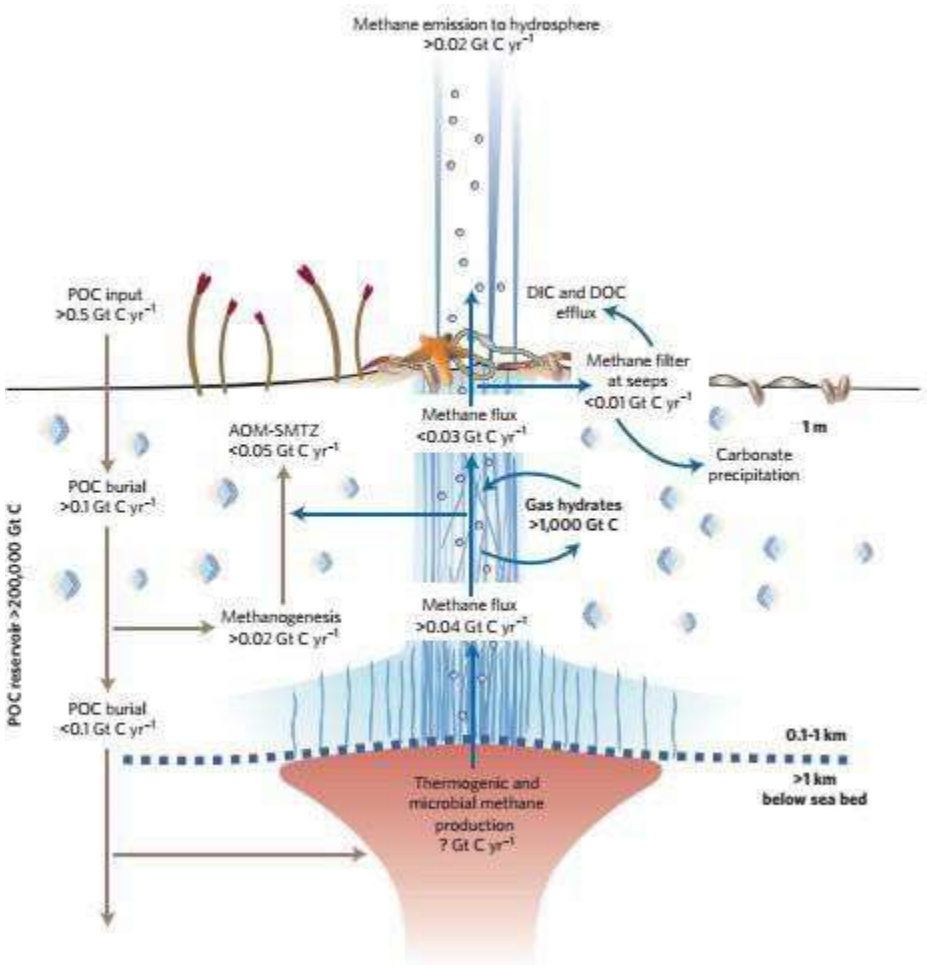

Figure 1.6: Carbon fluxes associated with marine methane seeps (Boetius and Wenzhöfer, 2013)

1.6 Recognizing the Methane Seepage Records from Sediment Records

Modern methane seepage can be detected using geochemical, geophysical, and remote sensing techniques, including pore water analysis, seafloor observations, and methane anomaly detection (e.g.MacDonald et al., 1993; Borowski et al., 1996; Coffin et al., 2008; Schwalenberg et al., 2010; Skarke et al., 2014). Methane biogeochemical signatures imprinted onto sedimentary record by such events are poorly constrained and require appropriate geological proxies that record methane seepage and quantify the timing of formation. This leaves a significant uncertainty regarding temporal and spatial variations of past methane seepage (Stott et al., 2002; Dickens, 2003; Li et al., 2016) and is an important part of the scientific challenge towards our understanding on the properties and processes governing the flow and storage of carbon in subseafloor (Bickle et al., 2011).

There have been many proposed proxies for identifying past methane flux events. Conceptual models (e.g. Dickens et al., 1995) provides an indirect framework for the role of past methane hydrate dissociation events in paleoclimate events. Authigenic mineral precipitates at seep setting are widely used proxy to study past seep records. Authigenic carbonates are perhaps the most widely studied paleo seep proxy in this context due to their distinct petrography, carbon isotope signatures indicative of methane-induced DIC sourcing, and redox-sensitive trace metal concentrations at seep setting (Roberts and Aharon, 1994; Naehr et al., 2000; Teichert et al., 2003; Feng et al., 2010b; Tribovillard et al., 2013; Hu et al., 2014; Crémière et al., 2016). Seep carbonates are also excellent archives for biomarker records of microbial consortia involved in AOM (Birgel et al., 2006b; Hagemann et al., 2013; Guan et al., 2018). Furthermore, the radioactive techniques, especially U-Th dating on seep carbonates provide unique insights to

temporal variability and drivers of the seepage (Aharon et al., 1997; Teichert et al., 2003; Feng et al., 2010b; Wirsig et al., 2012; Bayon et al., 2015; Cremiere, 2015; Sauer et al., 2017; Chen et al., 2019). However, such carbonates may not precipitate during events of high-intensity seepage (Karaca et al., 2010), fluid seepage with low dissolved methane concentrations, high bioturbation, or high sedimentation rates (Bayon et al., 2007).

Similarly, authigenic barite precipitates have been inferred as paleo-seepage indicators (Dickens, 2001). However, records of barite precipitation may be absent due to dissolution by upward migration of the SMTZ or low Ba flux to the sediment (Peketi et al., 2012). Other authigenic minerals of interests in methane laden diagenetic setting include Ikaite and glendonite (Schubert et al., 1997; Morales et al., 2017; Peckmann, 2017), gypsum (Sassen et al., 2004; Kocherla, 2013; Lin et al., 2016a; Zhang et al., 2018), greigite and pyrrhotite (Larrasoaña et al., 2007; Badesab et al., 2019), and vivianite (Hsu et al., 2014; Egger et al., 2015; Liu et al., 2018; März et al., 2018) etc. More recently sulfur isotope records of pyrite have gotten much attention to identifying present and past SMTZ (e.g. Peketi et al., 2012; Borowski et al., 2013; Peketi et al., 2015; Wang et al., 2015; Li et al., 2016; Lin et al., 2016c; Li et al., 2017b; Argentino et al., 2020). However, solely looking at pyrite geochemistry could be erroneous since the pyrite precipitated from a short duration of AOM is suggested not to imprint an enriched ^{34}S signal (Hu et al., 2017b). Also, the isotope signatures can be influenced by organoclastic sulfate reduction and the oxidative part of diagenetic sulfur cycle (Bazzaro et al., 2020). High $\delta^{56}Fe$ and $\delta^{34}S$ of pyrite can indicate enhanced Sulfate depended AOM signals (Lin et al., 2017). Sulfur isotope composition of barite and carbonate associated sulfate (CAS) provides important insights to the

porewater sulfate composition and rapid sulfate reduction at seep setting (Feng and Roberts, 2011; Feng et al., 2016; Gong et al., 2018).

Foraminifera have been extensively used to reconstruct methane seepage dynamics (Sen Gupta and Aharon, 1994; Rathburn et al., 2000; Hill et al., 2003; de Garidel-Thoron et al., 2004; Panieri et al., 2012; Panieri et al., 2014; Panieri et al., 2016; Schneider et al., 2018) However, their ubiquity as reliable seep proxy is debated due to diagenetic overprint, lack of defined seep endemic fauna, and isotopic signal sourcing from regional oceanography (Stott et al., 2002; Martin et al., 2004; Lobegeier and Sen Gupta, 2008; Burkett et al., 2015; Panieri et al., 2017).

The presence of seep-related biomarker compounds and their compound specific isotopes have led to the identification of numerous paleo seep sites as well as the flux variations (e.g., Peckmann and Thiel, 2004; Pape et al., 2005; Birgel et al., 2006a; Birgel et al., 2008; Birgel and Peckmann, 2008; Stadnitskaia et al., 2008; Peckmann et al., 2009; Haas et al., 2010; Birgel et al., 2011; Hagemann et al., 2013; Himmler et al., 2015; Guan et al., 2018). Biomarkers of interest in a seep setting predominantly include isoprene-based archaeal lipids derived from ANMEs, acetate-based lipids from SRB, as well as hopanoids and steroids from bacteria other than SRB including aerobic methanotrophs (Peckmann and Thiel, 2004; Birgel et al., 2008; Niemann and Elvert, 2008). In methane-rich settings, methanotrophic biomarker compounds will show strong to extreme depletion in ^{13}C ($\delta^{13}C$ values as low as -130‰; Elvert et al., 2000) in contrast to values normally observed for marine lipids of about -25‰.

To summarize, a great deal of progress has been made during the past two decades in interpreting the biogeochemical signals from the seep impacted marine sediments. These efforts are important steps to resolve the poorly understood temporal variability of methane venting in the past and their implications for future climate system (Peckmann and Thiel, 2004; Campbell, 2006; Dean, 2020). This dissertation aims to contribute to this scientific effort by characterizing the methane (and hydrocarbon) impacted sediment records from diverse geological settings to study the long-term records of carbon cycling associated with the geosphere-biosphere coupling at seeps.

CHAPTER II: DISSOLVED INORGANIC CARBON PUMP IN METHANE-CHARGED SHALLOW MARINE SEDIMENTS: STATE OF THE ART AND NEW MODEL PERSPECTIVES

Published as Akam, Sajjad A., Richard B. Coffin, Hussain AN Abdulla, and Timothy W. Lyons. "Dissolved Inorganic Carbon Pump in Methane-Charged Shallow Marine Sediments: State of the Art and New Model Perspectives." (2020). DOI: https://doi.org/10.3389/fmars.2020.00206

2.1 Abstract

Methane transport from subsurface reservoirs to shallow marine sediment is characterized by unique biogeochemical interactions significant for ocean chemistry. Sulfate-Methane Transition Zone (SMTZ) is an important diagenetic front in the sediment column that quantitatively consumes the diffusive methane fluxes from deep methanogenic sources toward shallow marine sediments via sulfate-driven anaerobic oxidation of methane (AOM). Recent global compilation from diffusion-controlled marine settings suggests methane from below and sulfate from above fluxing into the SMTZ at an estimated rate of 3.8 Tmol yr^{-1} and 5.3 Tmol yr^{-1} respectively, and wider estimate for methane flux ranges from 1—19 Tmol yr^{-1}. AOM converts the methane carbon to dissolved inorganic carbon (DIC) at the SMTZ. Organoclastic sulfate reduction (OSR) and deep-DIC fluxes from methanogenic zones contribute additional DIC to the shallow sediments. Here, we provide a quantification of 8.7 Tmol yr^{-1} DIC entering the methane-charged shallow sediments due to AOM, OSR, and the deep-DIC flux (range 6.4–10.2 Tmol yr^{-1}). Of this total DIC pool, an estimated 6.5 Tmol yr^{-1} flows toward the water column (range: 3.2–9.2 Tmol yr^{-1}), and 1.7 Tmol yr^{-1} enters the authigenic carbonate phases (range: 0.6–3.6 Tmol yr^{-1}). This summary highlights that carbonate authigenesis in settings dominated by diffusive methane

fluxes is a significant component of marine carbon burial, comparable to ~15% of carbonate accumulation on continental shelves and in the abyssal ocean, respectively. Further, the DIC outflux through the SMTZ is comparable to ~20% of global riverine DIC flux to oceans. This DIC outflux will contribute alkalinity or CO_2 in different proportions to the water column, depending on the rates of authigenic carbonate precipitation and sulfide oxidation and will significantly impact ocean chemistry and potentially atmospheric CO_2. Settings with substantial carbonate precipitation and sulfide oxidation at present are contributing CO_2 and thus to ocean acidification. Our synthesis emphasizes the importance of SMTZ as not only a methane sink but also an important diagenetic front for global DIC cycling. We further underscore the need to incorporate a DIC pump in methane-charged shallow marine sediments to models for coastal and geologic carbon cycling.

2.2 Introduction

Methane (CH_4) is an important greenhouse gas with a significant role in the geological evolution of Earth's carbon cycle and ongoing climate change. Compared to carbon dioxide (CO_2), methane has ~28 times higher warming potential (Stocker et al., 2014), and marine methane reservoirs constitute a large exchangeable carbon pool in the Earth's shallow subsurface, which is significant for carbon cycle dynamics (Kvenvolden, 2002). Continental margins are characterized by methane flux sites that involve transfer in dissolved and gaseous forms via diffusion and advection from subsurface reservoirs to the seafloor. Methane transport towards the seafloor creates a characteristic chemosynthetic ecosystem based on benthic microbial interactions and highly interconnected carbon cycling coupled with other elements such as sulfur, iron, calcium, and trace metals (Suess, 2010). They are thus sites of unique geosphere-

biosphere coupling that plays a significant role in the chemical and biological composition of the oceans, as well as the global carbon cycle (Judd and Hovland, 2009; Boetius and Wenzhöfer, 2013; Levin et al., 2016; Suess, 2018).

Some abrupt climate change events in paleoclimate records are potentially linked to massive dissociation of subsurface methane reservoirs into the oceans and atmosphere (e.g., Dickens et al., 1995; Hesselbo et al., 2000; Jiang et al., 2003). On the contemporaneous Earth, marine methane fluxes are effectively prevented from entering the atmosphere by microbial interactions in shallow sediments and water columns (Boetius and Wenzhöfer, 2013; Ruppel and Kessler, 2017). These processes convert methane carbon to inorganic and organic carbon pool (Fig. 2.1) and prevent the direct impact of methane on the climate system (Reeburgh, 2007). However, the fate of this methane-derived carbon pool is overlooked and could be relevant to oceanic carbon cycling (Dickens, 2003; Coffin et al., 2014; Aleksandra and Katarzyna, 2018). Here we quantify methane-derived carbon cycling in shallow marine sediments in settings characterized by diffusive methane fluxes. We do this by assessing the transformation of methane carbon to inorganic and organic carbon pools (Fig.2.1) with the goal to assess its contribution to global oceanic carbon budgets. We emphasize settings dominated by diffusive rather than advective methane transport because of relatively well-constrained porewater data availability for global diffusive fluxes of methane and sulfate.

2.3 Sulfate-Methane Transition Zones and Associated Carbon Cycling

Sulfate-Methane Transition Zone (SMTZ) is an important diagenetic front where the upward flux of methane encounters downward diffusive sulfate flux and undergoes sulfate-driven Anaerobic

Methane Oxidation (AOM) (Reeburgh, 1976; Borowski et al., 1996; Malinverno and Pohlman, 2011). During AOM, both methane and sulfate are consumed, and hydrogen sulfide (as HS^-) and dissolved inorganic carbon (DIC) present mostly as bicarbonate (HCO_3^-) are produced (Boetius et al., 2000; Orphan et al., 2001). The net reaction can be expressed as:

$$CH_4 + SO_4^{2-} \rightarrow HCO_3^- + HS^- + H_2O \quad (1)$$

AOM in shallow sediment effectively consumes the methane diffusion in marine sediments (Reeburgh, 2007; Knittel and Boetius, 2009). A recent compilation by Egger et al. (2018) from 740 sites of wide oceanographic settings suggests that 2.8–3.8 Tmol CH_4 undergoes sulfate-driven AOM annually. This range was higher than the average ~1 Tmol CH_4 yr^{-1} proposed by Wallmann et al. (2012), closer to 3-5.2 Tmol CH_4 yr^{-1} estimated by Henrichs and Reeburgh (1987), and much lower than the estimated 19 Tmol CH_4 yr^{-1} by Hinrichs and Boetius (2002). Here we highlight that SMTZ is not only important as a methane sink but also for DIC cycling in methane-charged shallow sediments. We do this by quantifying the sources and sinks of DIC cycling associated with the SMTZ at diffusive flux settings (Fig.2.1).

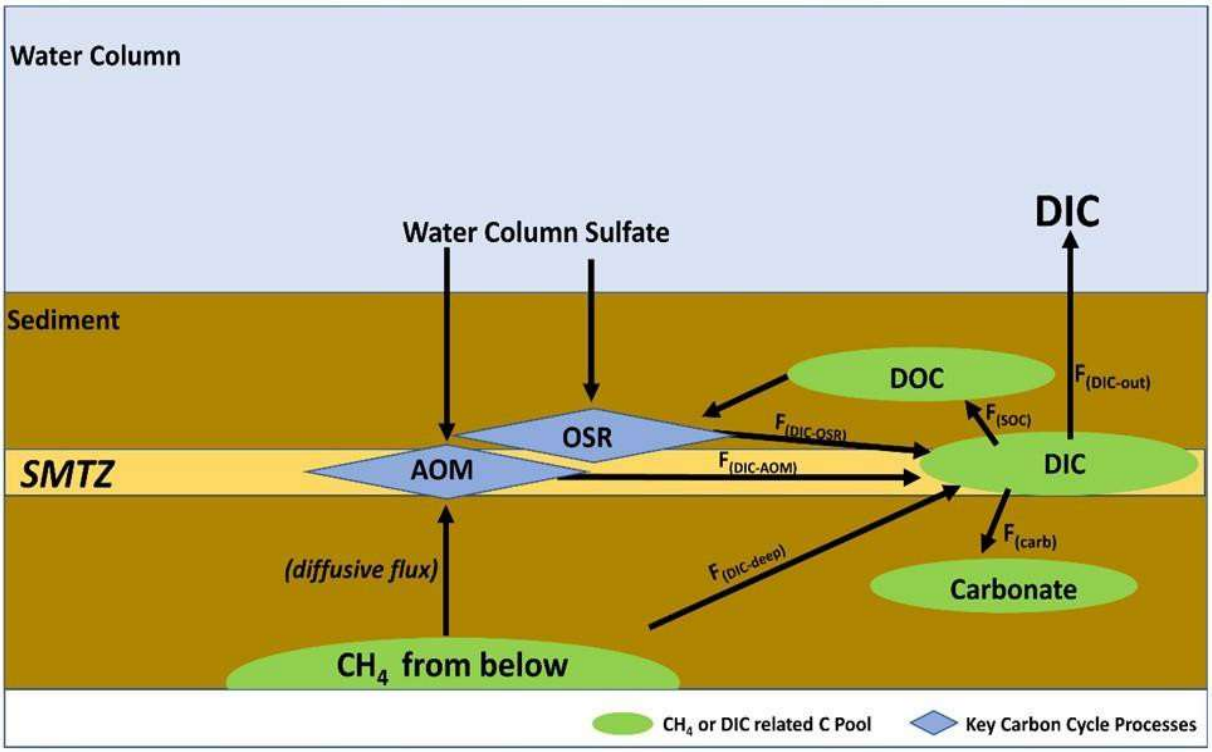

Figure 2.1: A simplified representation of DIC cycling at diffusion-controlled marine settings. Figure 2.4 provides DIC flux estimates. Refer to section 3 for descriptions of flux parameters.

2.3.1 DIC Sources at SMTZ

The SMTZ often contains higher DIC concentrations that can be accounted for AOM (Fig. 2.2). Organoclastic sulfate reduction (OSR, Eq. 2) and deep-DIC flux from methanogenic zones are the primary sources of this excess DIC (Chatterjee et al., 2011).

$$2CH_2O + SO_4^{2-} \rightarrow H_2S + 2HCO_3^- \qquad (2)$$

The SMTZ depth is largely controlled by the upward flux of methane (Borowski et al., 1996) as well as the rate of organic matter degradation, which then controls rates of OSR and methanogenesis (Meister et al., 2013). In diffusive settings, OSR and AOM consume the sulfate at the SMTZ supported by organic matter buried into the SMTZ as well as DOC that is produced

below the SMTZ and migrates upward (Berelson et al., 2005; Komada et al., 2016; Jørgensen et al., 2019a). An estimated 11-80 Tmol yr^{-1} of SO_4^{2-} is reduced globally in marine sediments (Jørgensen and Kasten, 2006; Thullner et al., 2009; Bowles et al., 2014). Egger et al., (2018) suggested that 5.3 Tmol yr^{-1} of this global marine SO_4^{2-} reduction occurs at sites where methane transport occurs through diffusion.

A global estimate for methane and sulfate fluxing to the SMTZ in diffusive settings yielded an average ratio (CH_4:SO_4^{2-}) of 1:1.4 (Egger et al., 2018). A combined effect of AOM and OSR (Berelson et al., 2005; Kastner et al., 2008; Komada et al., 2016; Jørgensen et al., 2019b), as well as cryptic C-S cycling within SMTZ (due to concurrent production and consumption of methane), have been suggested to be causing this higher sulfate flux relative to methane flux (Borowski et al., 1997; Hong et al., 2013; 2014; Beulig et al., 2019).

In addition to AOM and OSR, deep-DIC fluxing from methanogenic depths provides another important source for DIC through the SMTZ (Dickens and Snyder, 2009; Solomon et al., 2014). Methanogenesis in deeper sediment can produce DIC in the form of CO_2 which can be summarized as Eq. 3 (Meister et al., 2019b):

$$2CH_2O \xrightarrow{+H_2O} 2CO_2 + 4H_2 \rightarrow CO_2 + CH_4 \xrightarrow{-H_2O} \quad (3)$$

This CO_2 would dissociate to HCO_3^- and H^+, causing a pH decrease. This step, in turn, would favor weathering of silicate minerals in marine sediments (Marine Silicate Weathering-MSiW), resulting in alkalinity production and pH buffering (Aloisi et al., 2004; Wallmann et al., 2008; Solomon et al., 2014; Kim et al., 2016; Wehrmann et al., 2016, Eq. 4).

$$\text{Cation-rich silicate} + CO_2 \rightarrow \text{Cation-depleted silicates} + HCO_3^- + \text{Cations} \quad (4)$$

As a result of MSiW, methanogenic DIC enters the SMTZ as alkalinity instead of CO_2 (Wallmann et al., 2008). Additional deep-DIC could enter the methanogenic zone and shallow sediments due to fluid expulsion from greater depths (e.g., continental crust alteration [(Meister et al., 2011)]).

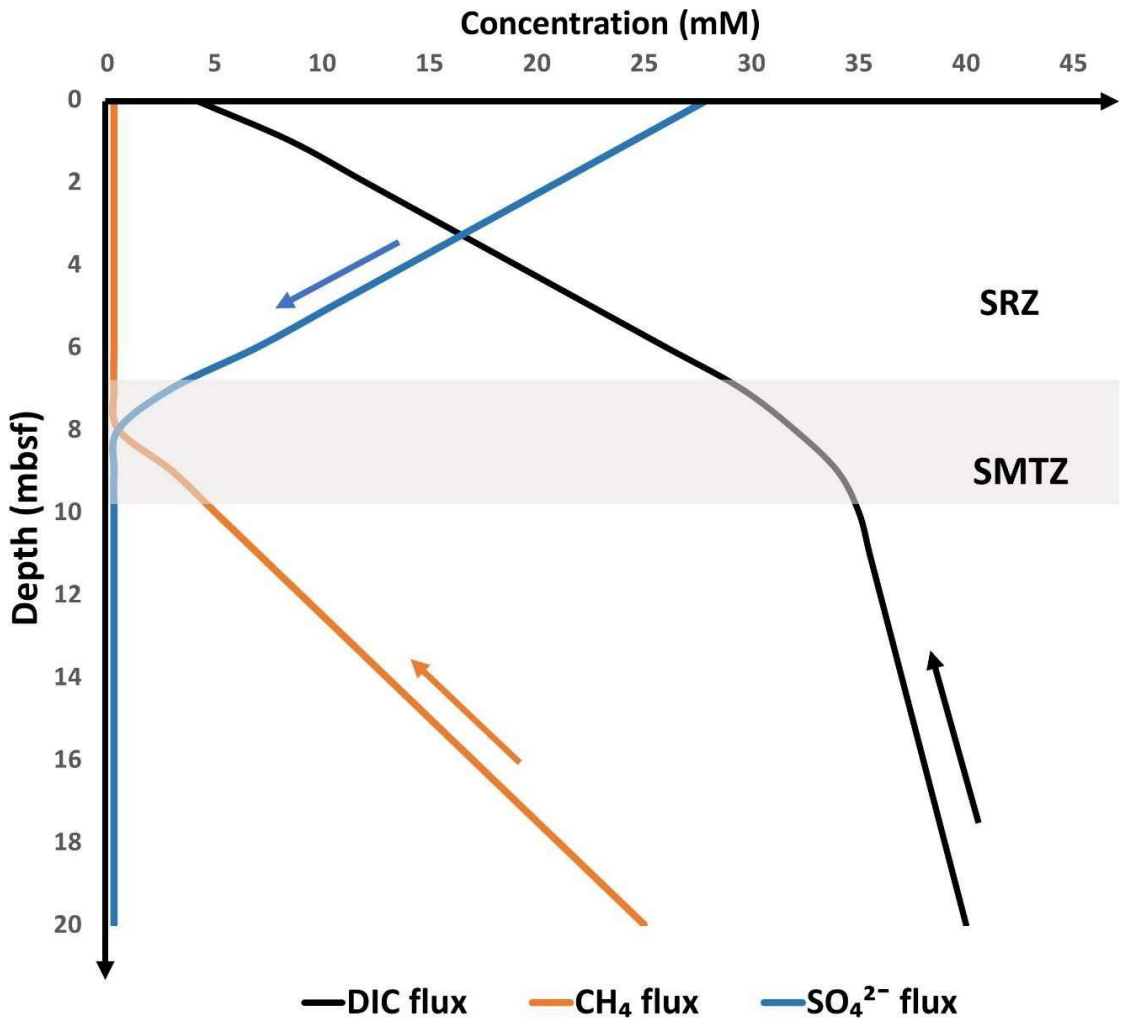

Figure 2.2: Schematic concentration (based on measured and modeled) profiles for CH_4, SO_4^{2-}, and DIC, at diffusive methane flux setting. Arrows indicate flux direction. SRZ indicates the sulfate reduction zone with dominant organoclastic sulfate reduction (OSR). The DIC concentration at the SMTZ is the result of AOM, OSR, deep-DIC input, and authigenic carbonate precipitation. Modified based on data from Snyder et al., (2007, Japan Sea), Malinverno and Pohlman (2011, IODP Site U1325, Cascadia Margin), Chatterjee et al., (2011 ODP Site 1244, Hydrate Ridge), and Wehrmann et al., (2011, IODP Site 1345, Bering Sea).

2.3.2 Fate of the DIC entering SMTZ

Fate of the DIC pool entering the SMTZ primarily involves precipitation as authigenic carbonate minerals, autotrophic microbial consumption, and transport toward the water column. AOM, OSR, and deep-DIC flux will increase the DIC concentration and carbonate alkalinity of pore fluids at SMTZ (Chatterjee et al., 2011; Yoshinaga et al., 2014). Higher carbonate alkalinity, in turn, will stimulate authigenic carbonate precipitation at SMTZ (Aloisi et al., 2002; Orphan et al., 2004; Naehr et al., 2007; Feng et al., 2010a; Crémière et al., 2012; Prouty et al., 2016) via the following reaction (Baker and Burns, 1985):

$$2HCO_3^- + Ca^{2+} \rightarrow CaCO_3 + CO_2 + H_2O \qquad (5)$$

A small portion of total DIC from SMTZ will be assimilated into biomass by autotrophic microbes and eventually become part of sedimentary organic carbon (SOC) (Sivan et al., 2007; Ussler III and Paull, 2008). The remaining DIC enters overlying sediment and eventually the water column if it is not involved in diagenesis on the way.

2.4. Calculations

The flux of DIC to the water column from methane charged sediments $F_{(DIC\text{-}out)}$, can be represented by Eqs. (6) and (7), respectively.

$$\mathrm{Total}_{(DIC)} = F_{(DIC-AOM)} + F_{(DIC-OSR)} + F_{(DIC-deep)} \quad (6)$$

$$F_{(DIC-0ut)} = (F_{(DIC-AOM)} + F_{(DIC-OSR)} + F_{(DIC-deep)}) - (F_{(carb)} + F_{(SOC)}) \quad (7)$$

As discussed below, $\mathrm{Total}_{(DIC)}$ represents the ratio of DIC from AOM, OSR, and deep flux to methane entering the SMTZ. $F_{(DIC\text{-}AOM)}$, $F_{(DIC\text{-}OSR)}$, and $F_{(DIC\text{-}deep)}$ represent the DIC input to $\mathrm{Total}_{(DIC)}$ via AOM, OSR, and deep flux, respectively. $F_{(DIC\text{-}OSR)}$ considers the depth-integrated DIC pool via OSR, which includes the SMTZ and sulfate reduction zone (SRZ) above. $F_{(Carb)}$, $F_{(SOC)}$, and $F_{(DIC\text{-}out)}$ represent the DIC output from $\mathrm{Total}_{(DIC)}$ via authigenic carbonate precipitation, microbial uptake to SOC, and DIC outflux toward the water column, respectively (Fig. 2.1). Net DIC fluxes from the sediment in methane-charged shallow sediments depend on the rates of these parameters.

We would also like to mention that DIC cycling in shallow marine sediments, in general, can be influenced by processes not directly related to methane cycling like carbonate dissolution, organic matter degradation using electron acceptors other than sulfate, as well as submarine groundwater discharge (e.g. Berelson et al., 2007; Higgins et al., 2009; Moore, 2010; Hu and Cai, 2011; Aleksandra and Katarzyna, 2018). However, we focus our attention on diffusive methane charged settings and hence to the parameters in Eqs. (6) and (7) for our DIC calculations, with an emphasis on their importance in marine DIC budgets.

2.4.1 Estimations of Parameter Values

$F_{(DIC\text{-}AOM)}$ and $F_{(DIC\text{-}OSR)}$: Modeling studies have shown that the methane flux at fluid advection rates of up to 60 cm $year^{-1}$ is almost completely consumed within shallow sediments (Luff and Wallmann, 2003; Luff et al., 2004), primarily via AOM. Hence, AOM efficiency would be lower in advective settings and higher in diffusive settings. As we focus on diffusive settings in this study, a 100% AOM efficiency is used for our budget calculation. Thus, for a 1:1.4 ratio of CH_4:SO_4^{2-} fluxing toward the SMTZ as a global average in diffusive settings (Egger et al., 2018), AOM accounts for 1 mol (70%) and OSR accounts for 0.4 mol (30%) of total SO_4^{2-} consumption.

$F_{(DIC\text{-}deep)}$: Deep-DIC flux to the SMTZ is prevalent in diffusive methane flux settings (e.g., Aloisi et al., 2004; Wallmann et al., 2008; Dickens and Snyder, 2009; Chatterjee et al., 2011; Scholz et al., 2013; Solomon et al., 2014). However, the global trend of this deep-DIC flux is not well established. If methane from deep below is biogenic, $F_{(DIC\text{-}deep)}$ should be 100% of the CH_4 flux. As a result of MSiW, methanogenic DIC contributes as alkalinity, and silicate-bond cations are released (Wallmann et al., 2008; Solomon et al., 2014; Pierre et al., 2016), resulting in deep-DIC sequestration via carbonate precipitation within methanogenic zones (Torres et al., 2020). Additional deep-DIC sinks coupled to Fe/Mn reduction in the methanogenic zones was proposed by Solomon et al (2014) and available literature reports also show a lower deep-DIC flux rate (Dickens and Snyder, 2009; Chatterjee et al., 2011; Wehrmann et al., 2011; Komada et al., 2016; Hu et al., 2017a; Zhang et al., 2019). Hence, we assume a conservative estimate of 50% of CH_4 flux to our budget as the average $F_{(DIC\text{-}deep)}$.

F_{carb}: Reported average DIC uptake by authigenic carbonates from the total DIC pool at the SMTZ varies from 7-36% (Luff and Wallmann, 2003; Snyder et al., 2007; Wallmann et al., 2008; Hong et al., 2013; Coffin et al., 2014; Komada et al., 2016; Chuang et al., 2019; Zhang et al., 2019), with upper estimates ranging up to 50% (Smith and Coffin, 2014). However, it is important to note that authigenic carbonates may not precipitate at all methane flux settings. Events of high-intensity fluxes (Karaca et al., 2010; Coffin et al., 2014), fluid flux with low dissolved methane concentrations, settings with intense bioturbation or high sedimentation rates (Luff et al., 2004; Bayon et al., 2007) can inhibit carbonate precipitation. Furthermore, dissolution of authigenic carbonates can occur under multiple conditions, including when aerobic methanotrophy produces CO_2, when sulfide oxidation produces acid, which is corrosive, (Matsumoto, 1990; Himmler et al., 2011); CO_2 produced from methanogenesis (Meister et al., 2011); and due to CO_2 produced in thermogenic gas seeps (Kinnaman et al., 2010)—among other drivers of dissolution. Rates of authigenic carbonate dissolution at diffusive methane flux sites are not well known. In our calculations, we assume a conservative estimate of 20% for F_{Carb} as an average, considering the still-limited global perspective. This value is comparable to the recent estimates of Zhang et al. (2019, 20%) and Komada et al. (2016, 25%), who treated all three parameters in Eq. 6 as $Total_{(DIC)}$.

F_{soc}: In exceptional cases, up to 85% incorporation of AOM induced DIC has been reported for the SOC pool (Coffin et al., 2015). However, in general, the production of new microbial biomass in anoxic sediments based on AOM is negligible due to low growth yield and accounts for only 1-3% of the methane consumption (Nauhaus et al., 2007; Treude et al., 2007). Hence the bulk SOC pool often does not represent the new biomass and the dissolved organic carbon

(DOC) produced via AOM (Ussler III and Paull, 2008; Coffin et al., 2014). Modeling studies have shown that AOM is the dominant process at SOC values <5% (Sivan et al., 2007). Hence, we use an F_{SOC}= 5% as an average estimate for DIC conversion to organic carbon at the SMTZ in our calculation.

$F_{(DIC\text{-}out)}$: With a portion of $Total_{(DIC)}$ going to authigenic carbonate and SOC, the remaining DIC from $Total_{(DIC)}$ (averaging 75% based on a F_{carb} = 20 and F_{SOC} = 5%) enters the overlying sediment and eventually the water column if it is not involved in diagenesis on the way. This DIC flux can, in turn, significantly impact ocean chemistry.

It is also important to mention that methane fluxes are highly variable in time, resulting in upward and downward movement of the SMTZ (e.g., Malone et al., 2002; Meister et al., 2007; Contreras et al., 2013; Meister, 2015; Meister et al., 2019a). Such dynamic conditions could lead to strong variations in the parameters discussed above and the net DIC sinks and sources. Hence, we consider an extended range of these parameters in Table 1 to address the flux variability. This approach also considers the still-limited global perspective of these parameters.

Table 2.1: Parameters controlling the DIC fluxes at SMTZ, with their average and extended range considered in carbon flux calculation.

Parameter	**Average Rate**	**Variable Range**	**Examples**
AOM:OSR (for consumption of total sulfate entering SMTZ)	70:30	100:0 - 30:70	(Kastner et al., 2008; Burdige and Komada, 2011; Boetius and Wenzhöfer, 2013; Meister et al., 2013; Hu et al., 2015; Komada et al., 2016; Wu et al., 2016; Hu et al., 2017a; Wurgaft et al., 2019; Zhang et al., 2019)
$F_{(DIC\text{-}deep)}$	50%	20-75%	(Luff and Wallmann, 2003; Snyder et al., 2007; Wallmann et al., 2008; Hong et al., 2013; Coffin et al., 2014; Komada et al., 2016; Hu et al., 2017a; Chuang et al., 2019; Zhang et al., 2019)
F_{carb}	20%	10-35%	(Luff and Wallmann, 2003; Wallmann et al., 2006; Snyder et al., 2007; Karaca et al., 2010; Hong et al., 2013; Coffin et al., 2014; Komada et al., 2016; Hu et al., 2017a; Chuang et al., 2019; Zhang et al., 2019)
F_{SOM}	5%	1-10%	(Nauhaus et al., 2007; Sivan et al., 2007; Treude et al., 2007; Ussler III and Paull, 2008; Contreras et al., 2013; Coffin et al., 2014; Jørgensen et al., 2019a)
$F_{(DIC\text{-}out)}$	75%	50-90%	(Aloisi et al., 2004; Wallmann et al., 2008; Dickens and Snyder, 2009; Chatterjee et al., 2011; Wehrmann et al., 2011; Scholz et al., 2013; Solomon et al., 2014; Zhang et al., 2019).

2.4.2 DIC production via AOM and OSR

We assume global average DIC production at SMTZ as suggested by Egger et al. (2018) along with their average CH_4:SO_4^{2-} fluxes to SMTZ of 1:1.4. This approach assumes quantitative methane consumption at SMTZ. AOM produces 1 mole of DIC for every mole of SO_4^{2-} consumed. OSR, on the other hand, would produce 2 moles of DIC for every mole of SO_4^{2-} consumed (Eqs.1 and 2)**.** For a global average CH_4:SO_4^{2-} flux to the SMTZ of 1:1.4, 1.8 moles of DIC will be produced by sulfate reduction via AOM and OSR—that is, of the total 1.4 moles of

SO_4^{2-} entering SMTZ, 1 mole DIC will be produced by 1 mole SO_4^{2-} reduction via AOM, and the remaining 0.4 moles of SO_4^{2-} yields 0.8 moles DIC via OSR. Thus, the SO_4^{2-}: DIC ratio from a CH_4: SO_4^{2-} flux ratio of 1:1.4 at the SMTZ will be 1.4:1.8 or 1:1.3 (Fig. 2.3).

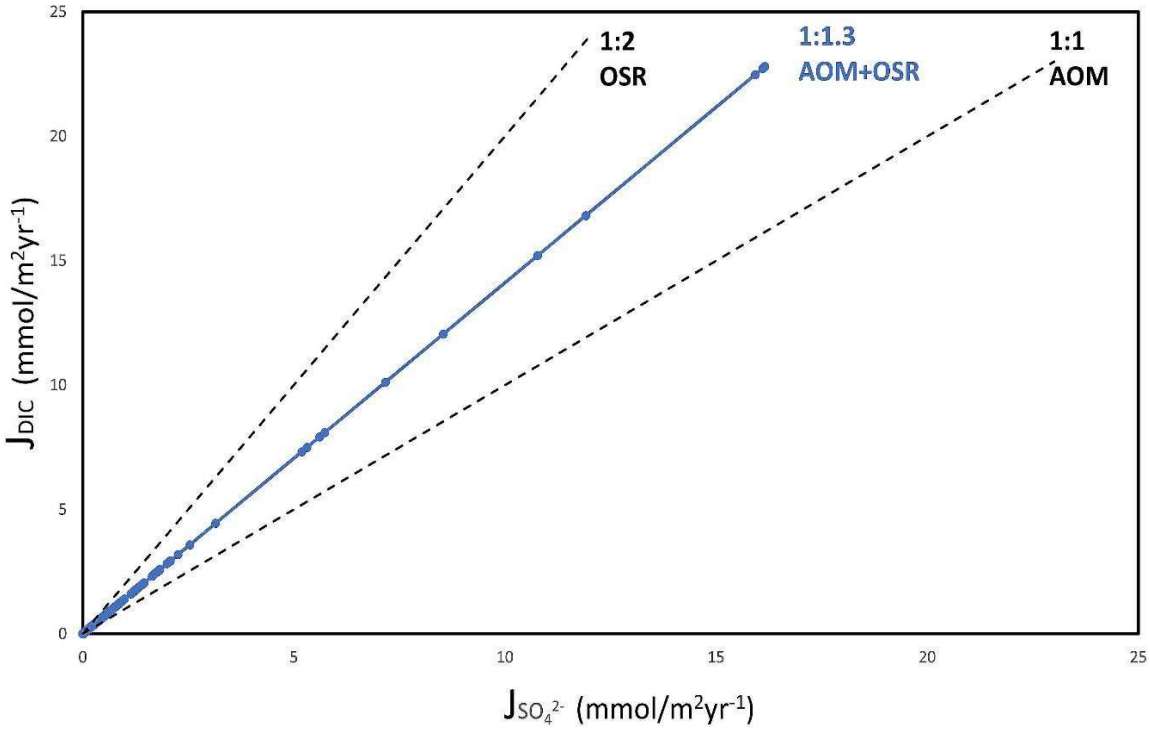

Figure 2.3: Plots for SO_4^{2-}: DIC ratio for AOM and OSR. Black slopes indicate AOM (1:1) and OSR (1:2). The blue slope indicates SO_4^{2-}: DIC plot calculated from 740 diffusion-controlled marine methane flux sites globally by Egger et al (2018), with SO_4^{2-} flux data from 509 sites. CH_4 concentrations were adjusted using a 1:1.4 flux ratio for CH_4: SO_4^{2-} and the combined effect of AOM and OSR results in a SO_4^{2-}: DIC ratio ~ 1:1.3

2.4.3 Total DIC through the SMTZ

Considering an average $F_{(DIC\text{-}deep)}$ of 50% of the CH_4 flux, $Total_{(DIC)}$ through the SMTZ for a CH_4: SO_4^{2-} flux ratio of 1:1.4 can be given as:

$$\mathrm{Total}_{(DIC)} = F_{(DIC-AOM)} + F_{(DIC-OSR)} + F_{(DIC-deep)}$$

$$= 1 + 0.8 + 0.5$$

$$= 2.3 \text{ moles.}$$

Of this $Total_{(DIC)}$, an estimated DIC outflow towards the water column can be calculated using an average estimate of $F_{Carb} = 20$, and $F_{SOC} = 5$ as:

$$F_{(DIC\text{-}out)} = \mathrm{Total}_{(DIC)} - (F_{Carb} + F_{SOC})$$

$$= 2.3 - (.20*2.3 + .05*2.3)$$

$$= 1.73 \text{ moles.}$$

Thus, on average, for every mole of CH_4 entering the SMTZ in diffusive setting, ~0.5 moles of DIC precipitates as authigenic carbonate and ~1.7 moles of DIC flow upward from the SMTZ toward the seafloor and water column.

2.4.4 Global Estimate

A global estimate of DIC cycling in diffusive methane-charged shallow sediments is derived using the recent compilation of global diffusive methane and sulfate fluxes into the SMTZ in marine settings from 740 sites by Egger et al. (2018, Tables 2–4).

Table 2.2: Global estimate of diffusive CH_4 and SO_4^{2-} flux based on 1:1.4 ratio, and average SMTZ depth compiled from 740 sites (Egger et al., 2018)

Region (water depth (m))	**SO_4^{2-} flux (Tmol yr^{-1})**	**CH_4 flux (Tmol yr^{-1})**	**Average SMTZ depth (mbsf)**
Inner shelf (0–10)	1.6	1.2	0.5
Inner shelf (10–50)	1.7	1.2	2
Outer shelf (50-200)	1	0.7	4
Slope (200-2000)	0.8	0.5	12.8
Rise (2000-3500)	0.07	0.05	143.4
>3500	0.1	0.07	168.9
TOTAL	**5.3**	**3.8**	

Table 2.3: Average values for parameters in Table 2, for a global CH4 flux of 3.8 Tmol yr-1 and SO42- flux of 5.3 Tmol yr-1. AOM and OSR consumes 70% and 30% of SO42- entering the SMTZ respectively, F(DIC-deep)= 50% of CH4 flux, Fcarb = 20%, FSOC = 5% and F(DIC-out)= 75% of the Total(DIC). All flux values are in Tmol yr-1

	From Egger et al., (2018)		**Calculated**						
Region (water depth (m))	**SO_4^{2-} flux**	**CH_4 flux**	**DIC Via AOM¶**	**DIC via OSR***	**DIC from deep sediments#**	**$Total_{(DIC)}$**	**DIC sequestered via Carbonates¶¶**	**DIC sequestered via SOC****	**DIC Out##**
Inner shelf (0–10)	1.6	1.2	1.2	0.8	0.60	2.60	0.52	0.13	1.95
Inner shelf (0–50)	1.7	1.2	1.2	1	0.60	2.80	0.56	0.14	2.10
Outer shelf (50-200)	1	0.7	0.7	0.6	0.35	1.65	0.33	0.08	1.24
Slope (200-2000)	0.8	0.5	0.5	0.6	0.25	1.35	0.27	0.07	1.01
Rise (2000-3500)	0.07	0.05	0.05	0.04	0.03	0.12	0.02	0.01	0.09
>3500	0.1	0.07	0.07	0.06	0.04	0.17	0.03	0.01	0.12
TOTAL	**5.3**	**3.8**	**3.8**	**3.0**	**1.9**	**8.7**	**1.7**	**0.4**	**6.5**

¶DIC via AOM = CH_4 flux (quantitative methane consumption)
**DIC via OSR = 2 * (SO_4^{2-}flux - CH_4 flux)*
*#DIC from deep sediments = 0.5*CH_4 flux*
*¶¶DIC sequestered via Carbonates (F_{carb}) = $Total_{(DIC)}$*0.2*
***DIC sequestered via SOC (F_{SOC}) = $Total_{(DIC)}$*0.05*
*## DIC Outflux ($F_{DIC\text{-}out}$) = $Total_{(DIC)}$*0.75*

Table 2.4: Range of DIC flux values (in in Tmol yr-1) based on variable ranges of DIC flux parameters in Table 2.1

Region (water depth (m))	From Egger et al., (2018)		Calculated						
	SO_4^{2-} flux	CH_4 flux	DIC Via AOM	DIC via OSR	DIC from deep sediments	$Total_{(DIC)}$	DIC sequestered via Carbonates	DIC sequestered via SOC	DIC Out
Inner shelf (0–10)	1.6	0.5—1.6	0.5—1.6	0—2.24	0.1—1.2	1.9—3.1	0.19—1.0	0.02—0.3	1.0—2.8
Inner shelf (10–50)	1.7	0.5—1.7	0.5—1.7	0—2.38	0.1—1.3	2.0—3.3	0.2—1.2	0.02—0.3	1.0—3.0
Outer shelf (50-200)	1	0.3—1	0.3—1	0—1.4	0.06—0.8	1.2—1.9	0.12—0.7	0.01—0.2	0.6—1.7
Slope (200-2000)	0.8	0.2—0.8	0.2—0.8	0—1.12	0.05—0.6	1.0—1.5	0.1—0.5	0.01—0.2	0.5—1.4
Rise (2000-3500)	0.07	0.02—0.07	0.02—0.07	0—0.098	0.004—0.1	0.08—0.13	0.01—0.05	0.001—0.01	0.04—0.12
>3500	0.1	0.03—0.1	0.03—0.1	0—0.14	0.01—0.1	0.1—0.2	0.01—0.07	0.001—0.02	0.06—0.2
TOTAL	**5.3**	**1.6—5.3**	**1.6—5.3**	**0—7.4**	**0.3—4.0**	**6.4—10.2**	**0.6—3.6**	**0.1—1**	**3.2—9.2**

2.5. Synthesis

We highlight the major DIC fluxes through the SMTZ in methane-charged shallow marine sediments under diffusion-controlled settings with the following estimated values (Fig. 2.4):

a. 8.7 Tmol yr^{-1} DIC input ($Total_{(DIC)}$) due to AOM, OSR, and deep-DIC flux (range: 6.4–10.2 Tmol yr^{-1}) enters the shallow sediments.

b. 6.5 Tmol yr^{-1} DIC outflux $F_{(DIC\text{-}out)}$ toward the seafloor and water column (range 3.2–9.2 Tmol yr^{-1}).

c. 1.7 Tmol yr^{-1} DIC sink via authigenic carbonate precipitation (F_{carb}) (range: 0.6–3.6 Tmol yr^{-1})

d. 0.4 Tmol yr^{-1} DIC enters the sedimentary organic carbon pool due to microbial uptake (F_{SOC}) (range 0.1–1Tmol yr^{-1}).

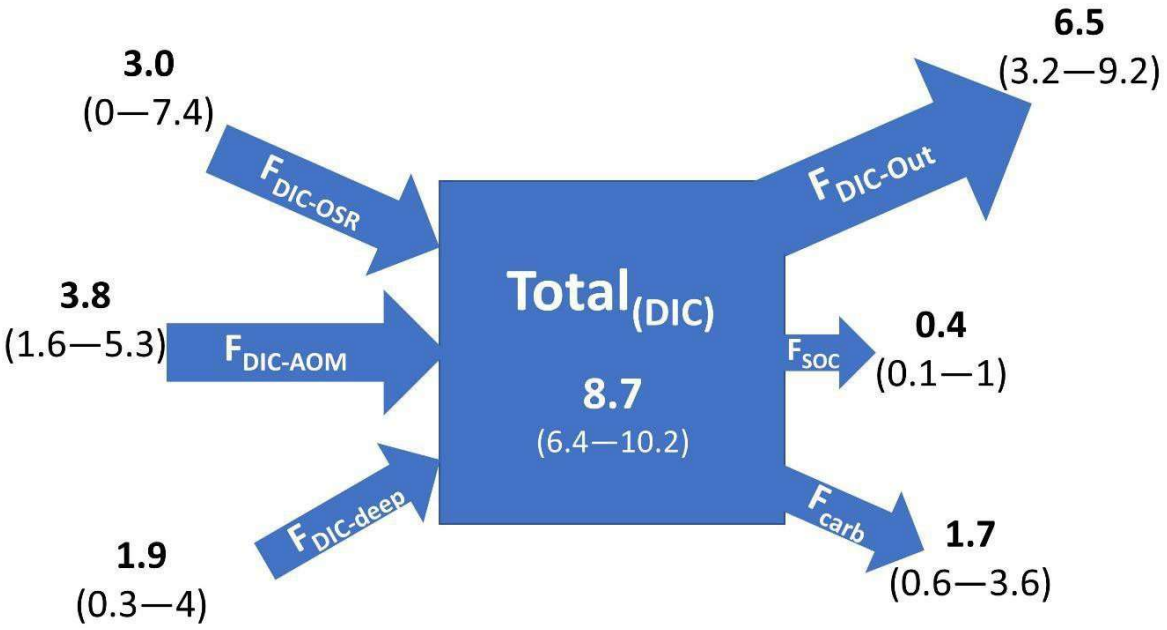

Figure 2.4: Sources and sinks of DIC through the SMTZ in methane-charged shallow sediments. The numbers in bold indicate flux values in Tmol yr^{-1}. Numbers in the parentheses indicate the flux values with an extended range of parameters considered in Table 2.1. Size of the arrows indicates relative DIC flux contribution.

We would like to point out that our model curve is determined from current turnover rates and methane fluxes would vary strongly over time. While data necessary to constrain the temporal variability of fluxes is not available, we acknowledge this limitation. Consideration of an extended range for all the parameters we used in our DIC budget aims to address this dynamic nature of methane fluxes. Furthermore, it is also important to note that present estimates on global marine methane fluxes are heavily dependent on data from continental margins. Methane venting in the deep sea remains to a great part unexplored (e.g., Boetius and Wenzhöfer, 2013). The uncertainty on global marine methane flux estimates is expected to narrow down in the

coming decade with rapidly improving mapping efforts and long-term flux monitoring programs. We also emphasize that we based our DIC flux estimates on the pore fluid data compiled by Egger et al (2018), due to an extensive geochemical database it considers (740 global sites from a wide range of oceanographic settings). Calculations based on the other estimates, ~1.2 Tmol CH_4 yr^{-1} by Wallmann et al. (2012) and 19 Tmol CH_4 yr^{-1} by Hinrichs and Boetius (2002) would provide much wider flux range (Supp. Table 3).

2.5.1 Importance of Methane Derived Authigenic Carbonate Precipitation

Methane-derived authigenic carbonate precipitation in diffusive settings averaging 1.7 Tmol yr^{-1} (range: 0.6–3.6 Tmol yr^{-1}) is close to the 1 Tmol yr^{-1} estimated by Sun and Turchyn (2014) and 1.5 Tmol yr^{-1} suggested by Wallmann et al. (2008, for a methane flux estimate of 5 Tmol yr^{-1}). Our estimated average corresponds to 11-15% of 11-15 Tmol yr^{-1} carbonate accumulation estimated for continental shelf sediments and 15% of ~11 Tmol yr^{-1} in pelagic oceans (Milliman, 1993; Archer, 1996; Milliman and Droxler, 1996; Iglesias-Rodriguez et al., 2002; Schneider et al., 2006; Wallmann and Aloisi, 2012).

However, this estimate is an order of magnitude higher than the recently suggested estimate of 0.14 Tmol yr^{-1} by Bradbury and Turchyn (2019). Multiple factors could be responsible for this mismatch. Previous estimates for global carbonate authigenesis were based primarily on the Ca^{2+} flux into sediments from the overlying water column and do not account for Ca^{2+} fluxes toward shallow sediment from deep methanogenic zones due to MSiW (Longman et al., 2019). Further, a higher authigenic carbonate sink is expected when Mg^{2+} fluxes into shallow marine sediments are also considered along with the Ca^{2+} fluxes (Berg, 2018; Berg et al., 2019).

Moreover, the CH_4 and SO_4^{2-} flux data used in this study from the compilation by Egger et al. (2018) covers a higher number of diffusive methane flux locations from IODP and non-IODP expeditions than those used by Sun and Turchyn (2014) and Bradbury and Turchyn (2019), which were based solely on the ODP/IODP database. Estimates of global methane flux-related processes based exclusively on the ODP/IODP dataset have important limitations. So far, only a handful of ODP/IODP expeditions (e.g., 146, 164, 204, X311, and X341S) were dedicated to methane/gas hydrate research. Further, to the best of our knowledge, ~33 drill sites have shown SMTZ depths below 10 mbsf. The data compilation used here from Egger et al. (2018) includes data from 323 non-IODP sediment cores (coring sites) globally with ~290 sites with an SMTZ depth of <10 mbsf, and the remaining sites have an SMTZ depth of <20 mbsf. Many of the past ODP/IODP sites do not have pore fluid measurements from the top 1 mbsf whereas the data from non-IODP sediment cores focused on diffusive methane flux sites shows ~100 global sites with an SMTZ less than 1 mbsf. Thus, the drilling-based dataset grossly underestimates DIC entering the SMTZs in coastal settings, which in turn constitutes ~65% of global diffusive methane flux. Hence, the combination of IODP and non-IODP sediment core data used here, based on Egger et al (2018), can provide better constraints to the global DIC cycling at diffusive methane flux settings.

Recently, it was postulated that carbonate cap rocks sealing the majority of hydrocarbon systems could be formed via AOM (Caesar et al., 2019). Further, carbonate authigenesis is suggested to be more dominant in slope settings, especially during the periods of widespread anoxia in geologic history, because of the prevalent anaerobic respiration in comparison to margins (Higgins et al., 2009; Schrag et al., 2013a). These studies suggest large unexplored authigenic

carbonate deposits that account for thousands of Gt C sequestration over millions of years. Authigenic carbonates formed below SMTZ in methanogenic zones ($Ca[Fe,Mg,Mn,Ba]CO_3$) with distinctly enriched $\delta^{13}C$ (>5‰) are well known (Rodriguez et al., 2000; Meister et al., 2011; Solomon et al., 2014; Teichert et al., 2014; Pierre et al., 2016; Phillips et al., 2018; Torres et al., 2020). If we assume 20-50% of the DIC from methanogenic zones is sequestered as authigenic carbonate below the SMTZ, net methane-induced authigenic carbonate precipitation at the SMTZ and in the methanogenic depths below would be 2.5-3.6 Tmol yr^{-1}, for a global 3.8 Tmol yr^{-1} of methane production suggested by Egger et al (2018). This range is consistent, at the lower end, with the estimate of 3.3-13.3 Tmol yr^{-1} by Wallmann et al. (2008) and the higher end of 1-4 Tmol yr^{-1} suggested by Torres et al., (2020). These estimates amount to a significant carbon sink that must be accounted for in global carbonate accumulation budgets.

2.5.2 Importance of DIC Outflux to the Water Column: Implication to C-S-Fe dynamics

In present-day settings, 6.5 Tmol yr^{-1} (range 3.2–9.2 Tmol yr^{-1}) of DIC flux toward the seafloor and water column from the SMTZ. In comparison, this amount is ~20% (range: 10-28%) of the ~33 Tmol yr^{-1} of global riverine DIC fluxing to the oceans (Meybeck, 1993; Amiotte Suchet et al., 2003; Aufdenkampe et al., 2011; Li et al., 2017a). Most of our estimated DIC outflux (98%) occurs in continental margin sediments with shallow SMTZ depths of ~13 mbsf (Table 2). Hence, this DIC flux can enter the water column, if it is not involved in diagenesis on the way, and impact ocean chemistry. As oceans continue to absorb rapidly rising atmospheric CO_2, the water column is prone to pH reduction with significant changes to ocean chemistry, associated biogeochemical cycling, and marine ecology (Doney et al., 2009). A pH reduction on the scale of 0.3-0.4 units has been predicted for the end of the 21st century (Feely et al., 2009). Further, under

advective conditions, methane can enter the water column and undergo aerobic methane oxidation, which consumes bottom water oxygen and contributes to acidification through the production of CO_2 (Biastoch et al., 2011; Boetius and Wenzhöfer, 2013; Boudreau et al., 2015).

Alkalinity contribution from the sediments to the water column has important implications for ongoing climate change as they can reduce the ocean acidification effect and even enhance the CO_2 absorption capacity of surface water (Chen and Wang, 1999; Chen, 2002; Thomas et al., 2008; Hu and Cai, 2011; Krumins et al., 2013; Brenner et al., 2016). Hence, evaluating the contribution of DIC outflux to the water column in terms of Total Alkalinity (TA) to DIC ratio is of great importance. Most (86%) of the DIC outflux at diffusive methane flux settings is occurring within SMTZ depths of ≤4 mbsf and bathymetry below 200 m (Tables 2-4). Minimum TA/DIC ratios in the water column 20 m above the seabed under oxygen-limited conditions on continental shelves (100-250m bathymetry) is generally ≤1 (Fig. 2.5). This relationship implies that if the DIC outflux has a TA/DIC ratio of >1, it is contributed as alkalinity to the water column.

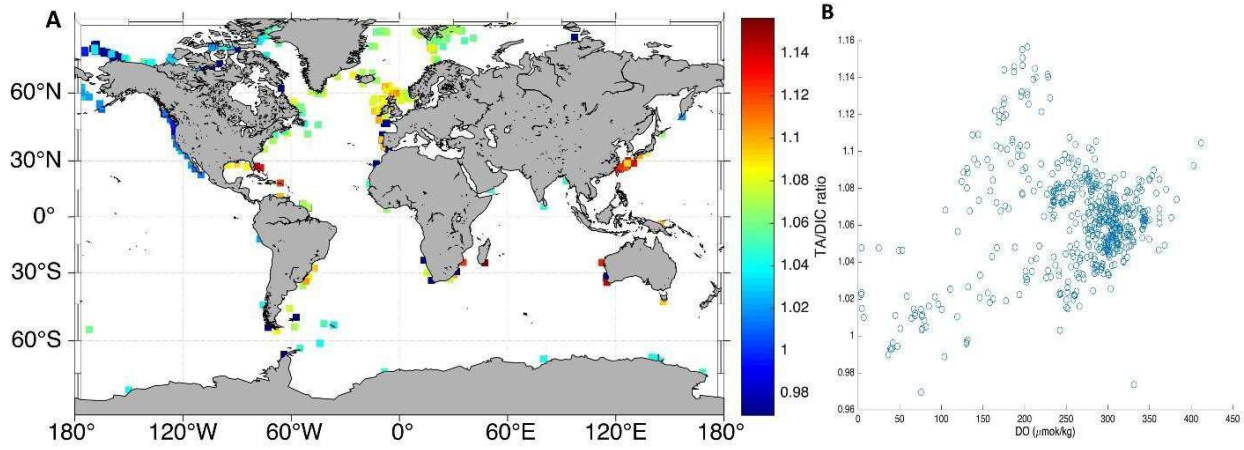

Figure 2.5. Global trend of TA/DIC ratio above the seafloor for oxygen-limited coastal setting.

A) Global distribution of TA/DIC at 100-250m bathymetry within 20m above the seabed. B) Global distribution of TA/DIC at different oxygen concentrations. It can be noticed that the minimum TA/DIC ratio is about 1, under oxygen-limited condition in the shallow bathymetry settings. Data Resource: GLODAPv2 (Key et al., 2015; Lauvset et al., 2016; Olsen et al., 2016)

TA/DIC for the net DIC entering the SMTZ and above in diffusive settings—considering inputs from AOM (TA/DIC ratio=2), OSR (TA/DIC ratio=1), the deep-DIC flux (TA/DIC ratio=1), and the average rates of DIC input parameters in Table 2.1—will produce a value ~1.4

$$\mathrm{TA/DIC}_{(\mathrm{Total-DIC})} = 2 * (\%_{(\mathrm{DIC-AOM})}) + 1 * (\%_{(\mathrm{DIC-OSR})}) + 1 * (\%_{(\mathrm{DIC-deep})}) \quad (8)$$

$$= [(2*.44) + (1*.34) + (1*.22)]$$

$$= 1.44$$

However, the TA/DIC flux ratio from this pool would be determined by the authigenic carbonate precipitation and the balance between sulfide burial and oxidation. As discussed below, sulfide burial relates to the extent of sulfide oxidation and related acid production. Otherwise, assuming the stoichiometry from Wallmann et al. (2008) ($H_2S + 2/5Fe_2O_3 \rightarrow 2/5FeS_2 + 1/5\ FeS + 1/5\ FeO + H_2O$), formation of sulfide minerals at the SMTZ would have no net impact on the TA/DIC ratio of DIC outflux. Carbonate precipitation would consume bicarbonate and reduce the total alkalinity by a factor of two. Thus, while methane derived authigenic carbonate precipitation sequesters a portion of total DIC entering the SMTZ, it will also contribute CO_2 to the water column from shallow sediments by reducing the alkalinity of the DIC outflux. Net TA/DIC of DIC outflux for our average DIC budget (Fig. 2.4) under hypothetical complete sulfide burial can be given by:

$$\mathrm{TA/DIC_{(DIC-0ut)}} = 2 * (\%_{(\mathrm{DIC-AOM})}) + 1 * (\%_{(\mathrm{DIC-OSR})}) + 1 * (\%_{(\mathrm{DIC-deep})}) - 2 * \mathrm{F_{carb}} \quad (9)$$

$$= [(2*.44) + (1*.34) + (1*.22)] - (2*.22)$$

$$=1.04$$

This relationship suggests that even with a hypothetical complete sulfide burial, F_{carb} >20% can cause DIC outflux to contribute CO_2 to the water column. Maximum and Minimum TA/DIC estimates for DIC outflux based on varying parameter ranges used in this model are provided in supplementary table 2.2.

Alkalinity flux would be different when sulfide oxidation occurs. AOM and OSR produce ~5.3 Tmol yr^{-1} sulfide at SMTZ (equivalent to total SO_4^{2-} consumption). Complete or at least significant sulfide burial (e.g., Hensen et al., 2003; Dickens, 2011) could result in a substantial alkalinity contribution from sediments. Oxidation of this entire sulfide pool can, in contrast, produce acid and effectively neutralize the alkalinity flux. It has been suggested that globally 5 to 20% of the sulfide produced in sediments is buried as iron minerals (e.g., FeS, FeS_2) or with organic matter and the remaining is reoxidized to sulfate (Berner, 1982; Jørgensen, 1982; Jørgensen and Nelson, 2004; Zopfi et al., 2004; Wasmund et al., 2017).

Since marine methane flux settings have diagenetic systems different than sites without methane fluxes (e.g., Formolo and Lyons, 2013), the sulfide burial rate at diffusive methane flux settings could differ from the global average (Dickens, 2011). For example, nearly quantitative precipitation of all reduced sulfur by AOM was reported for an iron-rich, non-steady-state setting (Hensen et al., 2003) and more recently, two thirds of sulfide produced via AOM and OSR at the

SMTZ was inferred to undergo burial (Wurgaft et al., 2019). Availability of reactive iron (for sulfide burial) as well as the ratio of burial versus oxidation of the sulfide produced at the SMTZ is thus an important parameter in determining the impact of methane induced carbon cycling at diffusive methane flux settings. In general, a combination of higher sulfide burial with lower carbonate precipitation rates can result in a DIC outflux that contributes alkalinity from sediments, and the opposite can result in DIC contribution as CO_2. We assume the latter to be dominant in the present-day setting—that is, inefficient sulfide burial and high carbonate precipitation—which implies that out fluxing DIC would be a contributor to ongoing ocean acidification. We also emphasize the importance of integrated C-S-Fe approach to understand how these subsurface processes affect water column chemistry. Future studies should quantify the rates of sulfide oxidation and carbonate authigenesis in diverse and globally distributed settings characterized by subsurface methane fluxes to improve on these first-order estimates.

2.6 Conclusion

We estimated DIC cycling in methane charged shallow sediments with global values for diffusive methane and sulfate fluxes into the SMTZ. Our synthesis highlights major diffusive methane-powered carbon fluxes with 8.7 Tmol yr^{-1} DIC (range 6.4–10.2 Tmol yr^{-1}) entering the shallow sediments due to AOM, OSR, and the deep-DIC flux. An estimated 6.5 Tmol yr^{-1} (range 3.2–9.2 Tmol yr^{-1}) of this DIC pool flows toward the water column. This DIC outflux will contribute alkalinity or CO_2 in different proportions to the water column, depending on the rates of authigenic carbonate precipitation and sulfide oxidation. At present, settings with pervasive authigenic carbonate precipitation and sulfide oxidation are contributing CO_2 and thus to ocean acidification. Our estimates also suggest that globally distributed precipitation of authigenic

carbonate minerals at SMTZ characterized by diffusive methane transport sequesters an average of 1.7 Tmol yr^{-1} (range: 0.6–3.6 Tmol yr^{-1}). This estimate is equivalent to ~15% of carbonate accumulation in neritic and in pelagic sediments, respectively. Our study also suggests the need for detailed pore fluid chemical analysis in future expeditions at diffusive settings, which would include quantification of $F_{(DIC\text{-}deep)}$, F_{carb}, and sulfide oxidation rates. Overall, we emphasize that settings characterized by diffusive methane fluxes may play an even larger role in oceanic carbon cycling via conversion of methane carbon to inorganic carbon, which contributes significantly to oceanic DIC pool and carbonate accumulation. These pathways must be included in coastal and geologic carbon models.

2.7 Supplementary Documents

A spreadsheet file with supplementary data can be obtained at https://drive.google.com/file/d/1Hxtcn-UReYNH5dtSlHOL5wEhexji9Qn-/view?usp=sharing.

CHAPTER 3: CARBON-SULFUR COUPLING AND TEMPORAL PATTERNS FOR CHAPOPOTE ASPHALT SEEPS IN THE SOUTHERN GULF OF MEXICO BASED ON CARBONATE GEOCHEMISTRY

For submission to Chemical Geology as Akam, S.A., Coffin, R.B., Bates, S.B., Lyons, T.W., D McGee, Reese, B.K., and C Clarkson; Carbon-Sulfur coupling and temporal patterns for Chapopote asphalt seeps in the southern Gulf of Mexico based on carbonate geochemistry

3.1 Abstract

Offshore hydrocarbon accumulations in the Gulf of Mexico (GoM) are often accompanied by natural seepage of oil and gas from subsurface reservoirs to shallow sediment and water column. This study investigated the carbon-sulfur (C-S) coupling associated with authigenic carbonates recovered from a crude oil seepage site in southern GoM (Chapopote asphalt volcano, Bay of Campeche) using stable C, O, and S isotopes and compared the results with multiple seep sites in the northern GoM where methane seepage is dominant (along with non-methane hydrocarbons). $\delta^{13}C$ and $\delta^{18}O$ from authigenic carbonates at Chapopote indicated a mixed contribution of methane and non-methane hydrocarbon to the dissolved inorganic carbon (DIC) pool for carbonate precipitation, consistent with previous results. A comparison of $\delta^{13}C_{carbonate}$ vs. $\delta^{34}S_{pyrite}$ from the carbonate samples showed noticeable differences at the Chapopote seep site (average $\delta^{13}C_{carbonate}$ -25‰ VDPB, $\delta^{34}S_{pyrite}$ -28‰ VCDT) relative to the methane seep-dominated samples from the northern GoM (average $\delta^{13}C_{carbonate}$ < -40‰ VDPB, $\delta^{34}S_{CRS}$ >0‰ VCDT). Our results point towards distinguishable variation in sulfate reduction coupled with oxidation of methane and non-methane hydrocarbon (crude oil), which produces the DIC pool. These results provide an important proxy for these distinctions in sedimentary records. U-Th age dating of Chapopote

seep carbonate samples yielded ages of 13.5 ka – 4.5 ka before present (BP), suggesting that Chapopote Asphalt seepage has been ongoing for thousands of years. The results are also consistent with previous studies from the northern GoM, supportive to the case that seeps along GoM slopes were very active during the last deglaciation.

3.2 Introduction

The tectonic and depositional conditions in the Gulf of Mexico (GoM) provide an ideal setting for the formation of oil and gas as well as its upward migration from subsurface reservoirs to the seafloor and water column (Sassen et al., 1998). Natural hydrocarbon seeps are suggested to account for ~47% of all crude oil entering the marine environment (Kvenvolden and Cooper, 2003), with an estimated 160 to 690 thousand barrels of oil entering the Gulf of Mexico annually (Kvenvolden and Harbaugh, 1983; Mitchell et al., 1999; National Research Council, 2003; MacDonald et al., 2015). These seepage sites have a significant impact on geology and biology of the seabed facilitated through complex microbially mediated biogeochemical processes (Judd and Hovland, 2009; Hovland et al., 2012; Coffin et al., 2015).

GoM seeps are characterized by large quantities of precipitates of authigenic minerals formed by chemosymbiotic microbial communities; resulting from biogeochemical turnover and the interaction between downward-diffusing seawater and upward advection of hydrocarbon-rich pore fluids (Roberts and Aharon, 1994; Sassen et al., 2004; Roberts and Feng, 2013; Suess, 2018). Furthermore, chemosymbiotic benthic fauna are supported by the microbially driven anaerobic oxidation of methane (AOM), which involves a microbial consortium of anaerobic methanotrophic archaea (ANME) and sulfate-reducing bacteria (SRB) that anaerobically

oxidizes methane while reducing sulfate at the sulfate-methane transition zone (SMTZ) with the following net reaction (Boetius et al., 2000):

$$CH_4 + SO_4^{2-} \rightarrow HCO_3^- + HS^- + H_2O. \qquad (1)$$

Authigenic carbonates are a common diagenetic mineral formed at methane (and other hydrocarbon) seepage sites (Aloisi et al., 2002). They are formed primarily through bicarbonate production via AOM, which results in supersaturation of carbonate ions in porewater at the SMTZ and induces carbonate precipitation (Baker and Burns, 1985):

$$2HCO_3^- + Ca^{2+} \rightarrow CaCO_3 + CO_2 + H_2O. \qquad (2)$$

Carbonate authigenesis at seep sites is a substantial carbon sequestration process and provides an excellent geologic recorder of carbon-sulfur (C-S) coupling at such sites. At present-day settings, for example, authigenic carbonate precipitation is considered to be a significant component of oceanic carbon sink (Wallmann et al., 2008; Torres et al., 2020), accounting for 10-15% carbonate accumulation in pelagic and neritic sediments, respectively (Sun and Turchyn, 2014; Akam et al., 2020). Studies of organic biomarkers in sediments from the GoM (Pancost et al., 2005) revealed disparities between measured rates of sulfate reduction versus methane oxidation that suggest other carbon sources in addition to methane (Joye et al., 2004; Bowles et al., 2011). Further, carbon isotope data from authigenic carbonates (Formolo et al., 2004) also suggest that AOM may not be the only process responsible for an increase in carbonate alkalinity at many seep sites. Rather, it seems likely that the oxidation of non-methane hydrocarbons coupled with sulfate reduction (AONM) (e.g., hexadecane, Eq. 3, propane, Eq. 4, Widdel and Rabus, 2001; Kniemeyer et al., 2007) provides a significant source of metabolic energy and bicarbonate

production at these locations (Formolo et al., 2004; Naehr et al., 2009; Mansour and Sassen, 2011; Smrzka et al., 2019; Sun et al., 2020).

$$C_{16}H_{34}+12.25SO_4^{2-} \rightarrow 16HCO_3^-+12.25HS^-+3.75H^++H_2O. \quad (3)$$

$$4C_3H_8 + 5SO_4^{2-} \rightarrow 6HCO_3^- + 5HS^- + 4\,H_2O + H^+. \quad (4)$$

Even though seeps dominated by heavy hydrocarbons (like crude oil) are less commonly than seeps dominated by light hydrocarbons (like methane), their occurrences are well documented globally (e.g., Hornafius et al., 1999; Noble et al., 2009; Valentine et al., 2010; Jones et al., 2014; Körber et al., 2014; Jiang et al., 2018) and are suggested to have an important effect on microbial diversity and associated biogeochemical cycling (Joye et al., 2004; Orcutt et al., 2010). Oil seeps are likely to persist over geologic time (Wilson et al., 1974). Characterizing and comparing the impacts of crude oil and methane seeps in present-day settings will enable better identification of these processes in the sediment record and their biogeochemical implications over geologic time (Peckmann and Thiel, 2004; Campbell, 2006; Bristow and Grotzinger, 2013). Furthermore, the hydrocarbon seeps are highly variable in response to changes in oceanographic and tectonic conditions (e.g., Aharon et al., 1997; Bayon et al., 2009; Berndt et al., 2014), and our current understanding of their temporal variations is weak. Such uncertainty also leaves a critical gap in our ability to assess the potential response of these seep systems during future climate change.

In this study, we examined authigenic carbonates using sulfur isotopes ($\delta^{34}S$) of pyrite and the Carbonate-Associated Sulfate (CAS) to unravel the details of sulfate reduction coupled with AOM and AONM and their relationships with the DIC pool. We focused our attention on the authigenic carbonates recovered from asphalt seep sites in Chapopote Knolls of Campeche Bay, which were suggested to be dominantly derived from crude oil oxidation. The study site is

characterized by extensive and repetitive asphalt flows, oil and gas seeps, and seafloor gas hydrate deposits, along with seep-associated chemosynthetic communities and authigenic carbonate deposits (MacDonald et al., 2004). These discoveries added a new dimension to the inventory of seafloor hydrocarbon seep processes (Bohrmann, 2013; Marcon et al., 2018). Given this importance, we compared the results from Chapopote seep carbonates with multiple seep sites from the northern Gulf of Mexico. As part of this study, we produced U-Th dates on the Chapopote seep carbonate to identify the timing and mechanisms of formation.

3.3 Study Area

The GoM basin is characterized by a large hydrocarbon reservoir overlying salt deposits, which are sealed by continental margin sediments. Differential sedimentary loading and density contrast with the overburden induce salt diapirism and consequent fault generation, paving way for hydrocarbon leakages toward seafloor (Brooks et al., 1990; Sassen et al., 1993; Roberts, 2001; Fisher et al., 2007; Kennicutt, 2017). The southern Gulf Coast region of Mexico is a relatively unexplored area with numerous hydrocarbon seeps. The southern GoM is characterized by two distinct active salt provinces: the Campeche and Sigbee Knolls, separated from the Mississippi-Texas-Louisiana salt province in the northern GoM by the Sigsbee Abyssal Plain (Bryant et al., 1991). These knolls consist of a series of domes and ridges formed by movement of the Jurassic salt deposits underlying the ~5-7 km thick continental margin sediments (Salvador, 1991; Ding et al., 2008). Extensive hydrocarbon transport from sediments to the sea-surface in the region is observable via satellite images as sea surface oil slicks (MacDonald et al., 2004; MacDonald et al., 2015; Suresh, 2015; Römer et al., 2019). This study employs carbonate samples collected at a water depth of 2902 m from Chapopote Knoll (21°54′N/93°26′W) located

on the northern slope of the Campeche Knolls province during the R/V Sonne SO174/2 (2003) and R/V M67/2 (2006). Campeche knolls province consists of a cluster of elongated knolls and ridges formed via salt tectonics (Garrison and Martin, 1973). The knolls have relief ranging from 450 to 800 m above the seafloor with 3000-3500 m water column depth (Ding et al., 2008).

Extensive and repetitive lava-like asphalt flows in Chapopote emanate from a central crater-like depression, generating extensive surface deposits of solidified asphalt with distinct surface textures—leading to the term 'asphalt volcano' (MacDonald et al., 2004). Seismic studies revealed that asphalt seeps derive from a large reservoir buried at shallow depths linked to a deep heavy petroleum source (Ding et al., 2008; Ding et al., 2010). Asphalt flow is accompanied by oil and gas seeps (Bohrmann, 2008) and seafloor gas hydrate deposits (Klapp et al., 2010), along with seep-associated chemosymbiotic communities and authigenic carbonate deposits (Bohrmann and Schenck, 2004; MacDonald et al., 2004; Naehr et al., 2009; Brüning et al., 2010; Sahling et al., 2016). Seepage systems support prolific microbial activity involving crude oil degradation and sulfate reduction (Schubotz et al., 2011a; Schubotz et al., 2011b) in otherwise deep pelagic sediments with low organic carbon input from surface waters. Surface sediments from Chapopote showed local high in total organic carbon content (0.9%) and a very high carbon-nitrogen atomic ratio (C/N_a) than the surrounding abyssal sediments (50 vs. 7), suggestive of highly localized hydrocarbon input (Escobar-Briones and García-Villalobos, 2009). These features of Chapopote added to the list of seafloor hydrocarbon seep processes (Bohrmann, 2013; Marcon et al., 2018). Authigenic carbonates collected from Campeche seeps allow us to investigate the role of crude oil oxidation during carbonate authigenesis (Naehr et al., 2009; Smrzka et al., 2016).

For comparison, we studied samples from relatively well-studied sites of northern continental slope of GoM Green Canyon Block 415 (GC 415, 27°33.48N/90°58.86W, water depths 950m; 27°32.61N/90°59.54W, water depth 1045m) and Bush Hill (GC 185, 27°46.97N/91°30.47W, water depths 547m). These sites were also among the expedition targets of R/V Sonne cruise 174. Similar to Campeche Knolls, these sites host widespread hydrocarbon seeps due to fractures in sedimentary strata induced by salt tectonics (Roberts and Aharon, 1994; Sassen et al., 2004; Feng et al., 2009). Preliminary analysis revealed a relatively higher contribution of methane to the DIC pool in many northern GoM seep carbonates compared to Chapopote seep carbonates (Akam et al., 2019). Further, we used published literature reports of C-S isotope values for seep carbonates collected from multiple sites in the northern GoM (Atwater Valley - AT340, Green Canyon – GC 180, GC 232, GC 234, GC 852 Garden Banks – GB 260, GB 382, GB 427, GB 647, and Mississippi Canyon MC 118, Fig. 3.1) (Formolo and Lyons, 2013; Feng et al., 2016; Sun et al., 2020).

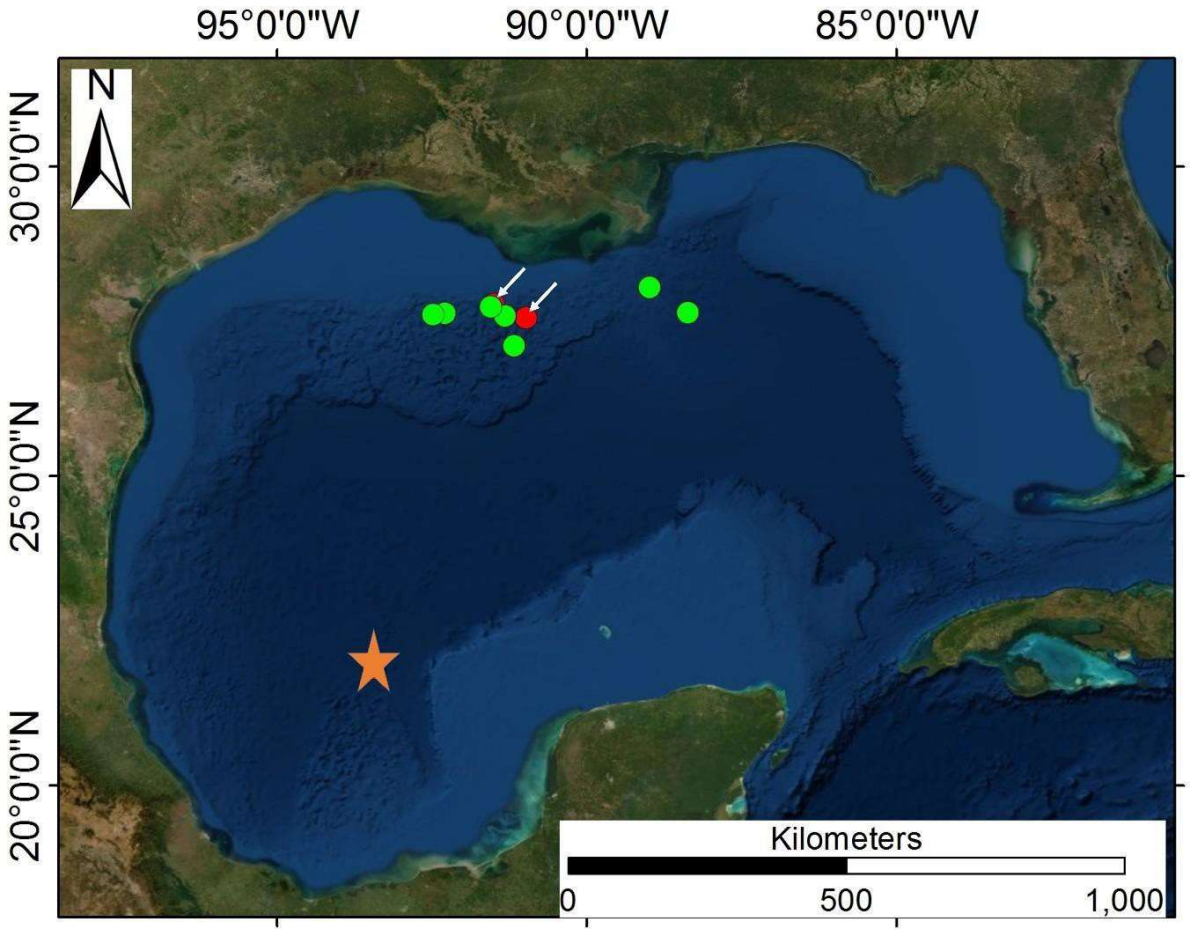

Figure 3.1: Study Area. The orange star represents the primary study site, Chapopote Knolls, with significant asphalt seeps. Red dots with an arrow indicate the locations (GC 415 and GC 185) for carbonates samples from northern GoM analyzed in this study. The green dots indicate locations from published literature where we used to compare the C-S isotope results.

3.4 Methods

Fifteen carbonate crusts were analyzed. These materials were split into multiple subsamples based on observations from hand specimens. The samples were collected via Video Guided Grab Sampling. Carbonate contents of the samples were determined by acid-leach weight-loss

procedure and are reported as weight percent $CaCO_3$. Bulk mineralogy was determined by X-ray diffraction (XRD) according to Naehr et al. (2000) at TAMUCC. One gram of crushed sample was mixed with 0.25 gm internal corundum standard (α-Al_2O_3) to prepare randomly oriented powdered slides. Scans were run from 20°- 60° using a Rigaku Ultima III X-ray diffractometer at TAMUCC at a scan speed of 0.01° 2θ/s. Relative proportion of magnesium content in carbonate was determined using the shift d spacing of the reflection (104) (Greinert et al., 2001). Calcite with $MgCO_3$ <4% is referred to as low-magnesium calcite (LMC), and 4-30% were considered high magnesium calcite (HMC) (Flügel, 2004). Polished thin sections of 50 x 75 mm size partially stained with Alizarin Red and Potassium Ferrocyanide were used for textural and compositional analysis using standard optical microscopy. Stable isotopes of carbon and oxygen from authigenic carbonates were determined using a Thermo Scientific Gasbench Device coupled to a Delta V Advantage Isotope Ratio Mass Spectrometer (IRMS) via a ConFlo IV inlet at the University of California, Riverside. Sample powders were microdrilled from polished slab surfaces. Carbon dioxide for $\delta^{13}C_{carb}$ and $\delta^{18}O_{carb}$ analysis was produced by reaction of samples with 103% orthophosphoric acid. Precision of $\delta^{13}C_{carb}$ and $\delta^{18}O_{carb}$ measurements is 0.2‰. The $\delta^{13}C_{carb}$ and $\delta^{18}O_{carb}$ are reported with reference to Vienna Pee Dee Belemnite (VPDB)standard.

Chromium reducible sulfur (CRS) was extracted using a modified method of Canfield et al (1986). Homogenized 5 g samples were reacted with 10 ml ethanol, 25 ml of 6M HCl, and 25 ml of a chromium chloride (1 M $CrCl_3.6H_20$ in 0.5 M HCl) solution. CRS was converted to H_2S gas and carried via a N_2 carrier to an $AgNO_3$-NH_4OH trap where it was quantitatively converted to silver sulfide (Ag_2S). Ag_2S precipitates were recovered on polycarbonate membrane filters using vacuum filtration before being dried and weighed to determine the CRS weight percent.

Carbonate Associated Sulfate (CAS) was extracted using a technique modified from Lyons et al (2004). Briefly, 1-2 g of micro-drilled sample were treated with a 10% NaCl rinse to remove any soluble sulfate minerals. Next, metastable sulfides and organically bound sulfur (e.g., ester bound sulfates) were removed with a 5% sodium hypochlorite rinse. Samples were then rinsed two times with DI H_2O before being dissolved with 4 N HCl with 5% (by weight) $SnCl_2$ (to inhibit pyrite oxidation). Resulting samples were then vacuum filtered to remove insoluble residues. Twenty five mL of 250g/L $BaCl_2$ solution (250 g/L) were then added to each sample to yield insoluble $BaSO_4$. $BaSO_4$ precipitates were filtered and dried prior to analysis for $\delta^{34}S$ values. Sample CAS concentrations were quantified by analysis of S yields during $\delta^{34}S$ measurement. $\delta^{34}S_{CRS}$ and $\delta^{34}S_{CAS}$ values were measured using a Thermo Scientific Delta V Plus IRMS connected to a Costech 4010 ECS via a ConFlo III interface at the University of California, Riverside. Standard deviation for $\delta^{34}S$ analysis was ± 0.23‰ (VCDT).

Thirty samples were initially screened for $^{238}U/^{232}Th$ ratios to determine whether they could be dated by U/Th methods. One milligram of sample was dissolved in 1.5 mL 0.5 M nitric acid, and U, Th, and Ca were measured by quadrupole ICP-MS at the MIT Center for Environmental Health Sciences to determine U concentrations and U/Th ratios. A gravimetric U/Th/Ca solution with similar abundances to the samples was used to calibrate the instrument, and a standard was run after every 15-20 samples to monitor instrument drift. Samples with $^{238}U/^{232}Th$ mass ratios greater than 2 were selected for U/Th dating analysis. Radioactive U/Th isotope dating of the carbonate crusts was performed Nu Plasma II-ES MC-ICP-MS at the MIT Department of Earth, Atmospheric and Planetary Sciences. Micro drilled carbonate powder samples ranging in weight from 10 to 70 mg were used. Samples were dissolved in 8 N HNO_3 and spiked with

a $^{229}Th/^{233}U/^{236}U$ tracer. Uranium and Th were separated following procedures by Edwards et al (1987) and Bayon et al., (2009). Raw data were corrected with an initial $^{230}Th/^{232}Th$ atomic ratio of $4.4 \pm 2.2 \times 10^{-6}$ assuming a typical upper continental crust value for $^{238}U/^{232}Th$, and the errors were arbitrarily assumed to be 50%. This initial $^{230}Th/^{232}Th$ ratio is consistent with values used in some prior studies of seep carbonates from the GoM and other areas (Feng et al., 2010; Chen et al., 2019), but we note that Aharon et al. (1997) used initial $^{230}Th/^{232}Th$ ratios ranging from 8-22 $\times 10^{-6}$. Use of a higher initial $^{230}Th/^{232}Th$ ratio would reduce in younger corrected ages; we note the need for future work to better constrain this ratio at our site. $\delta^{234}U_{initial}$ was calculated based on ^{230}Th age (T), that is, $\delta^{234}U_{initial} = \delta^{234}U_{measured} X e^{l234*T}$, and T is the corrected age. Decay constants for ^{230}Th and ^{234}U are from Cheng et al. (2013); the decay constant for ^{238}U is 1.55125×10^{-10} yr^{-1} (Jaffey et al., 1971).

3.5 Results

Petrographic observations of carbonate macro- and microfacies from Chapopote seep carbonates were previously reported by Canet et al., (2006) and Naehr et al (2009). The average carbonate content of Chapopote samples were 86% (Table 1). Aragonite was the primary composition for Chapopote seep carbonates. The siliciclastic components consisted of detrital quartz, feldspar, and clay minerals. Petrographic observations of the samples showed wide-ranging textural variations (Figure 2). Aragonite cement types included acicular, botryoidal, peloidal, and micritic cement. Microsparitic aragonite was the volumetrically dominant phase, commonly occurring as peloidal and clotted textures. Microcrystalline aragonites were yellow and gray in appearance, whereas acicular and fibrous aragonite cements were pink to clear. Aragonite crystals were often coated with crude oil residues. Coarse fractions consisted of intraclasts and bioclasts.

Macroscopically, the samples consisted of irregularly shaped large intraclasts and bioclasts that were held together by a microsparitic to sparitic aragonite cement. Intraclasts were primarily composed of mud- and siltstones. Bivalve and foraminiferal shells were the dominant bioclasts. Widespread primary pore spaces were present resulting from incomplete filling of voids between clast and microsparitic or fibrous cements (Fig. 3.2B). Secondary pores, potentially caused by carbonate dissolution and in-situ brecciation, were also observed (Fig. 3.2A). Framboidal pyrite was pervasive (Fig. 3.2F).

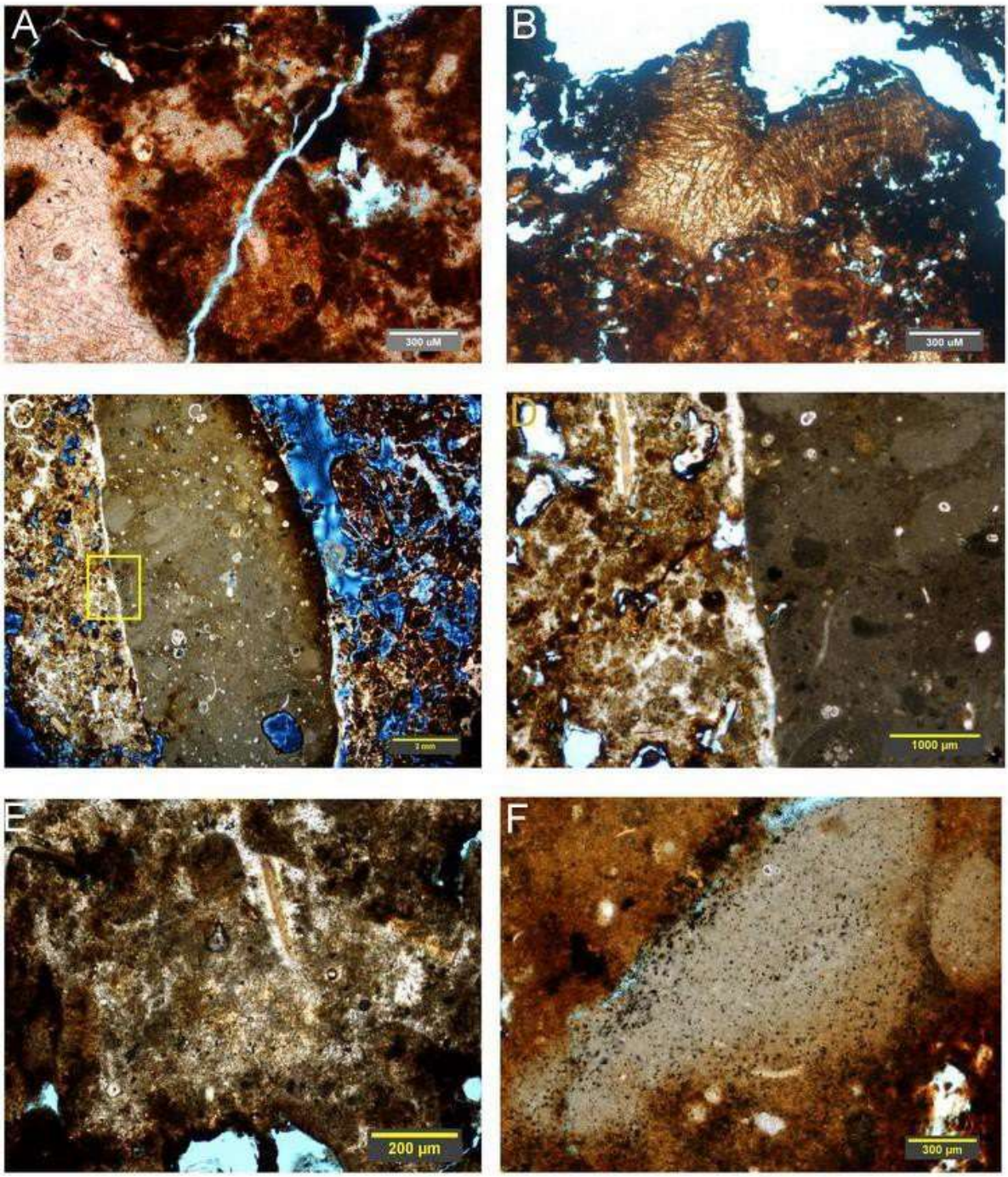
A
300 uM
B
300 uM
C
3 mm
D
1000 µm
E
200 µm
F
300 µm

Figure 3.2: Petrographic observations on Chapopote Seep Carbonates. A) Multiple cement types. A fracture event postdating cement formation can be seen. B) Acicular aragonite cement forming radial-fibrous fabric. C) Large clast cemented by microcrystalline aragonite. D) Zoomed view of the box marked in 2C. Microsparitic filling of spaces between clasts and cement lining the clasts is incomplete, leaving significant pore space. Aragonite cement fills pore spaces, creating a peloidal texture in the left half of the picture. E) Peloidal texture indicative of microbial activity and early diagenetic cementation. F) Abundant pyrite formation is indicative of extensive sulfate reduction. Clots of residual hydrocarbons (dark brown) can be seen around the pore spaces adjacent to cemented structures as well as coating on the aragonite cements. All images are in plane-polarized light, and blue color indicates pore spaces. These observations are indicative of authigenic carbonate formation in a dynamic hydrocarbon seep setting.

Observed values of $\delta^{13}C_{carbonate,}$ $\delta^{18}O_{carbonate}$, and $\delta^{34}S_{pyrite}$ from studied samples are shown in table 3.1. $\delta^{13}C_{carbonate}$ and $\delta^{18}O_{carbonate}$ from Chapopote samples averaged -25‰ and +4.5‰, respectively. Samples from the northern GoM, GC 185 and GC 415, gave average $\delta^{13}C_{carbonate}$ values -19.8‰ and 4.4‰ and $\delta^{18}O_{carbonate}$ -34.6‰ and +4.8‰, respectively (Table 3.1). $\delta^{34}S_{pyrite}$ values from Chapopote carbonates were noticeably depleted, ranging from -14‰ to -38.7‰, with an average value -27.4‰. Samples from GC 415 and GC 185 averaged -4.8‰ and +18.9‰, respectively. CAS yield was limited in the samples, exacerbated by the low sample sizes used. $\delta^{34}S_{CAS}$ values from Chapopote averaged -6.1‰. $\delta^{34}S_{CAS}$ for background (non-seep site) samples averaged 19.7‰ (close to the global seawater value) The average for northern GoM samples was +30‰ (Supp. Data file).

Table 3.1: $\delta^{13}C_{carbonate,}$ $\delta^{18}O_{carbonate}$, $\delta^{34}S_{pyrite}$, and pyrite content from studied samples. An extended database, which includes a compilation of published literature data from multiple seep sites in GoM, is provided in the supplementary datasheet.

Location	Water depth (m)	Sample ID	$\delta^{13}C_{carbonate}$ (VDPB)	$\delta^{18}O_{carbonate}$ (VDPB)	$\delta^{34}S_{CRS}$ (VCDT)	Pyrite Wt %	Carbonate Wt %
Chapopote Knoll (21°54.00, 93°26.40)	2902	22A	-25.0	4.2	-20.1	0.014%	96%
		22B	-24.8	3.8	-26.2	0.047%	90%
		22C	-24.5	4.6	-19	0.060%	97%
		22D	-24	4.4	-18.8	0.002%	91%
		23A	-27.6	5.7	-28	0.124%	84%
		23B	-26.2	3.8	-23.7	0.175%	88%
		23C	-26.9	3.7	-22.0	0.000%	70%
		24B	-25.0	5.9	-27.3	0.356%	87%
		24C	-26.3	4.4	-28.5	0.172%	85%
		24D-SHELL	-4.1	3.3	-27.5	0.003%	70%
		25A	-24.2	4.1	-27.6	0.214%	87%
		25B	-25.7	5.1	-24.4	0.530%	70%
		26A	-26.5	4.3	-21.7	0.081%	99%
		26B	-25.0	5.3	-21.6	0.256%	81%
		26C	-25.6	4.3	-28.5	0.159%	83%
		27A	-26.0	4.0	-34.8	0.078%	87%
		27B	-28.5	4.5	-33.4	0.378%	75%
		27C	-23.3	4.3	-33.4	0.138%	87%
		28A	-26.3	4.0	-31.3	0.055%	64%
		28B	-25.8	4.7	-38.4	0.023%	89%
		28C	-25.2	4.4	-26.5	0.023%	71%
		28D-SHELL	-23.0	4.3	-33.1	0.069%	96%
		29B	-25	4.6	-27.4	0.209%	96%
		29C	-27.4	4.9	-38.7	0.480%	99%
		29F	-26.9	3.9	-34.9	0.007%	91%
		BX3-2	-26.8	5.6	-27.6	0.472%	88%
		BX3-3	-29.4	5.1	-14.1	1.041%	85%
GC 185 (27°46.97, 91°30.47)	547	N10A1	-20.9	5.2	-18.5	0.232%	80%
		N10A2	-21.4	4.6	-18.5	-0.634%	84%
		N10B1	-16.3	4.2	-24.2	0.104%	71%
		N10B2	-20.5	3.8	-14.5	0.441%	54%
GC 415 (27°32.6, 90°59.54)	1045	N1-1	-32.0	5.8	-7.4	0.174%	69%
		N1-2	-27.4	5.0	-4.7	0.444%	83%
		N2-1	-31.3	5.6	-11.3	0.484%	74%
		N2-2	-39.3	4.9	-10.9	0.736%	74%
		N3-1	-24.3	4.7	2.3	0.070%	68%
		N3-2	-21.3	5.0	3.4	0.096%	62%

GC 415 (27°33.48, 90°58.86)	951	T-1	-35.14	5.09	N/A	N/A	90%
		T-2	-34.30	5.05	N/A	N/A	85%
		T-3	-37.78	5.40	N/A	N/A	91%
		T-4	-36.73	3.70	N/A	N/A	89%
		T-5	-32.97	4.38	N/A	N/A	92%
		T-6	-34.12	4.28	N/A	N/A	96%
		T-7	-34.29	3.90	N/A	N/A	91%
		T-8	-37.60	3.94	N/A	N/A	88%
		T-9	-42.3	4.9	N/A	N/A	91%
		T-10	-42.8	5.0	N/A	N/A	92%
		T-11	-40.6	4.9	N/A	N/A	86%
		T-12	-41.0	4.9	N/A	N/A	86%
		T-13	-33.1	4.9	N/A	N/A	86%

Of the 30 samples screened for U-Th dating, nine Chapopote samples had $^{238}U/^{232}Th$ greater than 2. These samples were analyzed for U/Th isotopic composition and dates (Table 2). The ^{238}U concentrations for these selected samples ranged from 5230 to 13200 ppb, and ^{232}Th concentrations ranged from 482 to 1220 ppb. $\delta^{234}U$ initial averaged 143‰; when corrected for detrital U (based on an initial $^{230}Th/^{232}Th$ atomic ratio of $4.4 \pm 2.2 \times 10^{-6}$ and assuming that $^{230}Th/^{238}U$ and $^{234}U/^{238}U$ activity ratios in detrital matter are 1 ± 0.1), the initial $\delta^{234}U$ of the carbonate fraction of the Chapopote samples is 147 ± 1‰, consistent with the average seawater composition of 146.8 ± 0.1‰ (Andersen et al., 2010). U-Th dates ranged from 4.5 ± 1.0 Kyr to 13.5 ± 2.1 Kyr (BP). $^{230}Th/^{232}Th$ atomic ratios were between 11.4×10^{-6} and 19.0×10^{-6}, making corrections for initial ^{230}Th large, which means that the uncertainties in the corrected ages are dominated by the uncertainty in the initial ^{230}Th correction.

Table 3.2: U-Th data from Chapopote Samples

Sample ID	$^{238}U \pm (2\sigma)$	$^{232}Th \pm (2\sigma)$	$^{230}Th/^{232}Th \pm (2\sigma)$	$\delta^{234}U \pm (2\sigma)$	$^{230}Th/^{238}U \pm (2\sigma)$	^{230}Th Age(ka BP) $\pm (2\sigma)$	^{230}Th Age(ka BP) $\pm (2\sigma)$	$\delta^{234}U$initial$\pm (2\sigma)$
	(ppb)	(ppb)	(atomic $\times 10^{-6}$)	(measured)	(activity)	(uncorrected)	(corrected)	(corrected)
TVG_6-21a	13150±260	1183 ± 24	19.0 ± 0.3	143 ± 2	0.1074±0.0017	10788 ±0.19	8.32 ± 1.2	146 ± 2
TVG_6-23a	6673 ± 133	1060 ± 21	13.4 ± 0.3	138 ± 0.3	0.1340±0.0029	13750 ±0.32	9.40 ± 2.2	141 ± 3
TVG_6-25a	7253 ± 145	1104 ± 22	11.6 ± 0.3	138 ± 0.3	0.1109±0.0028	11260 ±0.31	7.10 ± 2.1	140 ± 2
TVG_6-26a	7799 ± 156	1163 ± 23	18.0 ± 0.3	139 ± 0.3	0.1691±0.0028	17670 ±0.33	13.50 ± 2.1	143 ± 2
TVG_6-26c	5231 ± 105	1018 ± 20	13.7 ± 0.3	137 ± 0.3	0.1673±0.0036	17460 ±0.41	12.10 ± 2.8	141 ± 3
TVG_6-27a	7736 ± 155	1074 ± 22	14.1 ± 0.3	142 ± 0.3	0.1235±0.0026	12630 ±0.29	8.79 ± 1.9	144 ± 2
TVG_6-27c	6824 ± 482	482 ± 10	14.8 ± 0.3	143 ± 0.3	0.0659±0.0014	6507 ±0.15	4.55 ± 0.96	144 ± 2
TVG_6-28a	5990 ± 120	993 ± 20	15.4 ± 0.3	140 ± 0.3	0.1612±0.0031	16700 ±0.35	12.10 ± 2.3	144 ± 2
TVG_6-29d	10160±200	1221 ± 24	11.4 ± 0.3	142 ± 0.3	0.0864±0.0022	8630 ±0.23	5.32 ± 1.67	144 ± 2

3.6 Discussion

Petrographic observations indicate carbonate authigenesis in a dynamic seep setting with episodic fluid flow, microbial activity, and associated C-S-Fe interactions (Figs. 2 and 3). Peloidal micrite exhibiting a clotted fabric (Fig. 3.2E) has widely been reported from seep carbonates and is indicative of early-stage cementation resulting from microbial interactions (Peckmann et al., 2002; Flügel, 2004). Microbially oxidized crude oil coating aragonite crystals and pore spaces indicates a close association between carbonate authigenesis and hydrocarbon seepage from the subsurface. Abundant authigenic pyrite in the carbonate matrix (Fig. 3.2F) indicates sulfate reduction coupled to anaerobic hydrocarbon oxidation, which increases carbonate alkalinity while generating sulfide, the latter forming pyrite through reaction with reactive Fe phases (Peckmann et al., 2001; Peckmann and Thiel, 2004).

Indications for multiple seepage episodes include distinctly younger carbonate cementation around pore spaces and fractures through intraclasts (Fig. 3.3). We propose that the fracture filling carbonate cementation could be indicative of multiple seepage events as well as autoendolithic activity. It has been shown that authigenic carbonates serve as a unique microbial habitat for endolithic activities capable of continued anerobic hydrocarbon oxidation and carbonate aggregation even after their formation (Marlow et al., 2014; Marlow et al., 2015; Yanagawa et al., 2019). Pervasive fractures potentially caused by *in situ* brecciation, and subsequently filled by aragonitic seams, were commonly observed together with hydrocarbon inclusions, and may indicate episodic seepage and subsequent carbonate precipitation events via anaerobic hydrocarbon oxidation (Fig 3A-E). These signatures could thus be indicative of autoendolithic structures reflecting self-entombment of hydrocarbon-oxidizing microbes

(Marlow et al., 2015, Fig. 3F). In addition, Campeche seep carbonates were shown to entrap methane and other hydrocarbons (C_2 up to C_6) in the crystal spaces of carbonate minerals (Blumenberg et al., 2018). The presence of trapped gases may trigger anaerobic hydrocarbon oxidation coupled with sulfate reduction (considering the aragonite crusts are formed near the sediment-water interface with high porosity, allowing sulfate percolation), resulting in carbonate authigenesis and potentially autoendolithic activity.

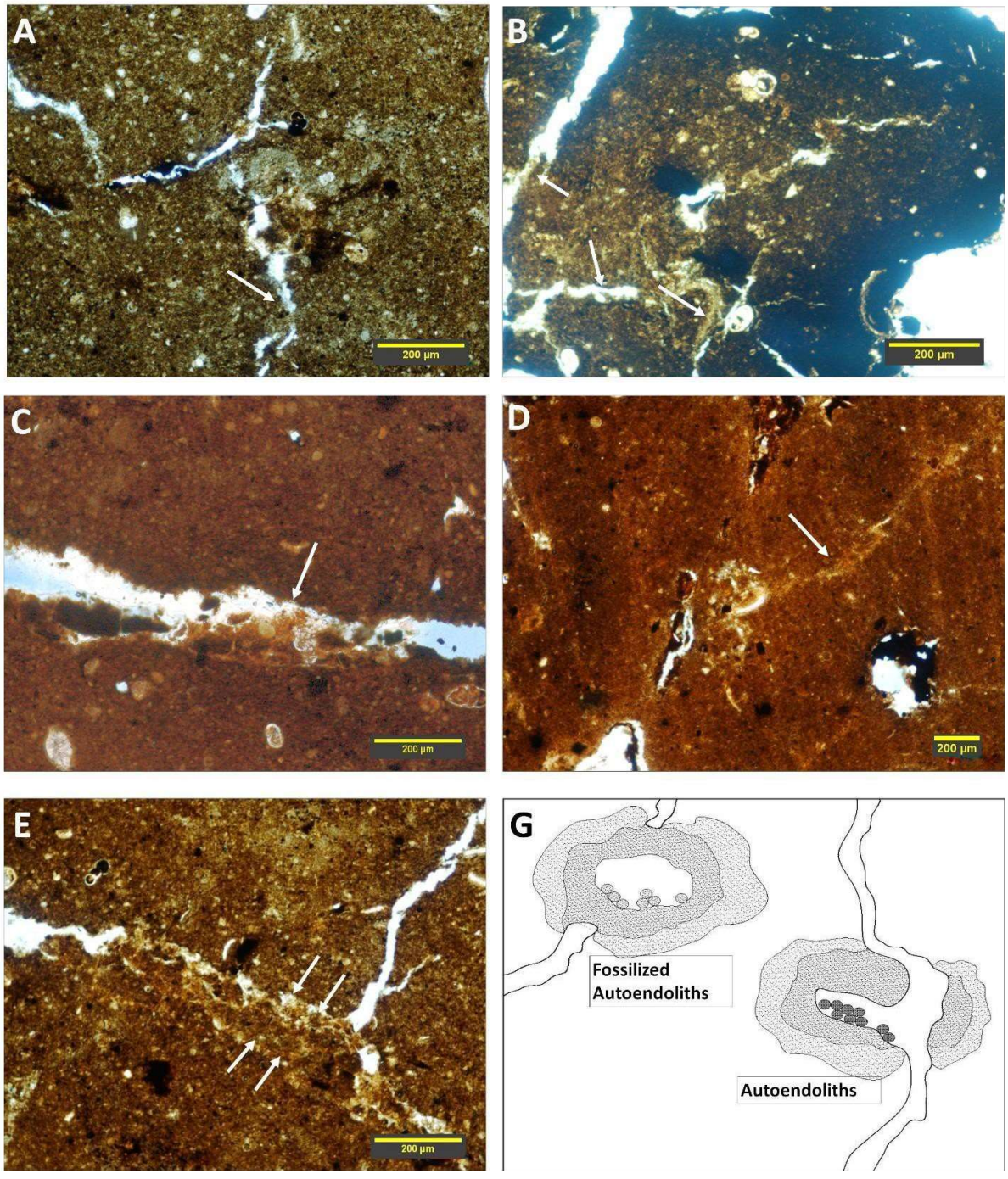
A
200 µm
B
200 µm
C
200 µm
D
200 µm
E
200 µm
G
Fossilized
Autoendoliths
Autoendoliths

Figure 3.3: Indicators for pervasive autoendolithic activity at Chapopote Seeps (A-E). Arrows mark sites of potential mineralization induced by autoendolithic activity. Figure F is a schematic representation for relative locations and microbe-rock interactions of endolithic organisms adapted from Marlow et al., 2015. Circles represents endoliths and gray shading represents autoendolithic carbonate precipitation.

Based on the average value of -25‰ of $\delta^{13}C_{Carbonate}$, a predominantly (up to 90%) crude oil source for carbon was suggested for Chapopote seep carbonates when we consider methane ($\delta^{13}C$ = -55‰), crude oil ($\delta^{13}C$ = -27‰), organic matter ($\delta^{13}C$ = -20‰), and DIC from seawater ($\delta^{13}C$ = +1‰) as end-members (Naehr et al., 2009). Measured $\delta^{18}O_{Carbonate}$ values ranged from 3.3 to 5.9 ‰, averaging 4.5‰. This was higher than the calculated $\delta^{18}O_{Carbonate}$ value (3.02‰) based on the measured bottom water temperature (4.02°C) and porefluid $\delta^{18}O$ values (0.09‰) of background samples, according to Kim et al. (2007) (Supp. data file). Porewater $\delta^{18}O$ enrichment sourced from shallow gas hydrate dissociation could explain this difference (Davidson et al., 1983; Naehr et al., 2009). These observations agree with Formolo et al. (2004), which suggested that at oil seep setting such as our study site, $\delta^{13}C$ of DIC (and $CaCO_3$) maybe swamped by AONM signals despite the presence of shallow pockets of gas hydrates, while the $\delta^{18}O$ signals of adjacent porewater ($CaCO_3$) are isotopically sensitive to $\delta^{18}O$ enrichment from shallow hydrate dissociation.

Multiple lines of evidence point to crude oil oxidation coupled with sulfate reduction as the dominant DIC source for carbonate precipitation of Chapopote:

(l) the $\delta^{13}C_{Carbonate}$ values averaging -25‰ are closer to crude oil signature;

(2) the presence of abundant biodegraded crude oil within the carbonate samples and in petrographic observations (Fig. 3.2);

(3) widespread crude oil degradation signals from organic geochemistry studies on asphalts, oily sediments, and seeping crude oil (Schubotz et al., 2011b);

(4) an abundant unresolved complex organic mixture (UCM) in the carbonate pore filling crude oil (Naehr et al., 2009) with an elevated baseline for the C15 to C30 range, indicative of degradation involving loss of labile n-alkanes and isoprenoids from crude oil (Mansour and Sassen, 2011; Schubotz et al., 2011b);

(5) recently reported evidence for a symbiotic consortium formed by short-chain alkanes degraders with the help of sulfate-reducing bacteria from the Chapopote seep sediments (Laso-Pérez et al., 2019);

(6) distinctive phase-specific enrichment of rare earth elements and U in Chapopote carbonates compared to methane-derived carbonates (Smrzka et al., 2016); and

(7) geochemical batch modeling suggestive of sulfate-driven crude oil oxidation contributing to carbonate precipitation at Campeche Knolls (Smrzka et al., 2019).

These multiple lines of evidence developed over the past 16 years of seep studies at Campeche knolls along, along with our petrographic observations and $\delta^{13}C_{Carbonate}$ data, elevate the value of the Chapopote seep carbonates as a template for recognizing authigenic carbonates sourced via AONM in other regions.

3.6.1 C-S Isotope Systematics of the AOM and AONM settings

We analyzed the $\delta^{13}C_{carbonate}$ versus $\delta^{34}S_{pyrite}$ relationships of Chapopote samples with those from GC 415 and GC 185 as well as from published data available from multiple seep settings in the northern GoM (Formolo and Lyons, 2013; Feng et al., 2016; Sun et al., 2020). This extensive database allowed us to compare and contrast the C-S isotope systematics of sulfide and DIC produced via sulfate driven AOM and AONM as recorded in GoM seep carbonates (Table 3.1 and Supp. data file). We could narrow down two dominant endmembers based on $\delta^{13}C_{carbonate}$ versus $\delta^{34}S_{pyrite}$ plots (Fig. 3.3):

(1) AOM-dominant seepage sites with strongly depleted $\delta^{13}C_{Carbonate}$ (< -40‰) and relatively enriched $\delta^{34}S_{pyrite}$ (>0‰) values, indicative of predominant AOM sourcing forDIC.

(2) Crude oil oxidation dominated sites with dominant AONM characterized by moderate $\delta^{13}C_{carbonate}$ depletion (~-25‰) and $\delta^{34}S_{pyrite}$ values with relatively strong depletion (<-10‰), indicative of DIC sourcing via AONM. These samples include virtually all (99%) of the Chapopote seep carbonates in this study and from northern GoM site GC 232, which was recently noted for crude oil seep carbonates by Sun et al. (2020).

The data points in between the two end-members indicate mixing from multiple sources (DIC and sulfide pools from AOM, crude oil oxidation, organic matter degradation, as well as DIC sourced from methanogenesis and water column. (e.g., Raiswell, 1987; Naehr et al., 2000; Crémière et al., 2012). Overall, as explained below, our results point towards distinguishable variation in sulfate reduction coupled with methane and non-methane hydrocarbon oxidation, which produces the DIC and sulfide pools. This observation also agrees with previously

observed disparities between measured rates of sulfate reduction and methane oxidation (Joye et al., 2004; Bowles et al., 2011). Those data suggest that sulfate reduction is not driven primarily by AOM—thus highlighting the complex C-S relationship due to sulfate reduction being coupled with both AOM and AONM at GoM seeps.

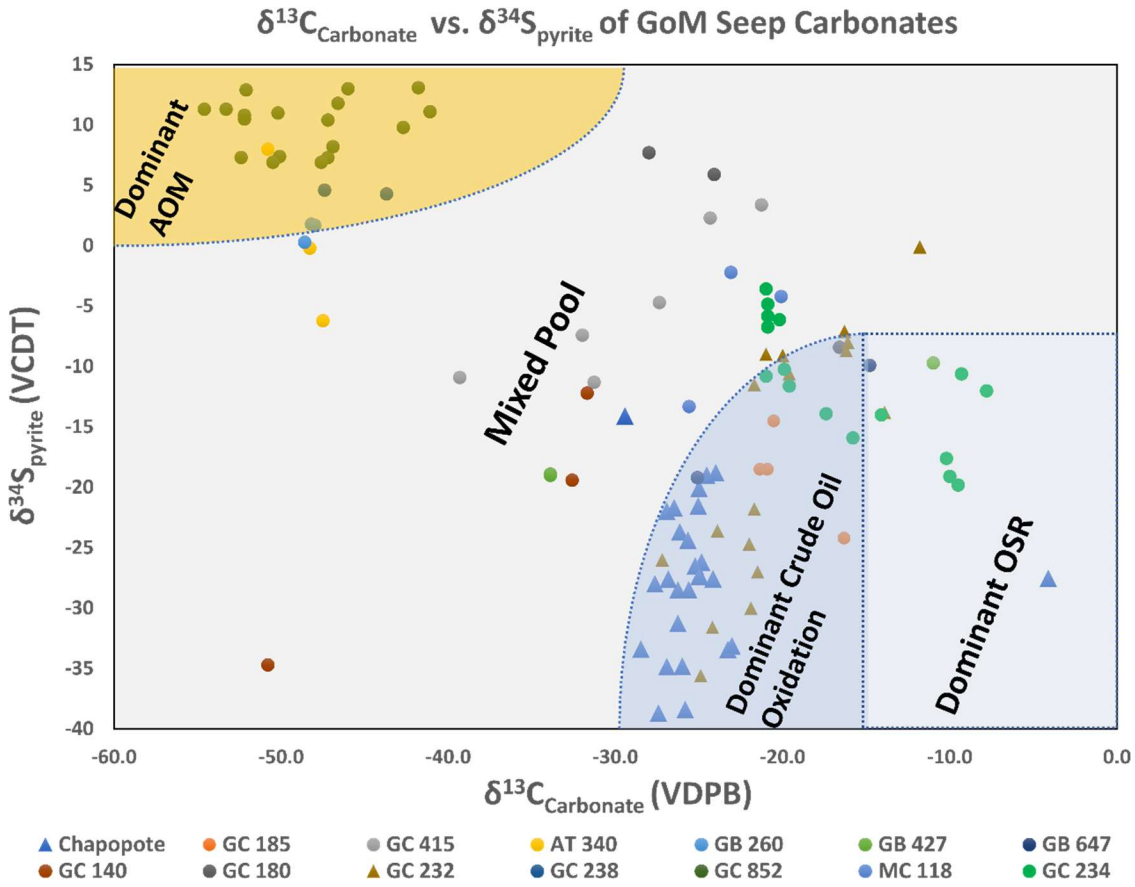

Figure. 3.4: $\delta^{13}C_{carbonate}$ vs. $\delta^{34}S_{pyrite}$ from *GoM seep carbonates with dominant endmembers contributing to the C-S coupling and associated DIC and sulfide sourcing. Refer to section 5.1 for details.*

Aharon and Fu (2000) reported that sulfate reduction rates at crude oil seeps and methane seeps in the GoM were higher than those at a non-seep reference site by up to 50 times and 600 times, respectively. This difference indicates that sulfate reduction coupled to AOM and AONM is distinctly different and that the isotopic composition of DIC and sulfide phases, produced via AOM and AONM, can be used to characterize these differences. The $\delta^{13}C_{DIC}$ signatures for methane and crude oil oxidation varies primarily because the $\delta^{13}C$ of methane and crude oil are different (Roberts and Aharon, 1994).

$\delta^{34}S_{sulfide}$ can also record the signatures of C-S coupling: $\Delta^{34}S_{sulfate-sulfide}$ ($\delta^{34}S_{seawater\ sulfate} - \delta^{34}S_{porewater\ sulfide}$) depends on the rate at which seawater sulfate exchanges with subsurface diagenetic horizons and the isotopic fractionation by sulfate-reducing microbes (Kump, 2012). In a normal marine setting without any significant methane seepage, organoclastic sulfate reduction (OSR) would predominate. In such setting, slow sulfate reduction rates causing high fractionation, along with non-limiting sulfate conditions (open-system) would result in depleted $\delta^{34}S_{sulfide}$ values (Chambers et al., 1975; Canfield, 2001, Fig. 3.4). Sites with subsurface methane flux often show high sulfate reduction rates due to AOM and exhaustion of sulfate in the local sulfate pool within the sediment column (closed-system), resulting in increased sulfide mineral precipitation at the SMTZ with enriched $\delta^{34}S_{sulfide}$ values (Jørgensen et al., 2004; Wang et al., 2008; Lim et al., 2011; Peketi et al., 2012; Fan et al., 2018). Provided sufficient Fe availability to form iron sulfide minerals, $\delta^{34}S_{pyrite}$ would be a good recorder for the porewater sulfide since isotopic fractionation associated with the pyrite formation from dissolved sulfide is only about 1‰ (Price and Shieh, 1979). Formolo and Lyons (2013), based on their observations from northern GoM site GC 234, suggested that Fe is limiting in these seep settings. Our results

suggest that small instantaneous fractionations associated with rapid sulfate consumption and/or a reservoir effect causing sulfate pool exhaustion via AOM results in initial sulfide to be isotopically heavy and be captured by available Fe early in the process (Fike et al., 2015 and references there in). In fact, multiple occurrences of sulfide minerals with distinctly enriched $\delta^{34}S$ values in sediment records is suggested to be a proxy for fossil SMTZs (Peketi et al., 2012; Borowski et al., 2013; Peketi et al., 2015; Li et al., 2016; Lin et al., 2016b; Li et al., 2017b; Wu et al., 2019; Argentino et al., 2020).

Seepage setting with anaerobic crude oil oxidation could result in sulfate reduction rates higher than OSR, but lower than AOM (Aharon and Fu, 2000; 2003). This could result in larger fractionation at lower sulfate reduction rates (in comparison to AOM) and less efficient removal of sulfate relative to replenishment, resulting in a relatively depleted $\delta^{34}S_{sulfide}$ signals when compared to AOM induced setting. Further, very high sulfide concentration [up to 13mM, Naehr et al., (2009)] and dominant anoxic conditions at the shallow sediment-seafloor of Chapopote would limit the overprinting of $\delta^{34}S_{pyrite}$ signals by sulfide oxidation and disproportionation processes. While some of the variability within the depleted $\delta^{34}S_{pyrite}$ values (-10 to-39‰) could be attributed to the diversity of hydrocarbon compounds involved, species and metabolic diversity, as well as secondary sulfide cycling (Kemp and Thode, 1968; Canfield and Teske, 1996; Detmers et al., 2001; Lyons and Gill, 2010; Sim et al., 2011; Gallagher et al., 2012; Colangelo-Lillis et al., 2019), when taken as overall, depleted $\delta^{34}S_{pyrite}$ values (<-10‰) indicates a sulfide sourcing distinctly different for AONM, in comparison to AOM. Chapopote samples with aragonite precipitation is likely to record these AOM versus AONM distinction since it is thought to form relatively close to the sediment-water column interface (e.g., Feng et al., 2016)

with sufficient Fe supply compared to the deeper sediments. It is also noteworthy that $\delta^{13}C_{carbonate}$ and $\delta^{34}S_{pyrite}$ values for Chapopote and GC 232, two sites with reported occurrence of authigenic aragonite precipitation via crude oil oxidation, shows similar $\delta^{13}C$ and $\delta^{34}S$ signals (Fig. 3.4). Hence, we interpret the enriched $\delta^{34}S_{sulfide}$ and depleted $\delta^{13}C_{DIC}$ values in our compilation to be sourced predominantly via AOM and relatively depleted $\delta^{34}S_{sulfide}$ with moderate depletion of $\delta^{13}C_{DIC}$ to be sourced primarily from crude oil oxidation (Fig. 3.4).

The aragonitic composition of Chapopote carbonates is indicative of a shallow origin in the presence of sulfate, low phosphate concentrations, and high Mg/Ca ratios (Burton and Walter, 1990; Burton, 1993). Aloisi et al., (2002) suggested that porewater sulfate concentration can have an important role in determining seep carbonate mineralogy since sulfate abundance inhibits Mg calcite precipitation and favors aragonite formation. Mansour (2014), in a compilation based on seep carbonates from multiple GoM sites, suggested that the aragonite is the dominant mineralogy at crude oil oxidation sites in comparison to methane gas seep settings, attributed to relatively lower sulfate reduction rates during crude oil oxidation. This was also recently reported to be the case at crude oil oxidation setting from GC 232 by Sun et al., (2020). Our results with aragonitic composition for Chapopote samples add additional evidence to these findings (Fig. 3.5). AOM-induced samples, on the other hand, showed a diverse mix of carbonate compositions spanning across aragonite, HMC, and LMC. We also highlight that sufficient Fe availability for iron sulfide mineral precipitation is necessary for considering $\delta^{34}S_{pyrite}$ as a faithful recorder of sulfate reduction processes, which is not always the case in many GoM seep settings, especially below the surface-most sediment layers (Formolo and Lyons, 2013). Hence aragonite samples, preferably formed closer to seafloor setting with high sulfide concentration

serve as an ideal target to analyze $\delta^{34}S_{pyrite}$ signals of AONM. Inclusion of CAS analysis along with CRS could be an effective way to overcome the limitation of the $\delta^{13}C_{carbonate}$ versus $\delta^{34}S_{pyrite}$ approach in an Fe-limited setting (Formolo and Lyons, 2013).

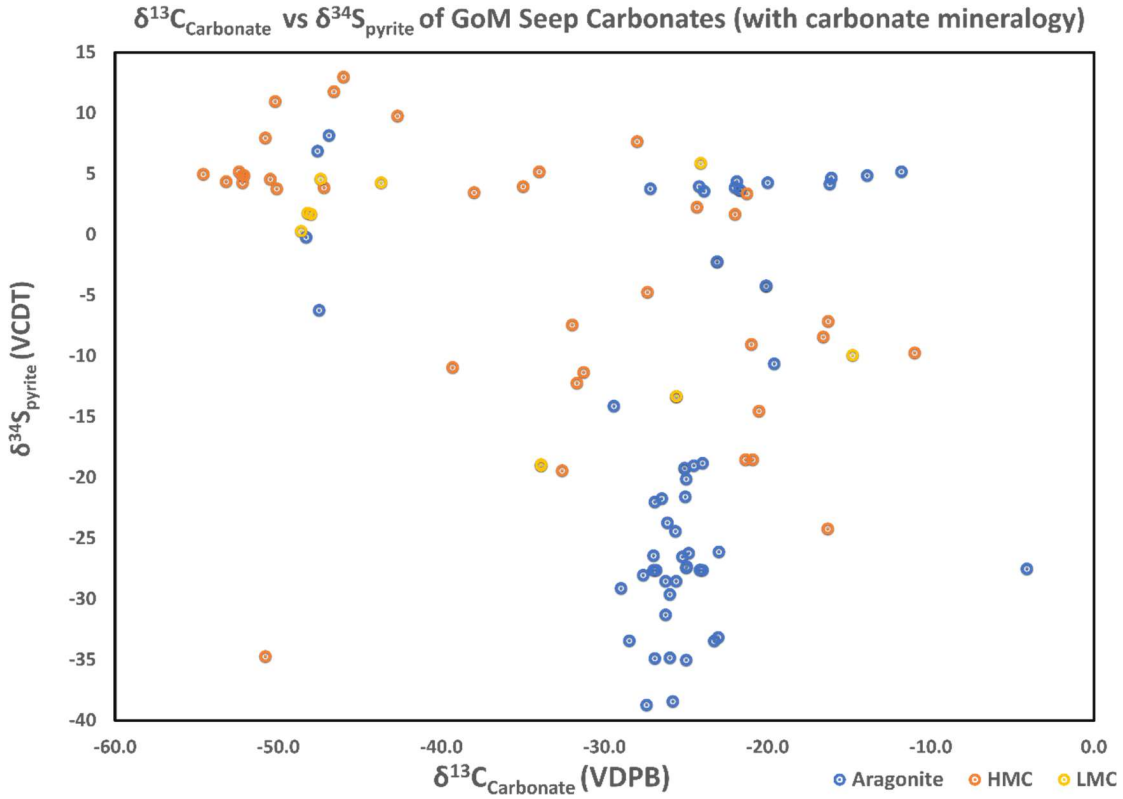

Figure 3.5: $\delta^{13}C_{carbonate}$ vs. $\delta^{34}S_{pyrite}$ values sorted by carbonate mineralogy. HMC = High Magnesium Calcite and LMC = Low Magnesium Calcite.

Our CAS analysis showed unusually depleted $\delta^{34}S_{CAS}$ as low as -23‰ and CAS concentrations as low as 31 ppm for Chapopote samples (Fig. 3.5 and supp. data). In contrast, CAS concentration from northern GoM samples from this study and Feng et al. (2016) averaged >200 ppm with $\delta^{34}S_{CAS}$ > +30‰ (Fig. 3.5). Background sediment samples from non-seep sites adjacent to Chapopote yielded $\delta^{34}S_{CAS}$ average +20‰, the modern seawater value, and CAS concentration averaging 109 ppm (Supp. data). Further, a bivalve shell with low pyrite content (0.07 wt%) and

high CAS concentration (510 ppm) yielded a $\delta^{13}C_{CAS}$ value of +19‰ (Fig. 3.5). Another suite of seep carbonate samples from Cascadia Margin that were analyzed simultaneously along with the Chapopote samples using the same methods yielded an average CAS concentration of 300 ppm and $\delta^{34}S_{CAS}$ ranging from +34 to +45.8‰ (Supp. data). Based on these observations, we suggest that the unusually depleted signals of $\delta^{34}S_{CAS}$ from Chapopote samples are likely a result of pyrite oxidation during CAS extraction, despite our efforts to minimize this effect, and are unlikely due to sulfide oxidation at the time of deposition. The high pyrite contents and low CAS concentrations of our samples elevated the risks during extraction. Thus, our results from Chapopote sites point to potential complications associated with CAS extractions of seep carbonates from crude oil-dominated seep setting. Further studies involving high-resolution $\delta^{18}O_{CAS}$ and $\delta^{34}S_{CAS}$ (e.g., Aharon and Fu, 2000; 2003; Antler et al., 2015; Feng et al., 2016) should be performed. We expect these results to provide a broader picture of diagenetic sulfur cycling, including the oxidative part of the cycle (Aharon and Fu, 2003). Further, our future work exploring the organic S pool that would also capture sulfide generated – particularly as Fe runs out, is expected to shed more light into S cycling in these settings.

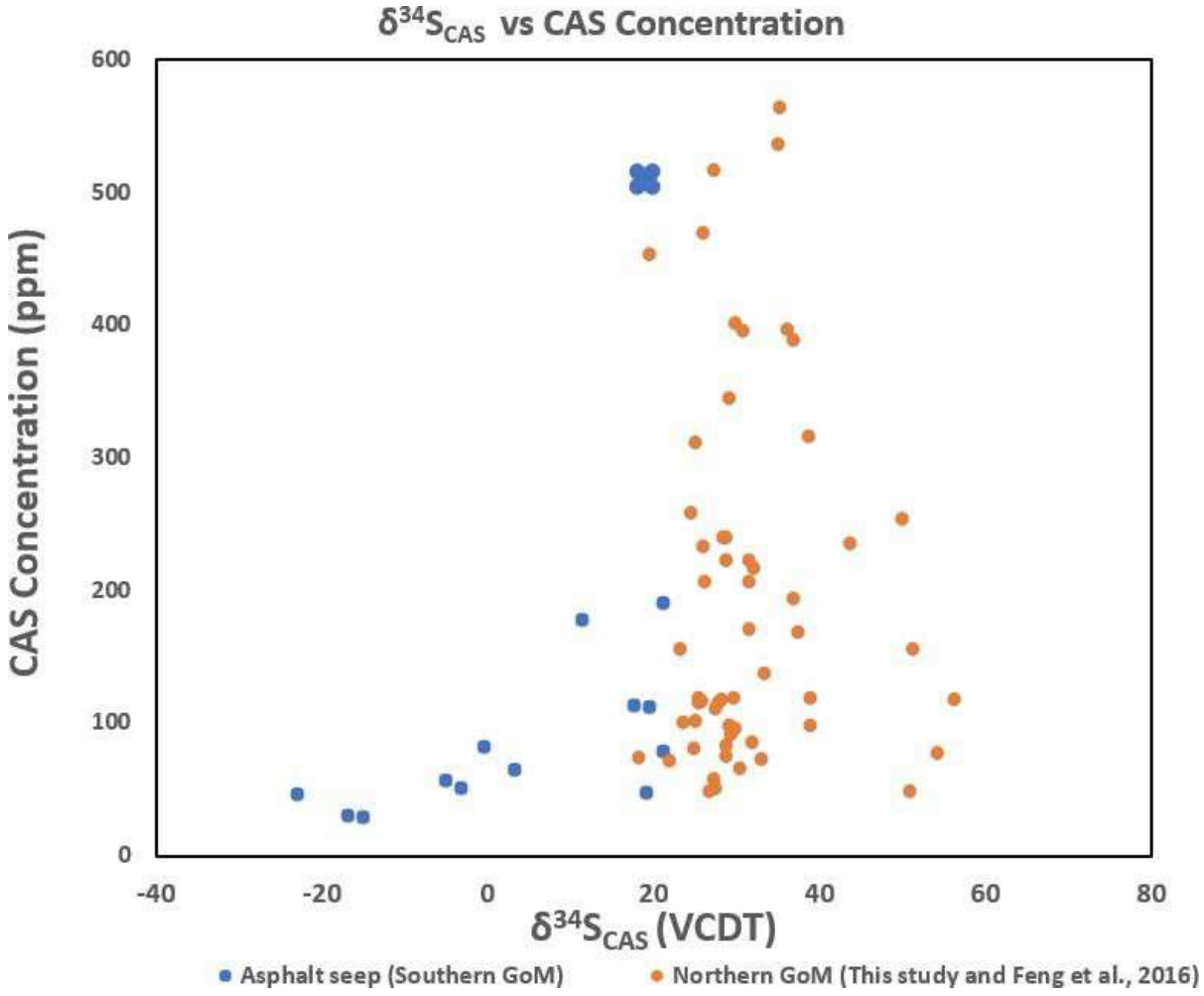

Figure 3.6. A plot of $\delta^{13}C_{CAS}$ vs. CAS concentration of seep carbonates from GoM. Chapopote samples (blue dots) showed distinctly depleted $\delta^{13}C_{CAS}$ and CAS concentration. The Chapopote samples with $\delta^{13}C_{CAS}$ ~ +21‰ are control samples from a non-seep site adjacent to the seep site. It is also noteworthy that a bivalve shell (cross marked) with low pyrite content (0.07 wt%) and high CAS concentration (510 ppm) showed a $\delta^{34}S_{CAS}$ value (+19‰) very close to that of modern seawater.

3.6.2 Implications for the sedimentary record

Carbonate systems constitute Earth's largest carbon reservoir, accounting for >60 million Gt C (Falkowski et al., 2000). Carbonate burial in marine sediments is an important part of carbon cycling through geological history, accounting for ~80% of the total carbon removal from Earth's surface (Derry, 2014; Sun and Turchyn, 2014; Berg, 2018). $\delta^{13}C_{carbonate}$ signals from the geologic records are an important sedimentary proxy for our understanding of the evolution of the carbon cycle and the chemical composition of the ocean-atmosphere system over geological history (Hayes et al., 1999; Berner, 2003; Katz et al., 2005). Variations in organic carbon burial through geologic time are recorded in the $\delta^{13}C_{carbonate}$ records. For example, a period of high organic carbon burial would cause enrichment in ^{13}C in DIC (and $CaCO_3$), since organic carbon has depleted $\delta^{13}C$ values compared to the remaining DIC in sea water (Berner, 2003; Canfield and Kump, 2013; Lyons et al., 2014). This approach can be used to reconstruct organic carbon burial and the oxygen content of the atmosphere (Shackleton, 1985; Kump and Arthur, 1999; Berner, 2004). Recently, authigenic carbonate precipitation was invoked as the third major carbon sink with major impact on $\delta^{13}C_{carbonate}$ fluctuations in the geological record (Schrag et al., 2013b). Further, authigenic carbonate precipitation is suggested to account for significant carbon sequestration, accounting for an average 1.7 Tmol annually in shallow marine sediments at present (Akam et al., 2020). Hence, better characterization of the sedimentary proxies for authigenic carbonates is an important goal (e.g., Bjerrum and Canfield, 2011; Bristow and Grotzinger, 2013; Zhao et al., 2016; Cui et al., 2017; Davis Barnes et al., 2019; Jiang et al., 2019).

Our results emphasize an important additional possibility for C-S coupling and resulting authigenic carbonate formation—crude oil oxidation (Formolo et al., 2004; Naehr et al., 2009; Mansour and Sassen, 2011; Formolo and Lyons, 2013; Smrzka et al., 2019), to the well-known processes of AOM and OSR (Bradbury and Turchyn, 2019; Akam et al., 2020). Further, we provide a sedimentary proxy using $\delta^{13}C_{carbonate}$ versus $\delta^{34}S_{pyrite}$ to identify these processes in geologic records, which can be confirmed with additional evidence, such as petrography and mineralogy (Mansour, 2014), biomarker analysis (particularly UCM indicative of petroleum degradation; Sassen et al., 2001; Naehr et al., 2009; Mansour and Sassen, 2011), trace metal concentration (Smrzka et al., 2016), and total organic carbon and total organic sulfur contents (Sun et al., 2020). Our $\delta^{13}C_{carbonate}$ versus $\delta^{34}S_{pyrite}$ compilation from GoM could serve as a template for data from additional sites and regions. Authigenic carbonate records have been used to estimate past methane fluxes (e.g., the Neoproterozoic caprocks; Kennedy et al., 2001; Jiang et al., 2003). An ability to better distinguish methane-driven carbonate authigenesis and that derived from oxidation of other hydrocarbons could allow us to better constraint on the temporal variations in methane fluxes over geologic history.

3.7 Temporal Variability of GoM Seeps

Since authigenic carbonates serve as a reliable geological archive for seepage events, constraining their precipitation ages should give us a glimpse of the temporal patterns, causes, controls, and consequences of seep systems. U-Th dating of seep carbonates is a proven tool for constraining past seep activity at diverse seep settings globally (Aharon et al., 1997; Teichert et al., 2003; Watanabe et al., 2008; Bayon et al., 2009; Mazumdar et al., 2009; Liebetrau et al.,

2010; Wirsig et al., 2012; Berndt et al., 2014; Crémière et al., 2016; Prouty et al., 2016; Mazzini et al., 2017; Sauer et al., 2017; Chen et al., 2019; Himmler et al., 2019; Judd et al., 2019).

To the best of our knowledge, our U-Th dates are the first for authigenic carbonates from the southern GoM. Only a few studies (Aharon et al., 1997; Feng et al., 2010b) have reported U-Th dates for seep carbonates in the GoM. Further, Bian et al., (2013) constrained the long-term seepage variability using ^{14}C dates on bivalve shell materials cemented in the seep carbonates. These studies were carried out in the northern GoM, and so the timing of seepage in the southern GoM has remained poorly understood. Sediment supply, sea-level changes, and salt deformation are suggested as the major factors that controlled recent hydrocarbon seeps in the GoM (Roberts and Carney, 1997). Previous results from northern GoM seeps along the lower continental margin and from upper bathyal depths to the abyssal plains showed concrete evidence of discontinuous fluid flux in these basins during the late Quaternary (Aharon et al., 1997; Feng et al., 2010b). Interestingly, it has been previously noticed that the ages of many carbonate samples clustered around 12 ka, suggestive of the role of changes in sediment loading and salt tectonics: A lower sea level would induce high sediment loading on slopes. Deglaciation will change this sediment loading and cause salt tectonic adjustment and the development of fault conduits for hydrocarbon seepage (Aharon et al., 1997; Feng et al., 2010b; Roberts and Feng, 2013). Our results also fall within that last deglaciation time frame, with the oldest being 13.5 ka and the youngest being 4.5 ka (BP).

While the northern GoM is dominated by sediment loading from Mississippi, southern GoM receives strong discharge from the Grijalva-Usumacinta River, the second largest river in the

GoM after the Mississippi (Salas-de-León et al., 2008). The salt activity of southern GoM is also suggested to be analogous to Texas-Louisiana Slope owing to its shared geological history (Garrison and Martin, 1973). Shallow sediment and salt structures, associated with regional salt tectonics are shown to have dominant control on seep distribution along Campeche knolls (Ding et al., 2008; Ding et al., 2010). These factors could hint towards possible fault activations for hydrocarbon seepage linked to changes in deglacial sediment loading in the Campeche Bay, similar to that of northern GoM (Feng et al., 2010b; Roberts and Feng, 2013). A case for sediment loading driven salt tectonics causing seep initiation in southern GoM, however, need support from more dataset and modelling. While the driving mechanisms is uncertain, our U-Th age data from the southern GoM combined with existing northern GoM data shows strong evidence that seeps along GoM slopes were very active during the last deglaciation.

Further, asphalt volcanoes are suggested to be a significant source of methane emission from the subsurface towards the water column and atmosphere (Valentine et al., 2010). Co-occurrence of gas and oil can indeed enhance methane emission via bubble coating (MacDonald et al., 2002; Solomon et al., 2009). Our age dating suggests that Chapopote asphalt volcanoes could be a source of greenhouse gas emissions to the water column and potentially the atmosphere at least since 13.5 ka. It is also noteworthy that GoM hydrocarbon seeps have been linked to carbon cycling at shallow sediments (Coffin et al., 2015) via benthic productivity (Hovland et al., 2012) as well as in the overlying water column (D'souza et al., 2016).

3.8 Conclusions

We examined the C-S coupling and temporal patterns for Chapopote asphalt seeps in the southern Gulf of Mexico based on carbonate geochemistry and compared with the data available from multiple northern GoM Seep sites. Carbonate petrography of Chapopote samples showed peloidal textures and autoendolithic features, indicative of a dynamic microbially driven biogeochemical process resulting in carbonate authigenesis. Our results indicated distinguishable variation in sulfate reduction coupled with methane and non-methane hydrocarbon oxidation, recorded in the sulfide and DIC pool. Authigenic carbonates samples from asphalt seeps at Chapopote knolls showed noticeable distinction in $\delta^{13}C_{carbonate}$ and $\delta^{34}S_{pyrite}$ values characterized by moderate $\delta^{13}C_{carbonate}$ depletion (~-25‰) and $\delta^{34}S_{pyrite}$ values with relatively strong depletion (<-10‰), indicative of DIC sourcing via AONM. AOM dominant seepage sites, in comparison, shows strongly depleted $\delta^{13}C_{Carbonate}$ (< -40‰) and relatively enriched $\delta^{34}S_{pyrite}$ (>0‰) values, indicative of predominant AOM sourcing for DIC. The spread of data in between the two indicate mixing from multiple sources (DIC and sulfide pools from AOM, crude oil oxidation, organic matter degradation, as well as DIC sourced from methanogenesis and water column). Our $\delta^{13}C_{carbonate}$ versus $\delta^{34}S_{pyrite}$ compilation from GoM could serve as a template for data from additional sites and regions. Unusually depleted $\delta^{34}S$ values (as low as to -23‰) for carbonate associated sulfate (CAS) combined with low CAS concentration and high pyrite wt% suggest pyrite oxidation during lab preparation, suggestive of necessary precautions in using CAS proxy for carbonates produced via crude oil oxidation. We presented the first U-Th based age report for seep carbonates from southern GoM. U-Th ages on Chapopote seep carbonates ranged from 13.5 ka to 4.5 ka (BP), suggesting that Chapopote asphalt seepage has been ongoing for thousands of years. These results warrants further investigation to the possibility that the GoM slopes might

have experienced vigorous seep activation during the last deglaciation owing to changes in sedimentary loading and associated salt-tectonic adjustment which provides fault conduits for hydrocarbon seeps.

3.9 Acknowledgment

SA would like to acknowledge the Graduate Research Grant Support from the American Association of Petroleum Geologist (AAPG), Geological Society of America (GSA), and Gulf Coast Association of Geological Societies (GCAGS). SA would also like to acknowledge scholarships from TAMUCC Fund, Air and Gulf Coast Chapter of Air & Waste Management Association (A&WMA), and Corpus Christi Geological Society (CCGS) for the support during this research work. Christine Chen, Ben Hardt, and Gabriela Serrato Marks at McGee Lab (MIT) are thanked for the assistance during the U-Th analysis. Lyons' group at UCR is acknowledged for the support to SA during the research visit to perform S isotope analysis. Samples for this study were obtained during R/V SONNE and R/V Meteor cruises SO174/2 and M67/2 and we would like to extend our thanks to the entire team involved in those expeditions.

3.10 Supplementary documents

A spreadsheet file with supplementary data can be obtained at

https://drive.google.com/file/d/1fCQB02Ma4YsVvYkw5t9lVq5wqRgg6Wlj/view?usp=sharing

CHAPTER 4: UNIQUE ISOMER PATTERNS OF ARCHAEAL BIOMARKER LIPIDS AT METHANE FLUX SETTINGS: IMPLICATIONS TO GDGT BASED PALEOCEANOGRAPHIC PROXIES

For submission to Geochimica et Cosmochimica Acta as : Akam, S.A., Coffin, R.B., Abdulla, H.A.N., and Y Zhang. Unique Isomer Patterns of Glycerol Dialkyl Glycerol Tetraethers at Methane Flux Settings – Implications to Paleoclimate Proxies

4.1 Abstract

Methane transport from the subsurface reservoir towards the seafloor is a wide-spread phenomenon on continental margins with important biogeochemical implications to ocean chemistry. Understanding the methane induced biogeochemical signatures recorded on sedimentary environments is an important task to develop geochemical proxies to reconstruct the magnitude and temporal framework of methane fluxes in geologic records. Isoprenoid Glycerol dialkyl glycerol tetraethers (GDGTs) derived from core lipid membranes of methane metabolizing archaea are often well preserved in sediment records, providing significant insights to the role methane induced biogeochemistry in sediment diagenesis. Methane Index (MI) is an organic geochemical proxy for methane seepage intensity which weighs in the relative proportion of GDGTs (GDGT-1,-2, and -3) preferentially synthesized by methanotrophic archaea with that of non-methane-related biomarker contribution from planktonic and benthic sources (Crenarchaeol and Cren_isomer). In this study, we analyzed the GDGT composition of sedimentary core lipids from IODP Site 1230 (Peru Margin) and Site U1426 (Japan Sea) by UPLC approach using two silica columns and high-resolution and accurate mass Orbitrap Fusion Mass Spectrometer. Our results report novel GDGT isomers with concentration peaking at the

SMTZ and nearly absent above and below the SMTZ. Our observations suggest that these characteristic isomers of GDGT compounds are sourced from methanotrophic archaea. Identification of these novel isomers has important implications in refining the MI as well as other GDGT based paleoceanographic proxies like TEX86.

4.2 Introduction

Methane (CH_4) is an important greenhouse with a significant role in the evolution of Earth's carbon cycle and the ongoing climate change. Compared to Carbon dioxide (CO_2), CH_4 has a higher global warming potential in terms of cumulative forcing by a factor of at least 84 over 20 years and 28 over a 100-year time frame (Myhre et al., 2013; Etminan et al., 2016). At present, CH_4 is the second most abundant greenhouse gas after CO_2 and the most abundant hydrocarbon present in the atmosphere accounting for 14% of global greenhouse gas emissions (Stocker et al., 2014). Continental margins that cover ~28% of ocean surface are important zones of methane production due to high rates of organic carbon loading and low oxygen availability in the sediments. The result is favorable conditions for methane production at relatively shallow depths via microbial activity and at greater depths through the thermal breakdown of organic matter. The methane formed in the gaseous or dissolved form at depth would migrate toward the seafloor and can be trapped in reservoirs, form gas hydrate structures under favorable pressure-temperature settings, oxidize in shallow sediments and the water column, or escape to the atmosphere (Barnes and Goldberg, 1976; Hovland et al., 1993; Judd et al., 2002). Our current estimate of methane reservoir in marine sediments range from 1000 Gt to 5000 Gt C (Milkov, 2011; Wallmann et al., 2012; Ruppel and Kessler, 2017). Areas along the world's continental margins are characterized by methane seepage from subsurface reservoirs to the seafloor. These

seepage sites have a significant impact on geology and biology of the seabed facilitated through complex, microbially mediated biogeochemical processes (Judd and Hovland, 2009).

Modern methane seepage can be detected using geochemical, geophysical, and remote sensing techniques, including pore water analysis, seafloor observations, and methane anomaly detection (e.g., MacDonald et al., 1993; Borowski et al., 1996; Coffin et al., 2008; Schwalenberg et al., 2010; Skarke et al., 2014). However, the biogeochemical signatures imprinted onto the sedimentary record by such events are still poorly constrained due to the uncertainty in selecting appropriate geological proxies that record methane seepage and the difficulty in quantifying the timing of such proxy formation, which leaves a significant uncertainty regarding the temporal variations of past methane seepage(Stott et al., 2002; Dickens, 2003; Li et al., 2016)

Methane seepage to the seafloor from deeper in the sediment column results in the formation of characteristic microbial consortia and associated biogeochemical reactions due to the interaction between downward-diffusing seawater and advection of hydrocarbon-rich pore fluids (Paull et al., 1995; Naehr et al., 2007). Anaerobic methane oxidation (AOM) that occurs within the sediment column, is a dominant methane-oxidizing processes consuming >80% of subsurface methane fluxes (Fig 1) (Boetius and Wenzhöfer, 2013). AOM involves a microbial consortium of anaerobic methanotrophic archaea (ANME) and sulfate-reducing bacteria (SRB) that anaerobically oxidizes methane while reducing sulfate in the so-called sulfate-methane transition zone (SMTZ) (Reeburgh, 1976; Boetius et al., 2000).

$$CH_4 + SO_4^{2-} \rightarrow HCO_3^- + HS^- + H_2O \quad (1)$$

ANMEs employ a metabolism depended on the transfer of reducing equivalents produced from methane oxidation to their SRB partners via multiple mechanisms (Knittel and Boetius, 2009; Knittel et al., 2019). SMTZ is an important diagenetic front as a methane sink as well as for dynamic dissolved inorganic pump in methane charged shallow sediments (Akam et al., 2020). The SMTZ depth is largely controlled by the upward flux of methane (Borowski et al., 1996) as well as the rate of organic matter degradation, which then controls rates of organoclastic sulfate reduction (OSR) and methanogenesis (Meister et al., 2013).

Biomarkers of interest in a seep setting predominantly include isoprene-based archaeal lipids derived from ANMEs, acetate-based lipids from SRB, as well as hopanoids and steroids from bacteria other than SRB including aerobic methanotrophs (Peckmann and Thiel, 2004; Birgel et al., 2008; Niemann and Elvert, 2008). In methane-rich settings, methanotrophic biomarker compounds will show strong to extreme depletion in ^{13}C ($\delta^{13}C$ values as low as -130‰; Elvert et al., 2000) in contrast to values normally observed for marine lipids of about -25‰ (Haas et al., 2010). The presence of seep-related biomarker compounds and their compound-specific isotopes have led to the identification of numerous paleo seep records, crucial to our understanding of ancient seep-influenced environments (Peckmann et al., 2002; Hinrichs et al., 2003; Peckmann and Thiel, 2004; Birgel et al., 2006b; Miyajima et al., 2020).

Glycerol dialkyl glycerol tetraethers (GDGTs) are organic compounds occurring in the core membrane lipids of archaea and bacteria with excellent preservation potential in the sediment record, serving as an important geological proxy for paleoclimate reconstructions (Schouten et al., 2002; Hopmans et al., 2004; Weijers et al., 2007; Schouten et al., 2013; Tierney, 2014;

Pearson et al., 2016). In methane-induced diagenetic settings, methane metabolizing archaea are shown to dominantly contribute to the net GDGT pool (Pancost et al., 2001; Blumenberg et al., 2004; Elvert et al., 2005; Rossel et al., 2008; Liu et al., 2011; Rossel et al., 2011; Weijers et al., 2011; Zhang et al., 2011).

Methane Index (**MI)** is a biomarker-based proxy proposed by Zhang et al (2011) to analyze the strength of AOM on archaeal GDGTs given as:

$$\mathrm{MI} = \frac{[\mathrm{GDGT}-1] + [\mathrm{GDGT}-2] + [\mathrm{GDGT}-3]}{[\mathrm{GDGT}-1] + [\mathrm{GDGT}-2] + [\mathrm{GDGT}-3] + [\mathrm{Cren}] + [\mathrm{Cren}']} \qquad (2)$$

Where GDGT-1, -2, and -3 are the lipid biomarkers preferentially synthesized by methanotrophic archaea while Cren (crenarchaeol) and Cren' (crenarchaeol regioisomer) indicate the non-methane-related biomarker contribution from planktonic and perhaps benthic sources (Fig. 4.1). The MI value ranges from 0 to 1, where a value >0.3 indicates an increased impact of AOM. This index serves as a tool to examine the past methane flux records as well as to screen GDGT based paleoceanographic reconstruction from methane induced diagenetic alterations. Effective application of MI to sediment cores can provide critical information about the temporal variability of methane flux in the study.

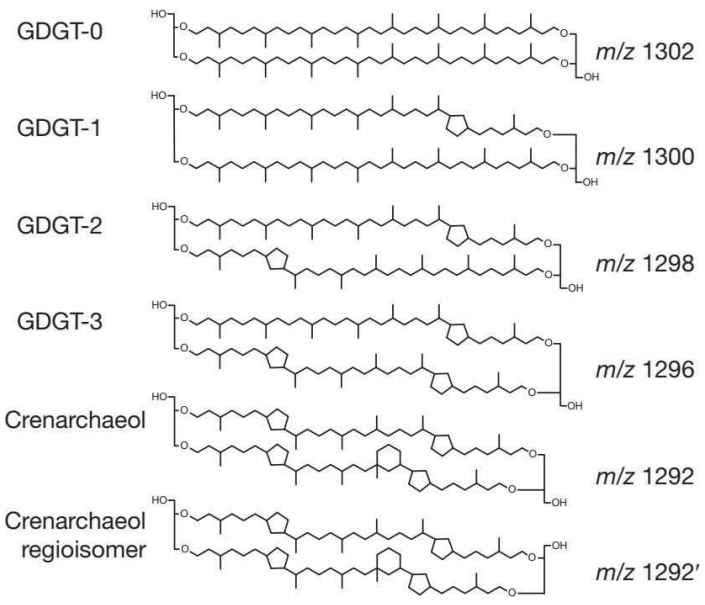

Figure 4.1: Core structures of the most common isoprenoidal GDGTs with mass-to-charge ratios (m/z)

In this study, we examined the GDGT composition of sedimentary core lipids from IODP Site 1230 (Peru Margin) and Site U1427 (Japan Sea) using a high-resolution Orbitrap Fusion Mass Spectrometer. Our study sites had very different oceanographic settings but a similar diagenetic setting of a diffusive methane flux with a shallow sulfate-methane transition zone (SMTZ) at 8 mbsf for Site 1230 and ~4.5 mbsf for U1427. Most of the GDGT based studies have reported elution of GDGTs 1-3 with leading shoulders, indicative of potential isomers (Tierney, 2014), however, their influence on GDGT based proxies at different environmental settings are poorly constrained (Becker et al., 2013). This study aimed at identifying these isomer patterns in a methane laden sedimentary setting to analyze their influence on MI.

4.3 Study Sites

ODP Site 1230 (9°6.7525′S, 80°35.010′W) is drilled at a water depth of 5086 meters below sea level (mbsl) on the lower slope of the Peru trench at the transition between accreted sediments

and the continental shelf during Leg 201 (Fig. 4.2). It is an active margin with fluid seepage from below and high phytodetritus sedimentation from the water column (Suess et al., 1990; D'Hondt et al., 2003). The presence of gas hydrates at the study site has been well documented by ODP legs 112 and 201. IODP Site U1427 (35°57.92′N, 134°26.06′E) was the shallowest site of the depth

transect of IODP Leg 346, at a water depth of 330 mbsl (Shipboard Scientific Party, 1990; Tada, 2015a) (Fig. 4.2). This is a site under the influence of Tsushima Warm Current (TWC) with an average sedimentation rate of ~300 meters per million years (m/m.y.), providing an excellent target for high-resolution paleoceanographic reconstruction (Tada, 2015b). In this study, we chose this site as the second core for the project since it showed porewater profiles very similar to that of Site 1230. No gas hydrates were observed in this site or the adjacent though noticeable microbial methane supply from the bottom sediment to the water column and a local methane plume with $\delta^{13}C$ values in the range -60‰ was recently reported from the eastern Yamato basin by Gamo et al. (2012), indicative of microbial methane flux occurring in the area.

Both the Sites U1427 and 1230 are highly productive margins with a high sedimentation rate (~100m/m.y for Pleistocene-Holocene sequence) with high organic carbon and carbonate content. Porewater profile showed a shallow SMTZ at ~8mbsf and 4 mbsf for Sites 1230 and U1427 respectively. We focused the top 22 mbsf with a 50cm depth interval for the study. Higher depth resolution was adopted for depths of interest, especially around the SMTZ depth. Distinctly convex upward alkalinity inflection, constant NH_4^+ gradient, and high concentration of dissolved HS^- were indicative of AOM derived SMTZ (Fig. 4.3). The total organic carbon (TOC)

contents for sediment samples for the top 22 mbsf for Site U1427 range from 1 to 2.2 wt% with an average 1.4 wt% (Tada et al., 2015a) and Site 1230 range from 2.07% to 3.22 wt%, with an average 2.5 wt% (Meister et al., 2005). Even though detailed pore water analyses and microbiological studies have provided a picture of present-day diagenetic conditions (Murray et al., 1992; Biddle et al., 2006; Inagaki et al., 2006; Miller and Dickens, 2017), little is known about the variation of these processes over geological time as well as the details of carbon cycling at these shallow SMTZs. A recent study at ODP Site 1229 by Contreras et al. (2013), with a deeper SMTZ (~30mbsf) without any significant upward methane flux, has found multiple and distinct layers of diagenetic barite and dolomite co-occurring with peaks of ^{13}C-depleted archaeol, which are biomarkers for ANME, at shallower depths than the modern SMTZ. These are indicative of variations in the SMTZ in the past with a unique insight into the non-steady-state nature of the deep-sea biosphere interacting with surface water productivity on glacial-interglacial cycles.

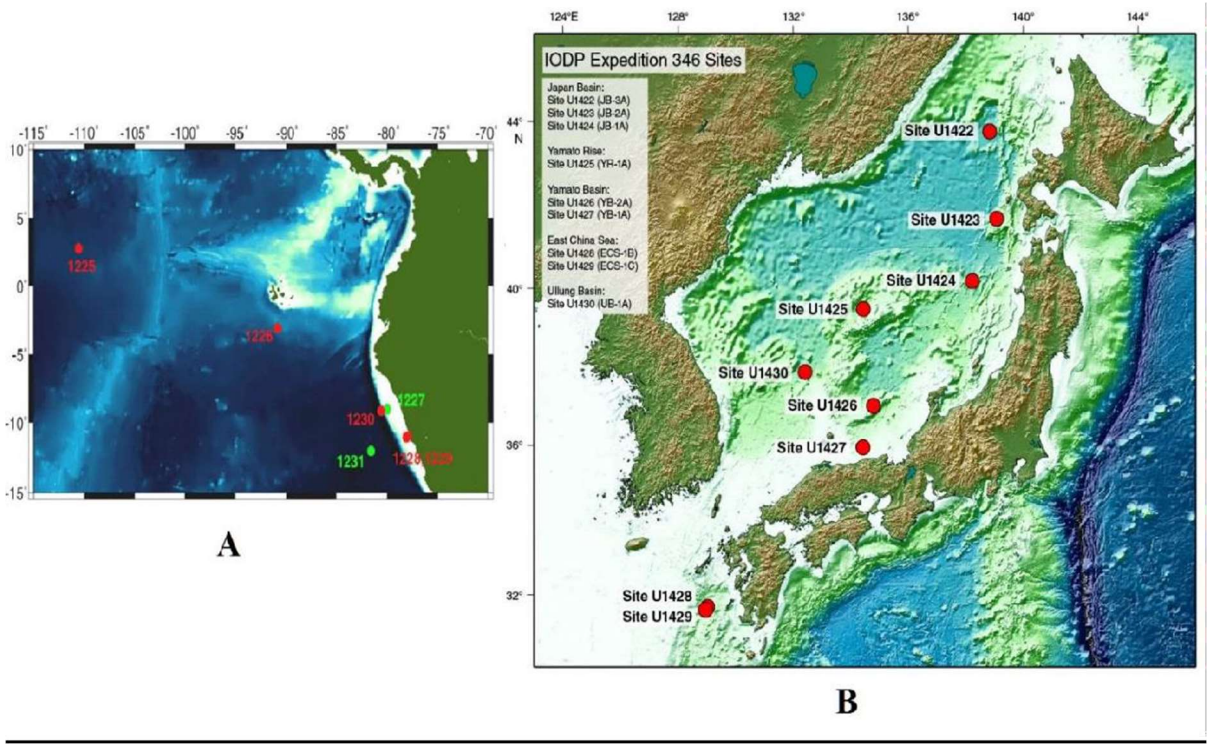

Figure 4.2: Study Area. A) Site 1230, ODP Leg 201, Peru Margin. B) Site U1427, IODP Leg 346, Japan Sea taken from cruise reports ODP Leg 204 and IODP Leg 346.

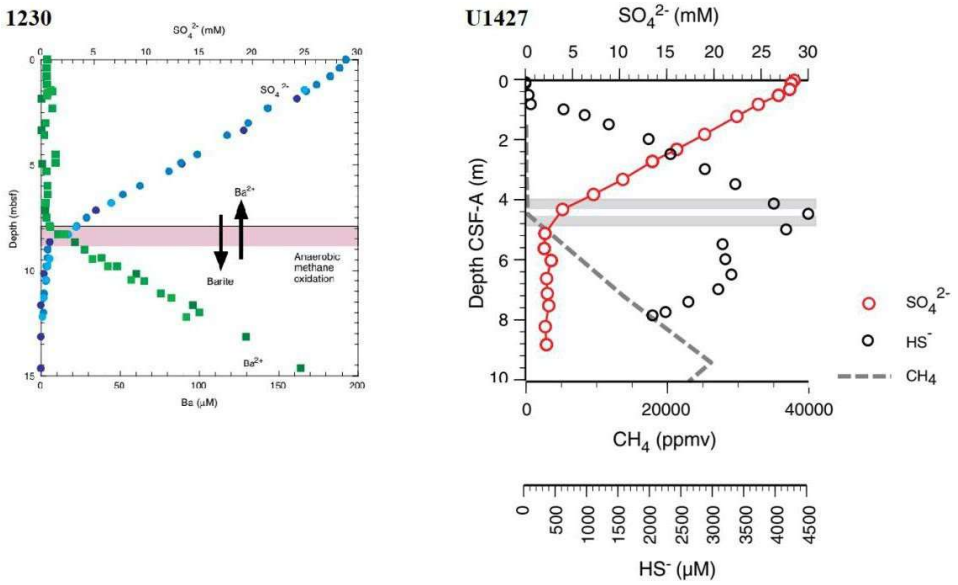

Figure 4.3: SMTZ depth for Sites 1230 and U1427 taken from cruise reports ODP Leg 204 and IODP Leg 346.

4.4 Methods

A modified Bligh/Dyer procedure was followed for total lipid extraction (e.g., Zhang et al., 2006; Zhang et al., 2011). A mixture of MeOH, Chloroform, Phosphate buffer (pH=7.4) in a 1:1:0.8 ratio was added to 5 g of freeze-dried sediment sample and kept in the sonic ice bath for ~12 hours. 2.5 ml of chloroform and 2.5 ml of MeOH were then added to this solution and the samples were centrifugated three times and the organic phase was extracted via pipette. The organic extracts were reduced under pure N_2 gas. 2ml of MeOH and HCl were added in a 95:5 ratio. The lipids were then transesterified by adding 2ml of MeOH and HCl in a 95:5 ratio and further heating at 70°C for 2 hours. Solid-phase extraction of the resulting lipid extracts was performed using a Varian Blond Elut C-18 column using 2ml of the following solvents to produce four fractions respectively: (i) Acetonitrile + Ethyl Acetate with a ratio of 3:1 (F1), (ii) Acetonitrile + Ethyl Acetate with a ratio of 1:1 (F2), (iii) Ethyl Acetate + Hexane with a ratio of 1:3 (F3), and (iv) Ethyl Acetate + Hexane with a ratio of 1:10 (F4). F3 fraction was used for GDGT analysis via Ultrapreformance liquid chromatography (UPLC) coupled with high-resolution Orbitrap Fusion Mass Spectrometer. Chromatographic methane based on two UHPLC silica columns in series (Hopmans et al., 2016) was adopted for GDGT separations with good resolution.

In brief, 5 uL of F3 fraction was analyzed on Vanquish UPLC - Orbitrap Fusion Tribrid Mass Spectrometer (UPLC-OT-FTMS). The analysis was performed on two UPLC silica column (1.7

μm BEH HILIC column 2.1 x 150 mm) in series and maintained at 30°C via atmospheric pressure chemical ionization (APCI). Eluent A was Hexane and eluent B was hexane:isopropanol (9:1, v/v). The following gradient was used: hold at 18% B for 25 min; ramp to 35% B for 25 min; ramp to 100% B for 30 min and hold for 10 min. A 20 min column re-equilibration with the starting ratio of eluents was carried out between sample analyses. The flow rate was 0.2 $ml \cdot min^{-1}$. The APCI setting was 5uA corona current, 35 Sheath gas, 10 Aux gas, 325°C ion transfer tube temp, and 200°C vaporizer temp. The Orbitrap full scan was run at 500,000 (FWHM at m/z 200) resolutions with a scan range of 600-1500 m/z and RF Lens at 60%. For MS^2, the isolation window was set at 0.7 m/z with preforming both collision-induced dissociation (CID) and higher-energy collisional dissociation (HCD) using ion trap mass spectrometer as the detector. The AGC was set at 1.0e4 and intensity threshold at 5.0e3.

Compound Discoverer software 3.01(Thermo Fisher) was used to identify the DOM compounds. The retention times (RT) of all chromatography spectra were aligned using the adaptive curve with a maximum shift of 0.8 min and 2 ppm mass tolerance.

4.5 Results and Discussions

Our high-resolution UHPLC approach using two silica columns and Orbitrap Fusion Mass Spectrometer provided excellent GDGT separation, showing a very diverse GDGT pool including GDGTs with different numbers of cyclopentane moieties (GDGT 0-4), Crenarchaeol and its regioisomer, branched GDGTS, Isoprenoidal H-shaped GDGT (H-GDGTs or GMGTs), hydroxy GDGTs (OH-GDGTs), glycerol dialkanol diethers (GDDs). In total, there were 2102 and 719 individual compounds identified by the mass spectrometry for sites 1230 and U1427

respectively. In this study, we focussed our attention on GDGTs 0-3, Crenarcheol, and its regioisomer. GDGT-0 and Cren were the dominant compounds in the study sites (Fig. 4.4). Distinct peaks of GDGT-1-3 were observable around the present-day SMTZ (Fig. 4.5).

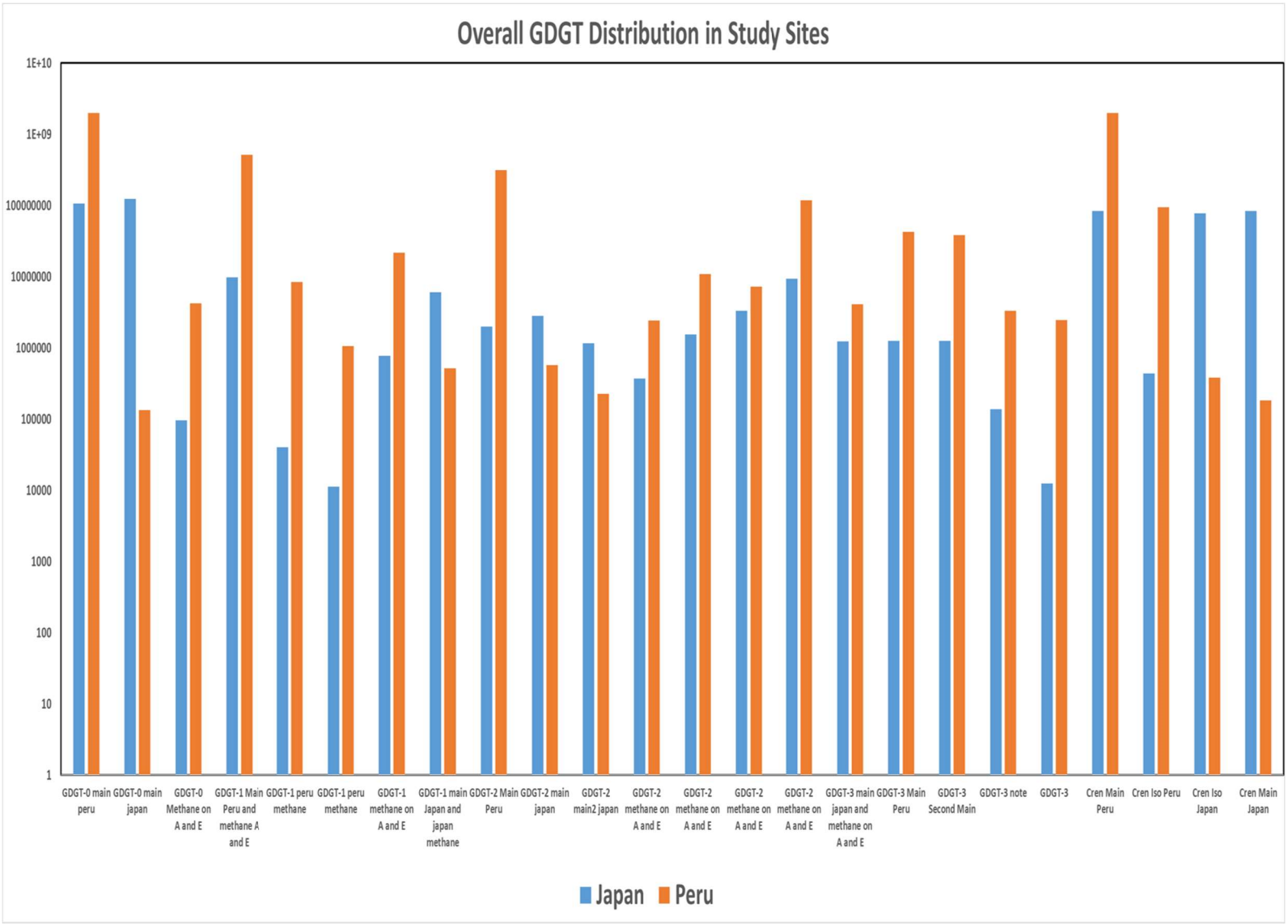
Overall GDGT Distribution in Study Sites
1E+10
1E+09
100000000
10000000
1000000
100000
10000
1000
100
10
1
GDGT-0 main peru
GDGT-0 main japan
GDGT-0 Methane on A and E
GDGT-1 Main Peru and methane A and E
GDGT-1 peru methane
GDGT-1 peru methane
GDGT-1 methane on A and E
GDGT-1 main Japan and japan methane
GDGT-2 Main Peru
GDGT-2 main japan
GDGT-2 main2 japan
GDGT-2 methane on A and E
GDGT-2 methane on A and E
GDGT-2 methane on A and E
GDGT-2 methane on A and E
GDGT-3 main japan and methane on A and E
GDGT-3 Main Peru
GDGT-3 Second Main
GDGT-3 note
GDGT-3
Cren Main Peru
Cren Iso Peru
Cren Iso Japan
Cren Main Japan
Japan
Peru

Figure 4.4: Bulk GDGT distribution. It can be seen that Peru margin samples (orange bars) gave relatively high GDGT distributions than Japan Margin (blue bar). GDGT-0 and Cren were the dominant compounds in both sites.

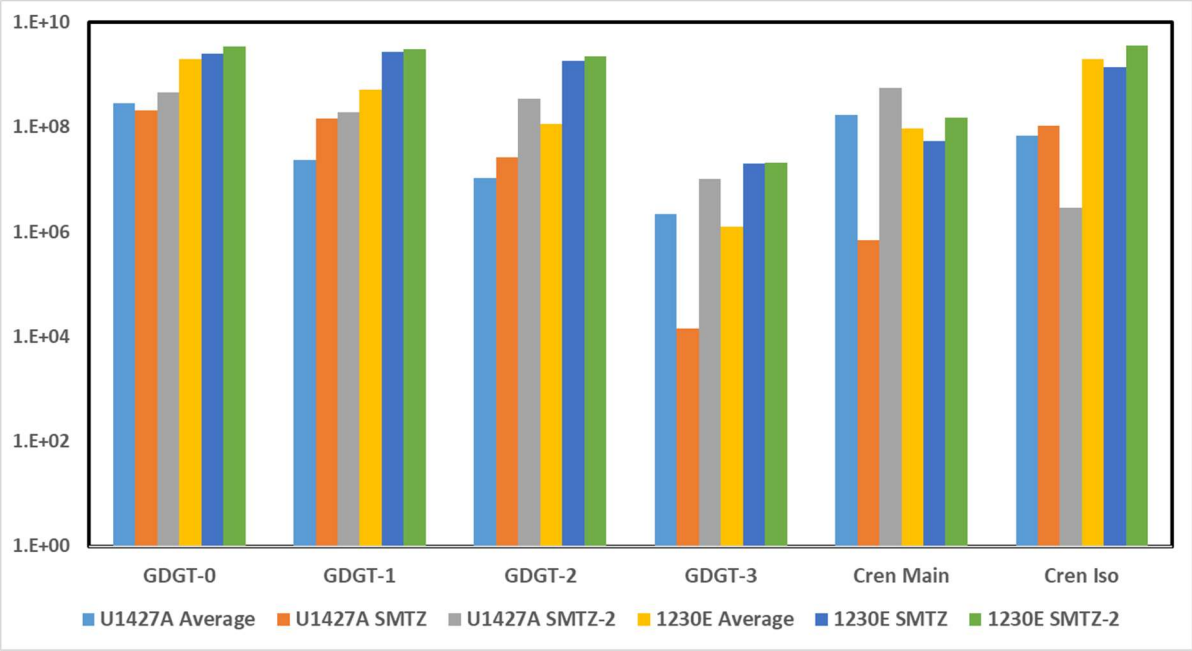

Figure 4.5: GDGT distribution at SMTZ intervals compared to average GDGT distribution throughout the sediment core. Relatively higher contribution of GDGTs 1 and 2 has a higher concentration than overall average GDGT distribution at the SMTZ.

4.6 Identification of different GDGTs Isomers:

Site 1230E showed a larger overall GDGT distribution through the sediment depth as well as higher intensities of different GDGTs isomers (Fig. 4.5). This can be explained from the Total Organic Carbon (TOC) for both sites; Site: average TOC reported for the top ~22 mbsf for Site 1230 averaged 2.5 wt% (Meister et al., 2005) whereas the average TOC for Site 1247 for the

depth range was 1.7 wt% . Hence we used the study site 1230E from Peru for the compound characterization.

GDGT-0 showed one isomer at retention time (RT) 16.53 (Fig. 4.6A). Preforming HCD and CID fragmentation techniques on m/z 1302, we have identified the following major m/z fragments 615.64, 651.66, 669.676, 689.68, 707.69, 725.70, 743.71, 1210.28, 1228.29,1246.30, 1269.29, and 1284.31. These fragments confirmed the structure of the GDGT-0 (Fig 4.6D-E). GDGT-0 could be sourced from multiple archaeal groups including methanogens (Koga et al., 1998; Pitcher et al., 2011). Depth profile plot of GDGT-0 did not show any noticeable variation down the sediment core, with regards to SMTZ (Fig. 4.11), which indicate that GDGT-0 sourcing from methane-metabolizing archaea is considerably low and potential sourcing from Thaumarchaeota, including ammonia-oxidizing archaea is dominant (Damsté et al., 2002; Jung et al., 2011; Pitcher et al., 2011). Multiple archaeal sources in different depth intervals are a likely scenario in this case, similar to the observation by Wakeham et al., (2003). GDGT0/crenarchaeol ratio was less than 2 throughout the sediment column, a proxy suggested to indicate relatively insignifcant GDGT-0 contributions from methanogens (Blaga et al., 2009). We can also discard the possibilities of halophilic archaeal sourcing for GDGT-0 (Turich and Freeman, 2011; Birgel et al., 2014; Natalicchio et al., 2017) in this setting, as we find no evidence for hypersaline conditions. It is also important that our study sites and the sediment depth of interest are well established to be ideal mesophilic setting.

Using the two silica columns UPLC-OT-FTMS method identified five distinct isomers of GDGT-1 at RT 18.064 min (named GDGT-1), 19.741, 18.974, and 17.404 min (named GDGT-

1a-c respectively, Fig 4.7). Plotting the GDGT-1 isomers at RT 18.064 and 19.741 min (named as GDGT-1 and GDGT-1a) showed unique peaking at the SMTZ depth (Fig. 4.11A). To verify the structures of the GDGT-1 at RT 18.064 min we performed CID fragmentation on mz/ 1300 for these specific isomers. We identified a list of m/z fragmentation signatures at 703.660, 739.681, 741.697, 1204.229, 1260.255, and 1278.266 m/z that verify the proposed structure of GDGT-1 (Fig 4.7D-E). Identifying a distinct peaking of one of the GDGT-1 isomers at the SMTZ agrees with the previous studies that reported predominant sourcing from methanotrophic archaea in methane laden settings (Pancost et al., 2001; Wakeham et al., 2003; Zhang et al., 2011).

For GDGT-2, we identified four distinct isomers at RT 20.051 min (named as GDGT-2), 19.786, 19.202, and, 17.986 min (named as GDGT-2a-c respectively). Plotting the depth profile of the four isomers shows the isomer at RT 19.786 (named as GDGT-2a) is the only isomer that has a distinct peak at the SMTZ region (Fig. 4.11B). CID fragmentation of m/z 1298 confirm the propose structure of GDGT-2 by detecting the following m/z fragments 553.555, 613.660, 667.697, 703.660, 705.676, 739.681, 741.697, 1206.245, 1224.255, 1262.271, and 1280. 281 (Fig 4.8D-E). Significant GDGT-2 presence at the SMTZ was previously reported from the Aarhus Bay by Weijers et al., (2011). Our results provide additional evidence for this inference and further, provide the characteristic GDGT-2 isomer specific to methanotrophic origin.

Using our modified UPLC-OT-FTMS we identified six distinct GDGT-3 isomers at RT 21.842 min (named as GDGT-3), 19.709, 21.118, 21.97, 21.214, and 22.245 min (named as GDGT-3a-e respectively) (Fig 4.9). Out of these isomers, only the isomer at RT 19.786 min (named as

GDGT-3a) showed a distinct peak at the SMTZ region ((Fig. 4.11C). The CID fragmentation of 1296 m/z shows these major m/z fragments 703.660, 705.676, 739.681, 741.697, 1205.229, 1260.255, and 1278.226 m/z, which all are distinct fragments of GDGT-3 propose structure. While a mixed sourcing of Thaumarchaeota and Euryarchaeota can be considered for the GDGT-3 sourcing (Schouten et al., 2008; Pitcher et al., 2011; Zhang et al., 2011; Schouten et al., 2013), our detection of isomers with distinctive depth would enable recognition of the ANME sourcing in the system.

Crenarcheol showed eight distinct isomer compounds (Fig. 4.10). However, none of these isomers showed any significant depth trend or correlation with SMTZ (Fig. 4.11D). This pattern is expected as the sources Crenarcheol is considered to be dominantly sourced from autotrophic ammonia-oxidizing Thaumarchaeota (Pitcher et al., 2010; Schouten et al., 2013). Hence, we expect these variations would reflect a dynamic mix of processes that include nitrification, carbon fixation in the water column, and perhaps some benthic sourcing, largely independent of the methane flux dynamics. Hence, with regards to our goal of refining the methane index (MI), we have focused on the two most prominent Crenarcheol isomers at RT (24.069 and 25.904). CID fragmentation of Crenarcheol show the distinct m/z fragmentations at 553.555, 555.571, 701.645, 719.655, 721.671, 737.665, 739.681, 1200.198, 1256.224, and 1274.234, which all confirm the structure of crenarcheol (Fig. 4.10D-E).

Overall, the abundance of GDGT 1-3, particularly at the SMTZ is highly indicative of an ANME-1 thriving environment, which is typical for diffusive settings with low-methane concentrations (Blumenberg et al., 2004; Elvert et al., 2005; Knittel et al., 2005; Pape et al.,

2005; Aquilina et al., 2010). A high methane flux setting, closer to the sediment seafloor with high sulfate concentration would be dominated by ANME-2 clades, characterized by the minimal presence of GDGTs (Niemann and Elvert, 2008; Rossel et al., 2011; Timmers et al., 2015). The most significant output of these results is the identification of isomer patterns potentially sourcing from ANME and thereby significantly reducing the uncertainty about their biological precursors, a fundamentally significant step towards the applicability of lipid biomarkers to paleoceanographic and paleodiagenetic studies.

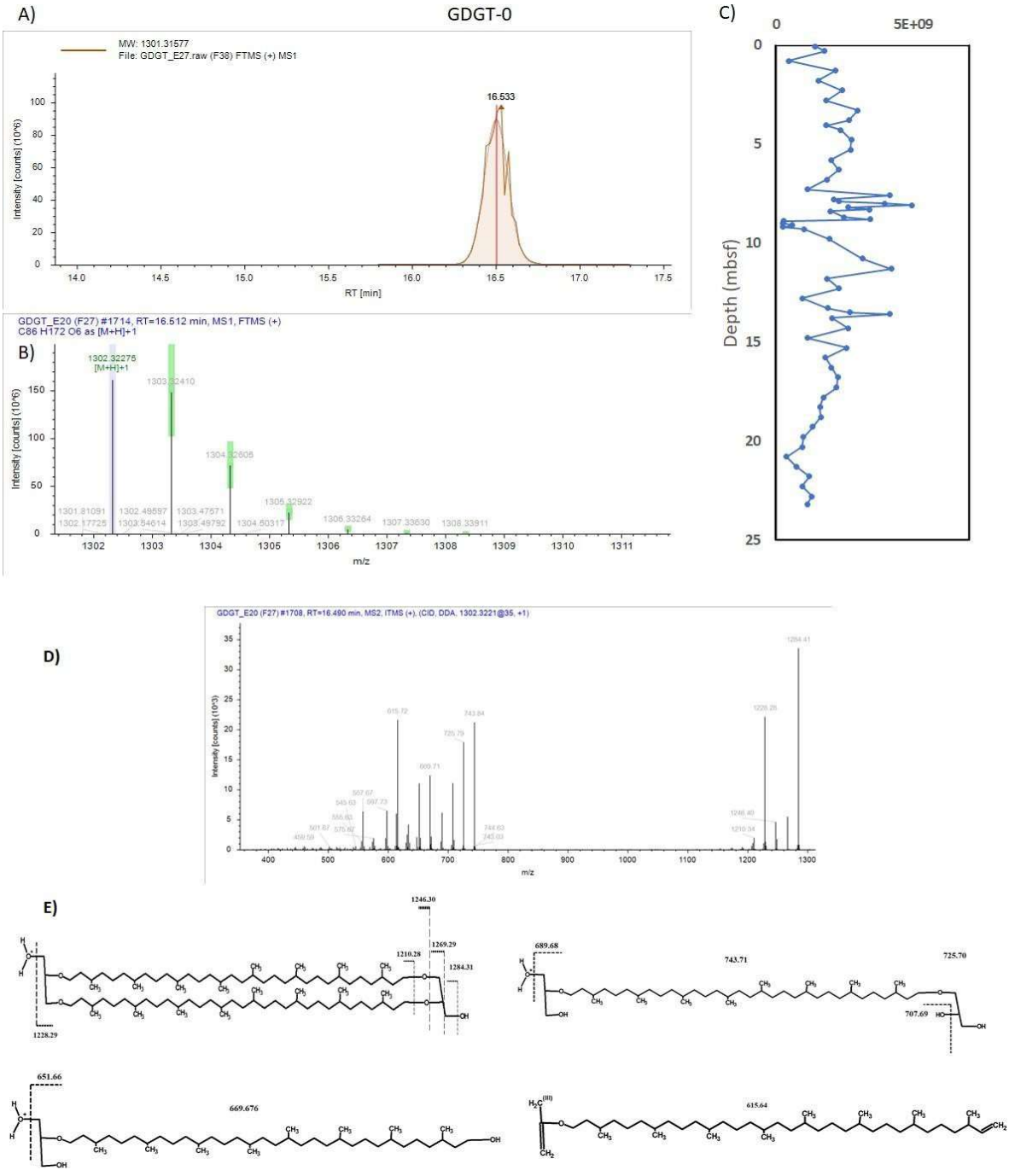

Figure 4.6: a) UPLC chromatogram of GDGT-0 b) isotope pattern of GDGT-0 c) depth profile of GDGT-0 d) CID fragmentation spectrum of m/z 1302 e) Fragmentation structures that for the major fragments of GDGT-0.

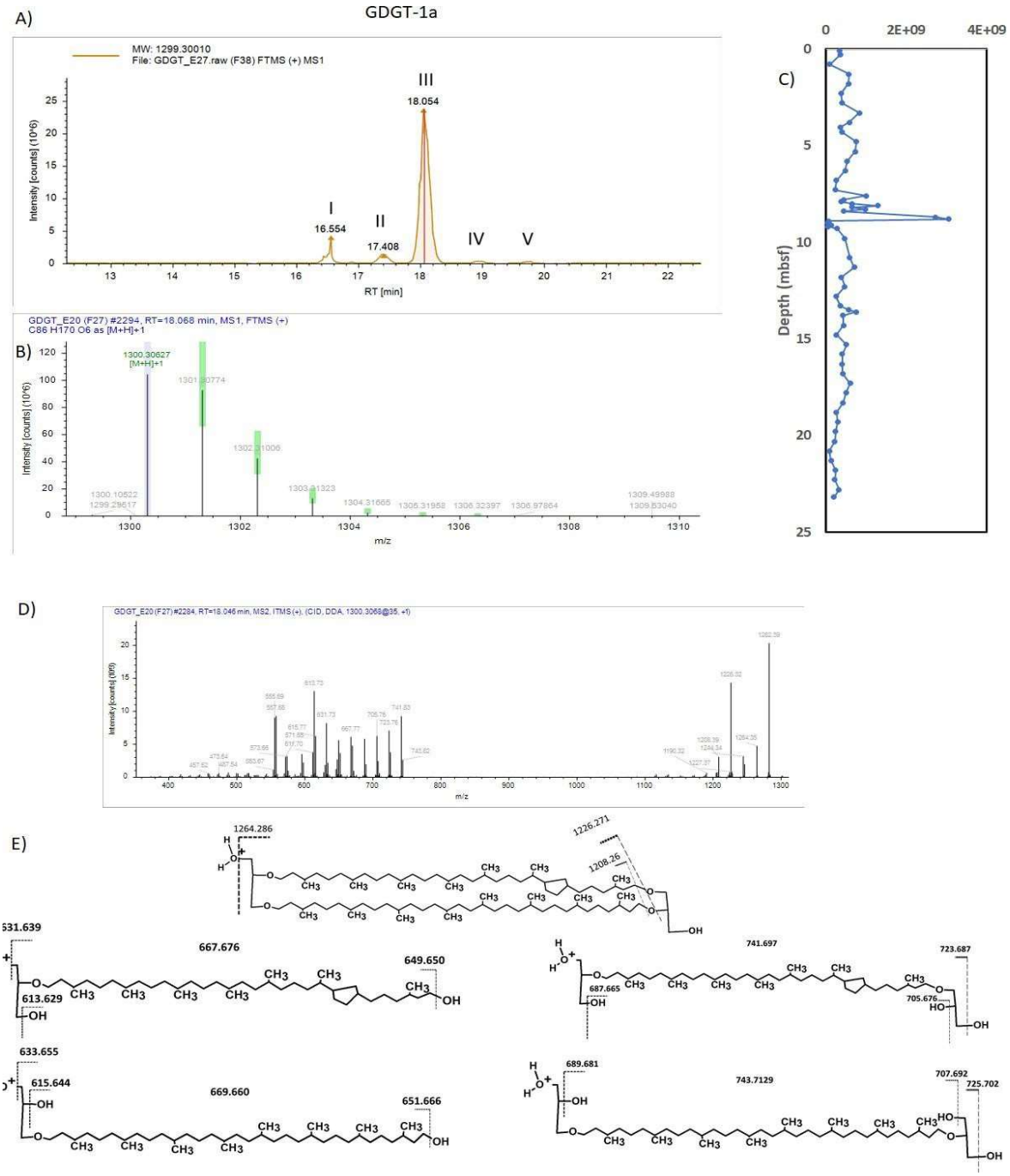

Figure 4.7: a) UPLC chromatogram of GDGT-1 highlighting the different detected isomers b) isotope pattern of GDGT-1 c) depth profile of GDGT-1 isomer III d) CID fragmentation spectrum of m/z 1300 for GDGT-1 isomer III e) fragmentation structures for the major detected fragments of GDGT-1-III isomer.

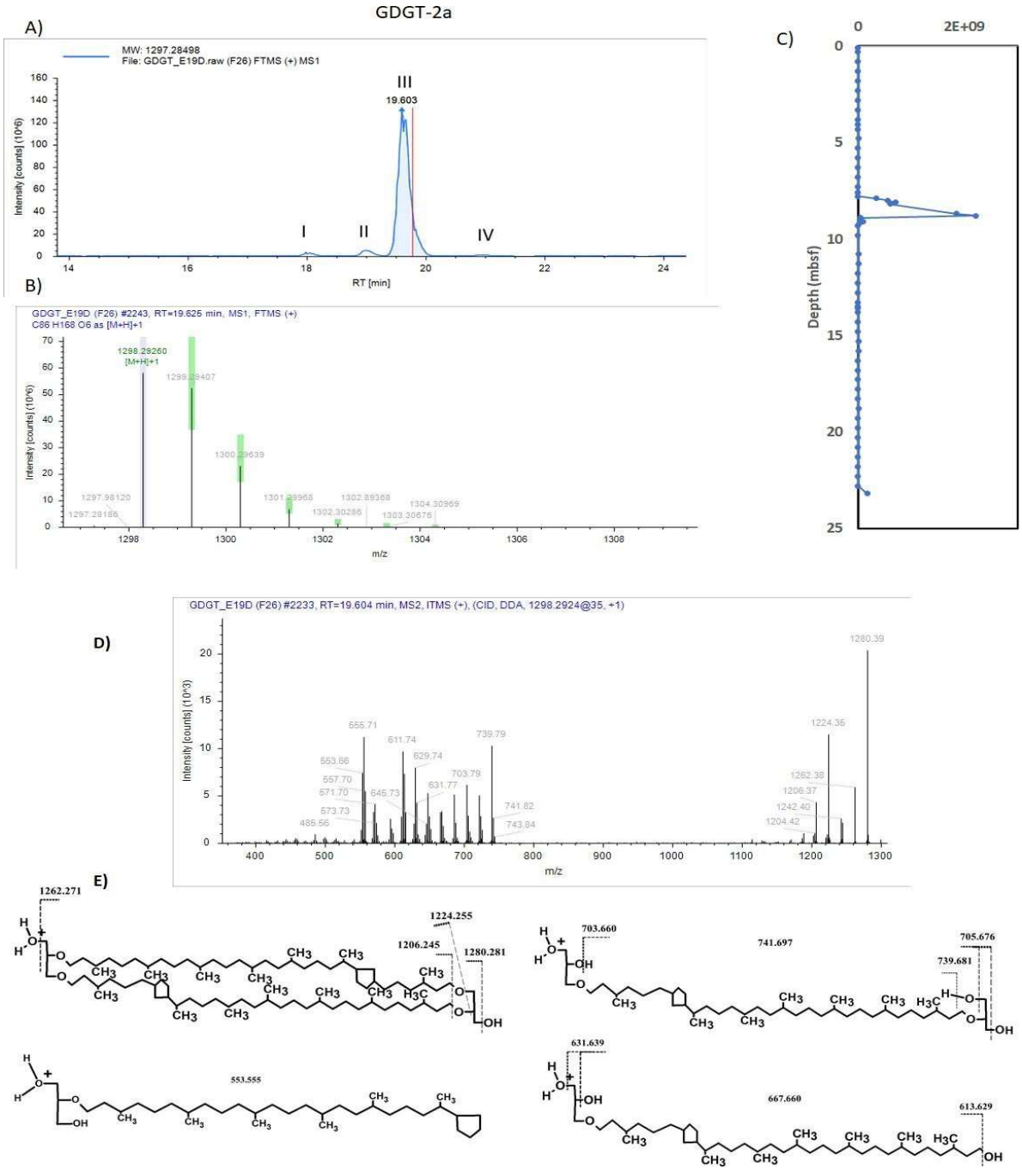

Figure 4.8: a) UPLC chromatogram of GDGT-2 highlighting the different detected isomers b) isotope pattern of GDGT-2 c) depth profile of GDGT-2 isomer III d) CID fragmentation spectrum of m/z 1298 for GDGT-2 isomer III e) fragmentation structures for the major detected fragments of GDGT-2-III isomer.

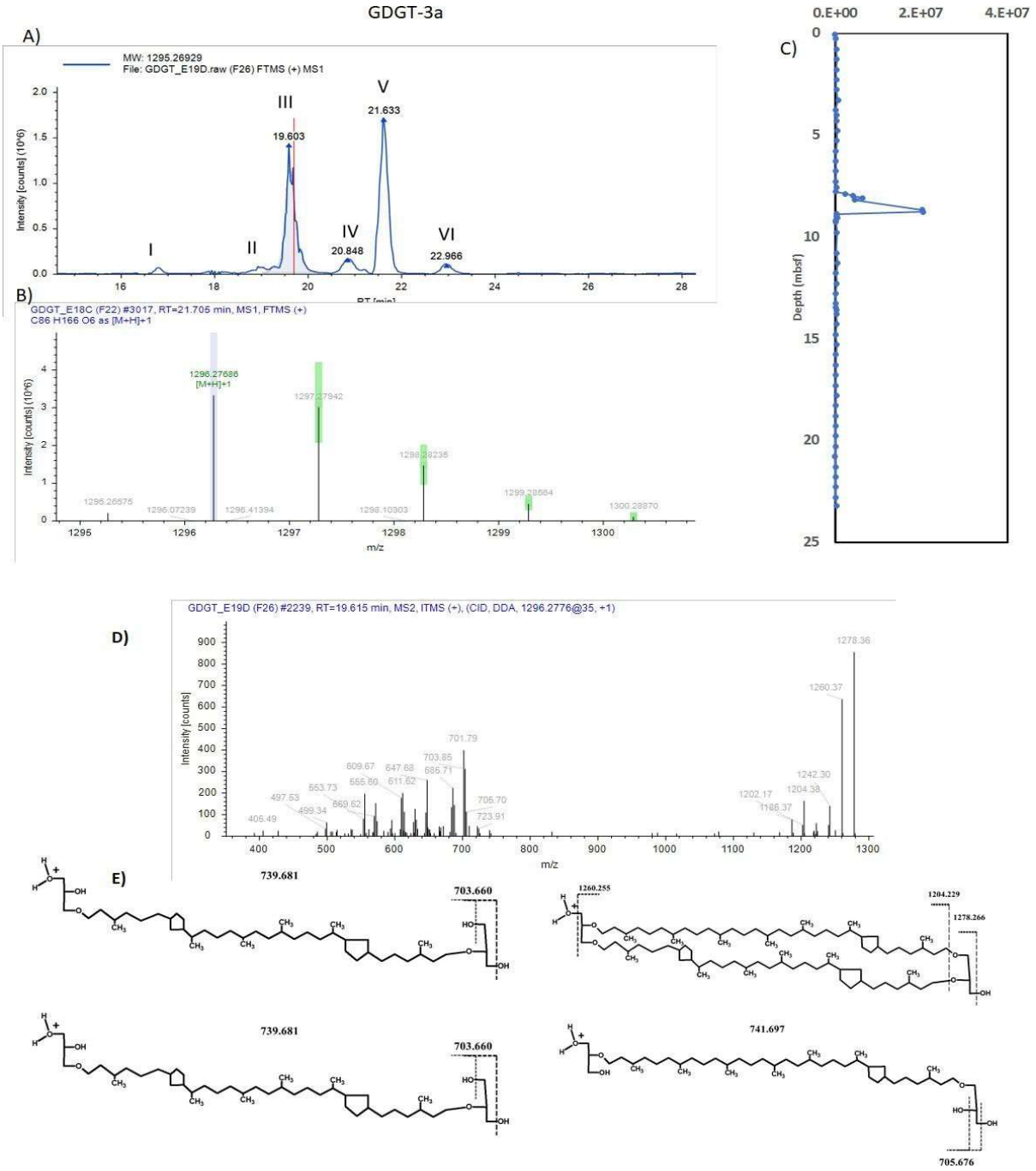

Figure 4.9: a) UPLC chromatogram of GDGT-3 highlighting the different detected isomers b) isotope pattern of GDGT-3 c) depth profile of GDGT-3 isomer III d) CID fragmentation spectrum of m/z 1296 for GDGT-3 isomer III e) Fragmentation structures for the major detected fragment of GDGT-1-III isomer.

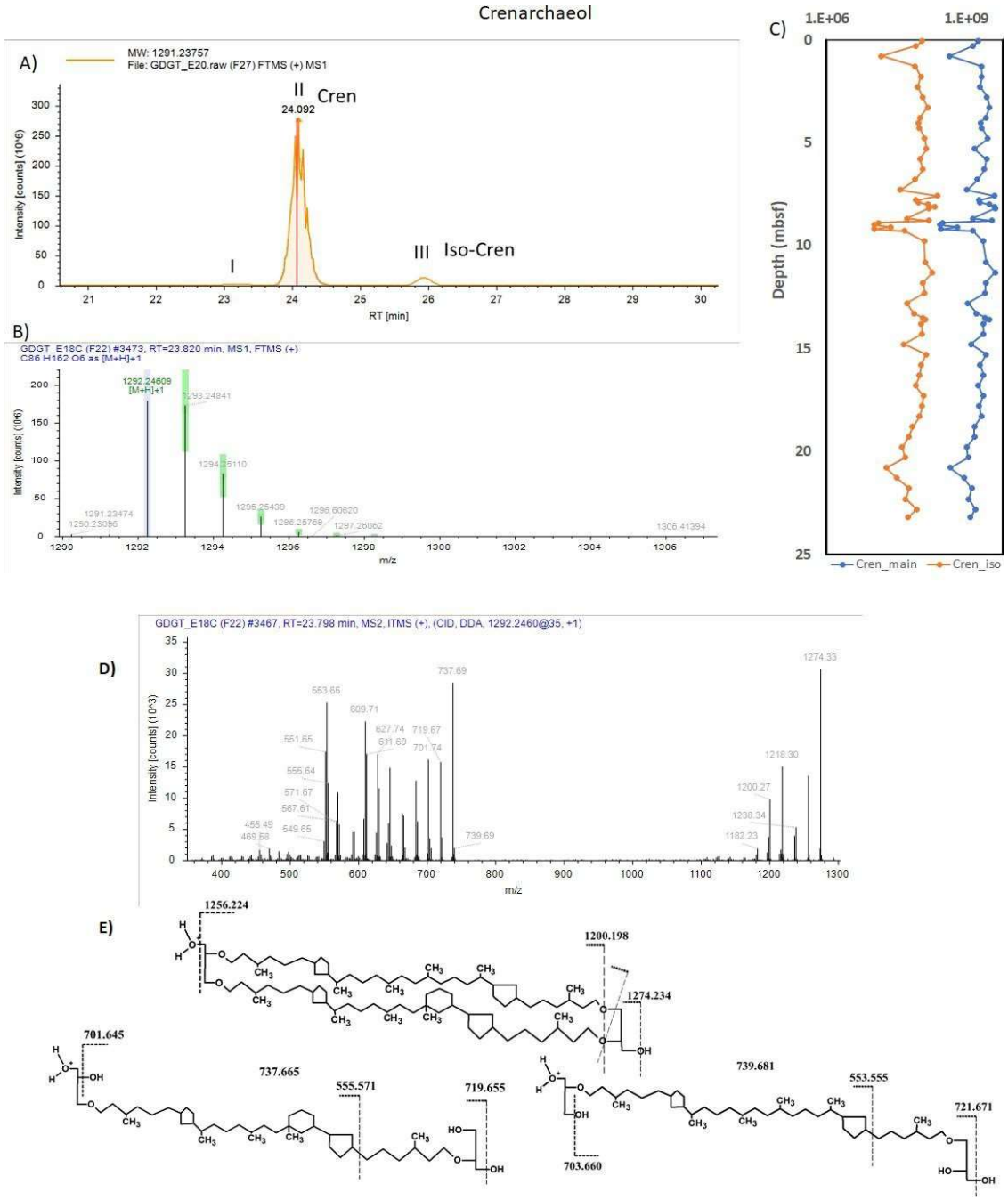

Figure 4.10: a) UPLC chromatogram of Crenarcheaol highlighting the different detected isomers b) isotope pattern of Cren c) depth profile of Cren and iso-Cren isomers d) CID fragmentation spectrum of m/z 1292 for Cren main isomer e) Fragmentation structures for the major detected fragment of Cren main isomer.

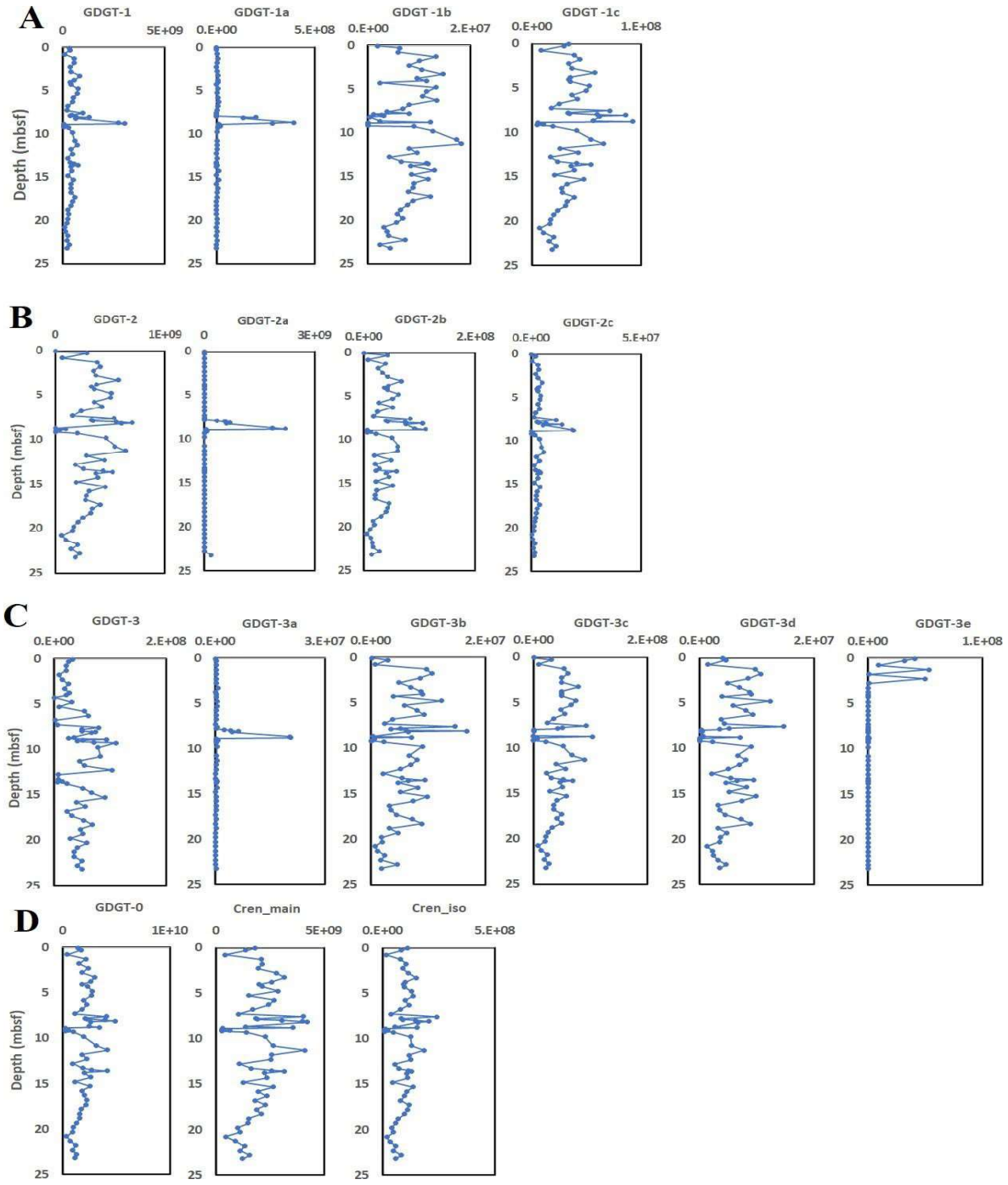

Figure 4.11: Depth profiles of All GDGTs and their isomers in this study. A) GDGT-1, B) GDGT-2, C) GDGT-3, D) GDGT-0, Cren and Cren'. Note the distinct peaks for GDGT 1a, 2a, and 3a at the SMTZ and almost absence of it above and below the SMTZ, indicative of methanotrophic archaeal sourcing.

4.7 Detection of GDGT Isomers Unique to ANME: Implications to MI

Calculating the methane index (MI) using the modified method, based on using two silica UPLC column coupled to high resolution and mass accuracy Fusion Orbitrap mass spectrometer show MI ranged from 0 to 0.89 and 0.15 to 0.7 in Site U1427 and 1230E respectively, with the highest values at the SMTZ intervals in both sites. Site U1427 showed an additional peak at depth 20.9 mbsf, potentially indicative of a paleo SMTZ (Fig. 4.15 C). MI values here show as an additional confirmation of the SMTZ depth in the sediment column, which when combined with porewater methane and sulfate profiles. Considering the measurement of methane concentration in porewater is prone to error due to degassing (Egger et al., 2018) and that additional cryptic sulfur cycling is pervasive in a diffusive setting (Beulig et al., 2019; Jørgensen et al., 2019a), MI can serve as an independent verification for porewater based SMTZ detection.

Application of the high-resolution approach in this study and the resulting capability of isomer separation enabled a great improvement in the MI values. We demonstrate that the inclusion of GDGT shoulders due to co-elution with previously uncharacterized isomers can cause significant changes to MI values and other GDGT based indices. Figure 4.14A shows the MI values obtained from the traditional HPLC method using a single-column separation for Site 1230. This MI index is significantly improved through the double-column separation (Fig. 4.14B). Further, the double-column separation allows the calculation of MI by including the GDGT isomers that are specific for ANME. This step brought MI values to go almost zero above and below the

SMTZ and a dominant peak at the SMTZ for Site 1230E (Fig. 14C). A similar refinement of MI values was observed for Site U1427 as well (Fig 15). The relative isomer peaks unique to SMTZ were limited for U1427, in comparison to Site 1230E. However, MI values showed significant improvement when the MI was calculated using the isomers with SMTZ peaking, in comparison to MI calculated using all the GDGT compounds (Fig 15C).

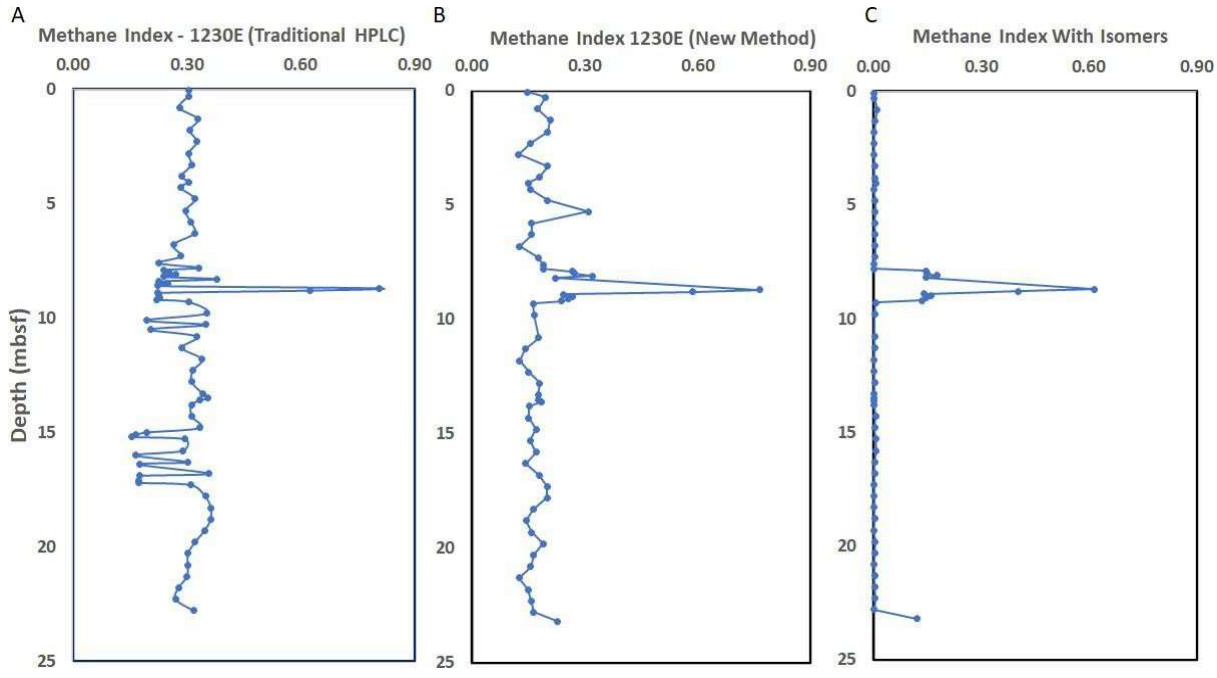

Figure 4.12: A comparison of MI values obtained from the traditional approach and the improved resolution approach used in this study. A) MI values from the traditional HPLC method using single-column separation. B) high-resolution method approach in this study using two silica column HPLC. MI values considered all the GDGT isomers in this case. C) MI values using only the specific Isomers that showed characteristic variation with regards to SMTZ (GDGT1a, 2a, and 3a). It can be seen that our method enables significant noise reduction by identifying the isomers sourcing from ANME with that of non-Non ANME origin.

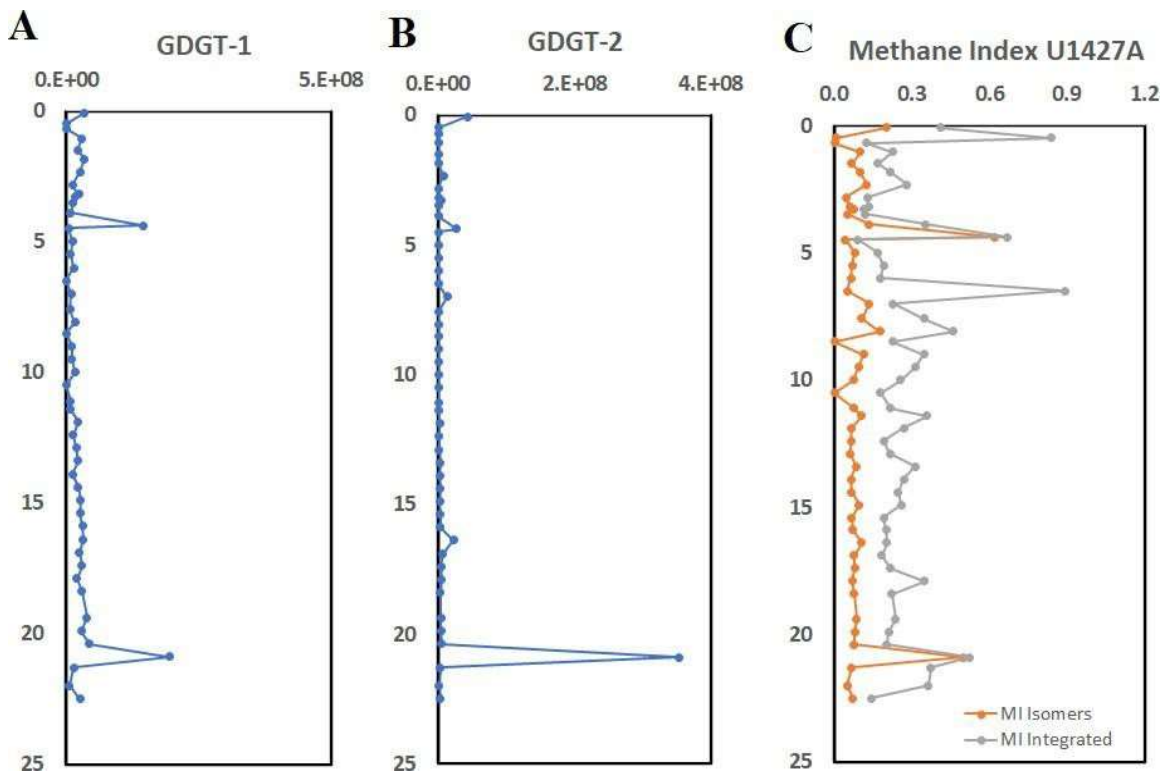

Figure 4.13: A and B) Characteristic GDGT isomers with SMTZ peaks C) MI values using all the GDGT compounds and only the characteristic isomers with SMTZ peaking. The peak at depth 20.9 mbsf indicates a paleo SMTZ front. Note the isomer patterns identify the SMTZ zone from a false-positive peak (grey peak) below the SMTZ.

An important applications of the MI proxy has been to screen methanotrophic GDGT sourcing from archaea other than marine Thaumarchaeota, as the latter sourcing is a key requirement for the fidelity of TEX_{86} based SST reconstructions (Schouten et al., 2013; Tierney, 2014; Hollis et al., 2019). This study suggest a significant impact of methane metabolizing archaeal GDGTs to the net GDGT pool in diffusive methane flux setting. This is in agreement with a previous study from Aarhus Bay where significant methanotrophic GDGT-2 was reported at SMTZ (Weijers et

al., 2011). Our observations suggest that methanotrophs contribute GDGT 1-3 to the overall GDGT pools with GDGT 2 being the most abundant methanotrophic contribution followed by GDGT 1 and 2 respectively.

Perhaps the most important highlight of this result is the enhancement of our existing GDGT based biomarker inventory by identifying isomer patterns that are unique for potential methanotrophic sourcing. These novel isomer patterns would considerably aid diagenetic imprints of methane fluxes from subsurface towards seafloor with an important global biogeochemistry/climate perspective. Further, these isomer patterns indicate to significant refinement in future for other GDGT based paleoceanography proxies like GDGT0/Cren (Blaga et al., 2009), TEX86 (Schouten et al., 2002), Ring Index (RI), RI_{TEX}, and |ΔRI| (Zhang et al., 2016), GDGT-2/GDGT-3 (Dong et al., 2019), etc. Considering there is a significant uncertainty existing regarding the temporal variations of methane fluxes as well as the carbon cycling associated with subsurface methane transport in ancient environments (Bristow and Grotzinger, 2013; Hancock, 2018), the high-resolution approach and the recognition of these novel isomer patterns reported here will considerably contribute to our existing geochemical proxy tools for investigations in this direction.

4.8 Conclusion

We analyzed GDGT core lipids from sediment cores of two diffusive methane flux sites off Peru (Site 1230E) and Japan margin (Site U1427A). Our high-resolution HPLC approach using two silica columns and Orbitrap Fusion Mass Spectrometer provided excellent GDGT separation, showing a very diverse GDGT pool. Our observations suggest a significant impact of methane

metabolizing archaeal GDGTs to the net GDGT pool in the study sites. MI values showed a strong peak at the SMTZ interval. Site U1427A showed an MI peak below the SMTZ, indicative of paleo SMTZ. Additionally, we report novel GDGT isomers with concentration peaking at the SMTZ and almost absent above and below the SMTZ. Our observations suggest that these characteristic isomers of GDGT compounds are sourced from methanotrophic archaea. Identification of these novel isomers and our high-resolution approach has important implications in refining the MI as well as other GDGT based paleoceanographic proxies like TEX86.

4.9 Supplementary documents

A spreadsheet file with supplementary data can be obtained at the following weblinks for the Peru and Japan margin sites, respectively:

https://drive.google.com/file/d/1f5oyVTOf_ld1Zx8xnxQuz3O7QDLCF2lB/view?usp=sharing

https://drive.google.com/file/d/1Vr0RFApIrbp3muOsqzdjEXOB53lQNh1k/view?usp=sharing

CHAPTER 5: SUMMARY AND FUTURE WORKS

Methane is an important greenhouse gas with a significant role in the evolution of Earth's carbon cycle and the ongoing climate change. Subsurface marine methane reservoirs constitute a large exchangeable carbon pool significant for the climate system. Ocean margins are often characterized by the transport of subsurface methane towards the seafloor. Some of the abrupt climate change events in paleoclimate records are potentially linked to massive dissociation of subsurface methane reservoirs into the oceans and atmosphere. Furthermore, recent studies have shown that methane seepage sites can significantly impact regional organic carbon cycling.

Modern methane fluxes in the ocean floor can be detected using geochemical, geophysical, and remote sensing techniques. Methane induced biogeochemical signatures imprinted onto sedimentary records by such events are poorly constrained and require appropriate geological proxies that record methane seepage and quantify the timing of formation. This uncertainty hinders our ability to reconstruct the temporal and spatial variations of past methane seepage and is an important scientific challenge towards our understanding of the properties and processes governing the flow and storage of carbon in subseafloor. This dissertation studied the impact of subsurface methane transport towards the shallow sedimentary environments at the present-day setting intending to improve our ability to evaluate methane induced biogeochemistry in ancient environments from sediment records.

The first chapter introduced methane induced biogeochemistry in shallow sediment settings. This chapter highlighted a significant methane carbon pool in the subsurface that can

interact with shallow sediments and the water column-atmosphere system to support a methane-powered carbon cycling, relevant to ocean chemistry and climate system.

The second chapter provided a quantification of methane induced carbon cycling in diffusive methane flux settings in a global context. In diffusion controlled-settings, methane entering from the subsurface is almost completely consumed within the shallow sediments at a sediment interval known as the sulfate-methane transition zone (SMTZ), where microbially driven anaerobic oxidation of methane (AOM) process converts the methane carbon to dissolved inorganic carbon (DIC). This chapter quantified DIC cycling in methane charged shallow sediments and reported a significant carbon flux contribution from the SMTZ towards the water column and to sediment carbon burial. The study highlighted the importance of SMTZ as not only a methane sink but also an important diagenetic front for global DIC cycling.

The first two chapters emphasized that marine methane reservoirs and their interaction to shallow sediment-water column-atmosphere system acts as an important intermediate in the global carbon cycle (Fig. 5.1)

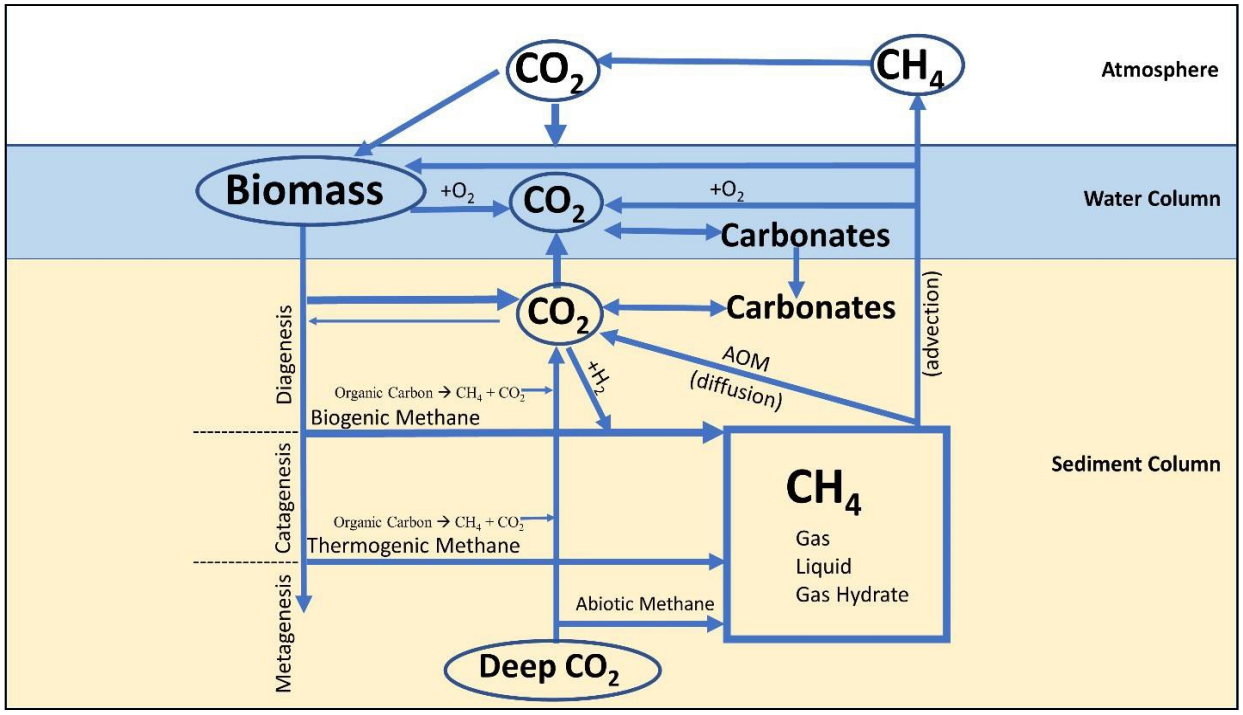

Figure 5.1 Generalized representation of marine methane cycle acting as an intermediate in the global carbon cycle.

The third chapter studied authigenic carbonates, an important geological archive for past methane seepage events, to reconstruct the carbon-sulfur geochemical coupling associated with a seep system from the southern Gulf of Mexico (GoM). Authigenic carbonates in seep settings are formed due to the alkalinity production resulting from the sulfate reduction coupled to hydrocarbon oxidation. This study reported distinguishable variation in sulfate reduction coupled with methane and non-methane hydrocarbon oxidation, recorded in the sulfide and DIC pool, that can be recognized from sedimentary records using stable isotope records of carbonate carbon ($\delta^{13}C_{carbonate}$) and pyrite sulfur ($\delta^{34}S_{pyrite}$). This study also provided additional evidence to the existing hypothesis that vigorous seep activation could have occurred in the GoM slopes

during the last deglaciation, based on the evidence from radioactive U-Th dates of seep carbonates.

The fourth chapter studied the organic molecular fossil records imprinted on sediment records from the Japan Sea and Peru Margin. This study focused on the Isoprenoid Glycerol dialkyl glycerol tetraethers (GDGTs), which are core lipid membranes produced by Archaea, often well preserved in sediment records. Using a high-resolution HPLC approach involving two silica columns and Orbitrap Fusion Mass Spectrometer, this study reports novel GDGT isomers with concentration peaking at the SMTZ and almost absent above and below the SMTZ. The observations suggested that these characteristic isomers of GDGT compounds in the study sites are sourced from methanotrophic archaea and their identification serves an important paleoceanographic tool to study the temporal variations of methane fluxes in the past from sediment records.

Key areas of future works to expand on the results obtained from this dissertation include (i) inclusion of advective settings to the global DIC budget prepared for diffusive methane charged settings (ii) quantification on the rates of sulfide oxidation and carbonate authigenesis in diverse and globally distributed settings characterized by subsurface methane fluxes to improve existing understanding on the impact of DIC outflux to ocean chemistry (iii) additional S isotope studies involving $\delta^{18}O$ and $\delta^{34}S$ of CAS as well as $\delta^{34}S$ of organic S pool to provide a broader picture of diagenetic sulfur cycling at seeps (iv) additional biomarker works from methane flux settings incorporating hopanoids of BSR to provide additional insight into the sulfate reduction processes (v) expansion of methane index to incorporate ANME 2 compounds and thereby an

opportunity for semi quantitative reconstruction of methane flux intensities from sediment records.

REFERENCES

Aharon, P. (2000). "Microbial processes and products fueled by hydrocarbons at submarine seeps," in *Microbial sediments*. Springer), 270-281.

Aharon, P., and Fu, B. (2000). Microbial sulfate reduction rates and sulfur and oxygen isotope fractionations at oil and gas seeps in deepwater Gulf of Mexico. *Geochimica et Cosmochimica Acta* 64**,** 233-246.

Aharon, P., and Fu, B. (2003). Sulfur and oxygen isotopes of coeval sulfate–sulfide in pore fluids of cold seep sediments with sharp redox gradients. *Chemical Geology* 195**,** 201-218.

Aharon, P., Schwarcz, H.P., and Roberts, H.H. (1997). Radiometric dating of submarine hydrocarbon seeps in the Gulf of Mexico. *Geological Society of America Bulletin* 109**,** 568-579.

Akam, S.A., Coffin, R.B., Abdulla, H.a.N., and Lyons, T.W. (2020). Dissolved Inorganic Carbon Pump in Methane-Charged Shallow Marine Sediments: State of the Art and New Model Perspectives. *Frontiers in Marine Science* 7, 206

Akam, S.A., Coffin, R.B., Lyons, T., Bates, S.M., Reese, B.K., and Clarkson, C.C. (2019). "Reconstructing the Carbon-Sulfur Geochemistry of Hydrocarbon Seeps at the Gulf of Mexico from Authigenic Carbonates", in: *AGU Fall Meeting 2019*: AGU).

Aleksandra, B.-G., and Katarzyna, Ł.-M. (2018). Porewater dissolved organic and inorganic carbon in relation to methane occurrence in sediments of the Gdańsk Basin (southern Baltic Sea). *Continental Shelf Research* 168**,** 11-20.

Alexander, T., Toelle, B., Baihly, J., Boyer, C., Clark, B., Waters, G., Jochen, V., Le Calvez, J., Lewis, R., Miller, C., and Thaeler, J. (2011). Shale Gas Revolution. *Oilfield Review* 23.

Aloisi, G., Bouloubassi, I., Heijs, S.K., Pancost, R.D., Pierre, C., Sinninghe Damsté, J.S., Gottschal, J.C., Forney, L.J., and Rouchy, J.-M. (2002). CH4-consuming microorganisms and the formation of carbonate crusts at cold seeps. *Earth and Planetary Science Letters* 203**,** 195-203.

Aloisi, G., Wallmann, K., Drews, M., and Bohrmann, G. (2004). Evidence for the submarine weathering of silicate minerals in Black Sea sediments: possible implications for the marine Li and B cycles. *Geochemistry, Geophysics, Geosystems* 5 (4)

Amiotte Suchet, P., Probst, J.L., and Ludwig, W. (2003). Worldwide distribution of continental rock lithology: Implications for the atmospheric/soil CO2 uptake by continental weathering and alkalinity river transport to the oceans. *Global Biogeochemical Cycles* 17 (2).

Andersen, M., Stirling, C., Zimmermann, B., and Halliday, A. (2010). Precise determination of the open ocean 234U/238U composition. *Geochemistry, Geophysics, Geosystems* 11 (12).

Antler, G., Turchyn, A.V., Herut, B., and Sivan, O. (2015). A unique isotopic fingerprint of sulfate-driven anaerobic oxidation of methane. *Geology* 43**,** 619-622.

Aquilina, A., Knab, N., Knittel, K., Kaur, G., Geissler, A., Kelly, S., Fossing, H., Boot, C., Parkes, R.J., and Mills, R. (2010). Biomarker indicators for anaerobic oxidizers of methane in brackish-marine sediments with diffusive methane fluxes. *Organic Geochemistry* 41**,** 414-426.

Archer, D., Buffett, B., and Brovkin, V. (2009). Ocean methane hydrates as a slow tipping point in the global carbon cycle. *Proceedings of the National Academy of Sciences* 106**,** 20596-20601.

Archer, D.E. (1996). An atlas of the distribution of calcium carbonate in sediments of the deep sea. *Global Biogeochemical Cycles* 10**,** 159-174.

Argentino, C., Johnson, J., Conti, S., Fioroni, C., and Fontana, D. (2020). Preservation of 34 S-enriched sulfides in fossil sulfate-methane transition zones: new evidence from Miocene outcrops of the northern Apennines (Italy). *Geo-Marine Letters***,** 1-12.

Aufdenkampe, A.K., Mayorga, E., Raymond, P.A., Melack, J.M., Doney, S.C., Alin, S.R., Aalto, R.E., and Yoo, K. (2011). Riverine coupling of biogeochemical cycles between land, oceans, and atmosphere. *Frontiers in Ecology and the Environment* 9**,** 53-60.

Badesab, F., Gaikwad, V., and Dewangan, P. (2019). Controls on greigite preservation in a gas hydrate system of the Krishna-Godavari basin, Bay of Bengal. *Geo-Marine Letters*.

Baker, P.A., and Burns, S.J. (1985). Occurrence and formation of dolomite in organic-rich continental margin sediments. *AAPG Bulletin* 69**,** 1917-1930.

Bange, H.W. (2006). Nitrous oxide and methane in European coastal waters. *Estuarine, Coastal and Shelf Science* 70**,** 361-374.

Bange, H.W., Bartell, U., Rapsomanikis, S., and Andreae, M.O. (1994). Methane in the Baltic and North Seas and a reassessment of the marine emissions of methane. *Global biogeochemical cycles* 8**,** 465-480.

Barnes, R., and Goldberg, E. (1976). Methane production and consumption in anoxic marine sediments. *Geology* 4**,** 297-300.

Bayon, G., Henderson, G., and Bohn, M. (2009). U–Th stratigraphy of a cold seep carbonate crust. *Chemical Geology* 260**,** 47-56.

Bayon, G., Henderson, G.M., Etoubleau, J., Caprais, J.-C., Ruffine, L., Marsset, T., Dennielou, B., Cauquil, E., Voisset, M., and Sultan, N. (2015). U-Th isotope constraints on gas hydrate and pockmark dynamics at the Niger delta margin. *Marine Geology* 370**,** 87-98.

Bayon, G., Pierre, C., Etoubleau, J., Voisset, M., Cauquil, E., Marsset, T., Sultan, N., Le Drezen, E., and Fouquet, Y. (2007). Sr/Ca and Mg/Ca ratios in Niger Delta sediments: implications for authigenic carbonate genesis in cold seep environments. *Marine Geology* 241**,** 93-109.

Bazzaro, M., Ogrinc, N., Relitti, F., Lucchi, R.G., Giani, M., Adami, G., Pavoni, E., and De Vittor, C. (2020). Geochemical signatures of intense episodic anaerobic oxidation of methane in near-surface sediments of a recently discovered cold seep (Kveithola trough, NW Barents Sea). *Marine Geology***,** 106189.

Beal, E.J., House, C.H., and Orphan, V.J. (2009). Manganese-and iron-dependent marine methane oxidation. *Science* 325**,** 184-187.

Becker, K.W., Lipp, J.S., Zhu, C., Liu, X.-L., and Hinrichs, K.-U. (2013). An improved method for the analysis of archaeal and bacterial ether core lipids. *Organic Geochemistry* 61**,** 34-44.

Berelson, W., Balch, W., Najjar, R., Feely, R., Sabine, C., and Lee, K. (2007). Relating estimates of CaCO3 production, export, and dissolution in the water column to measurements of CaCO3 rain into sediment traps and dissolution on the sea floor: A revised global carbonate budget. *Global Biogeochemical Cycles* 21 (1).

Berelson, W.M., Prokopenko, M., Sansone, F., Graham, A., Mcmanus, J., and Bernhard, J.M. (2005). Anaerobic diagenesis of silica and carbon in continental margin sediments: discrete zones of TCO 2 production. *Geochimica et Cosmochimica Acta* 69**,** 4611-4629.

Berg, R.D. (2018). *Quantifying the deep: The importance of diagenetic reactions to marine geochemical cycles. Ph.D. Thesis, University of Washington, Washington, D.C.*

Berg, R.D., Solomon, E.A., and Teng, F.-Z. (2019). The role of marine sediment diagenesis in the modern oceanic magnesium cycle. *Nature communications* 10**,** 1-10.

Berndt, C., Feseker, T., Treude, T., Krastel, S., Liebetrau, V., Niemann, H., Bertics, V.J., Dumke, I., Dünnbier, K., and Ferré, B. (2014). Temporal constraints on hydrate-controlled methane seepage off Svalbard. *Science* 343**,** 284-287.

Berner, R.A. (1982). Burial of organic carbon and pyrite sulfur in the modern ocean: its geochemical and environmental significance. *Am. J. Sci.;(United States)* 282.

Berner, R.A. (2003). The long-term carbon cycle, fossil fuels and atmospheric composition. *Nature* 426**,** 323-326.

Berner, R.A. (2004). *The Phanerozoic Carbon Cycle : CO_2 and O_2.* Cary, UNITED STATES: Oxford University Press, Incorporated.

Beulig, F., Roy, H., Mcglynn, S.E., and Jorgensen, B.B. (2019). Cryptic CH_4 cycling in the sulfate-methane transition of marine sediments apparently mediated by ANME-1 archaea. *ISME J* 13**,** 250-262.

Bian, Y., Feng, D., Roberts, H.H., and Chen, D. (2013). Tracing the evolution of seep fluids from authigenic carbonates: Green Canyon, northern Gulf of Mexico. *Marine and petroleum geology* 44**,** 71-81.

Biastoch, A., Treude, T., Rüpke, L.H., Riebesell, U., Roth, C., Burwicz, E.B., Park, W., Latif, M., Böning, C.W., and Madec, G. (2011). Rising Arctic Ocean temperatures cause gas hydrate destabilization and ocean acidification. *Geophysical Research Letters* 38 (8).

Bickle, M., Arculus, R., Barrett, P., Deconto, R., Camoin, G., Edwards, K., Fisher, F., Inagaki, F., Kodaira, S., and Ohkouchi, N. (2011). Illuminating Earth's Past, Present and Future The Science Plan for the International Ocean Discovery Program 2013-2023.

Biddle, J.F., Lipp, J.S., Lever, M.A., Lloyd, K.G., Sørensen, K.B., Anderson, R., Fredricks, H.F., Elvert, M., Kelly, T.J., and Schrag, D.P. (2006). Heterotrophic Archaea dominate sedimentary subsurface ecosystems off Peru. *Proceedings of the National Academy of Sciences of the United States of America* 103**,** 3846-3851.

Birgel, D., Elvert, M., Han, X., and Peckmann, J. (2008). 13 C-depleted biphytanic diacids as tracers of past anaerobic oxidation of methane. *Organic Geochemistry* 39**,** 152-156.

Birgel, D., Feng, D., Roberts, H.H., and Peckmann, J. (2011). Changing redox conditions at cold seeps as revealed by authigenic carbonates from Alaminos Canyon, northern Gulf of Mexico. *Chemical Geology* 285**,** 82-96.

Birgel, D., Guido, A., Liu, X., Hinrichs, K.-U., Gier, S., and Peckmann, J. (2014). Hypersaline conditions during deposition of the Calcare di Base revealed from archaeal di- and tetraether inventories. *Organic Geochemistry* 77**,** 11-21.

Birgel, D., and Peckmann, J. (2008). Aerobic methanotrophy at ancient marine methane seeps: a synthesis. *Organic Geochemistry* 39**,** 1659-1667.

Birgel, D., Peckmann, J., Klautzsch, S., Thiel, V., and Reitner, J. (2006a). Anaerobic and aerobic oxidation of methane at Late Cretaceous seeps in the Western Interior Seaway, USA. *Geomicrobiology Journal* 23**,** 565-577.

Birgel, D., Thiel, V., Hinrichs, K.-U., Elvert, M., Campbell, K.A., Reitner, J., Farmer, J.D., and Peckmann, J. (2006b). Lipid biomarker patterns of methane-seep microbialites from the Mesozoic convergent margin of California. *Organic Geochemistry* 37**,** 1289-1302.

Bjerrum, C.J., and Canfield, D.E. (2011). Towards a quantitative understanding of the late Neoproterozoic carbon cycle. *Proceedings of the National Academy of Sciences* 108**,** 5542-5547.

Blaga, C.I., Reichart, G.-J., Heiri, O., and Damsté, J.S.S. (2009). Tetraether membrane lipid distributions in water-column particulate matter and sediments: a study of 47 European lakes along a north–south transect. *Journal of Paleolimnology* 41**,** 523-540.

Blumenberg, M., Pape, T., Seifert, R., Bohrmann, G., and Schlömer, S. (2018). Can hydrocarbons entrapped in seep carbonates serve as gas geochemistry recorder? *Geo-Marine Letters* 38**,** 121-129.

Blumenberg, M., Seifert, R., Reitner, J., Pape, T., and Michaelis, W. (2004). Membrane lipid patterns typify distinct anaerobic methanotrophic consortia. *PNAS* 101**,** 11111-11116.

Bock, M., Schmitt, J., Möller, L., Spahni, R., Blunier, T., and Fischer, H. (2010). Hydrogen isotopes preclude marine hydrate CH4 emissions at the onset of Dansgaard-Oeschger events. *Science* 328**,** 1686-1689.

Boetius, A., Ravenschlag, K., Schubert, C.J., Rickert, D., Widdel, F., Gieseke, A., Amann, R., Jørgensen, B.B., Witte, U., and Pfannkuche, O. (2000). A marine microbial consortium apparently mediating anaerobic oxidation of methane. *Nature* 407**,** 623-626.

Boetius, A., and Wenzhöfer, F. (2013). Seafloor oxygen consumption fuelled by methane from cold seeps. *Nature Geoscience* 6**,** 725-734.

Bohrmann, G. (2008). *Fluid Seepage in the Southern Gulf of Mexico (Campeche Bay): M67, Leg 2a, Cristobal-Tampico, 14 March-31 March, 2006: M67, Leg 2b, Tampico-Bridgetown, 3 April-25 April, 2006.* Fachbereich Geowissenschaften, Universität Bremen.

Bohrmann, G. (2013). "Asphalt Volcanism," in *Encyclopedia of Marine Geosciences,* eds. J. Harff, M. Meschede, S. Petersen & J. Thiede. (Dordrecht: Springer Netherlands), 1-3.

Bohrmann, G., and Schenck, S. (2004). RV SONNE cruise report SO174, OTEGA II, Balboa− Corpus Christi− Miami (1 October− 12 November, 2003). *GEOMAR report* 117**,** 130.

Borowski, W.S., Paull, C.K., and Ussler Iii, W. (1997). Carbon cycling within the upper methanogenic zone of continental rise sediments; an example from the methane-rich sediments overlying the Blake Ridge gas hydrate deposits. *Marine Chemistry* 57**,** 299-311.

Borowski, W.S., Paull, C.K., and Ussler, W. (1996). Marine pore-water sulfate profiles indicate in situ methane flux from underlying gas hydrate. *Geology* 24**,** 655-658.

Borowski, W.S., Rodriguez, N.M., Paull, C.K., and Ussler, W. (2013). Are 34 S-enriched authigenic sulfide minerals a proxy for elevated methane flux and gas hydrates in the geologic record? *Marine and Petroleum Geology* 43**,** 381-395.

Borrel, G., O'toole, P.W., Harris, H.M., Peyret, P., Brugere, J.-F., and Gribaldo, S. (2013). Phylogenomic data support a seventh order of methylotrophic methanogens and provide insights into the evolution of methanogenesis. *Genome biology and evolution* 5**,** 1769-1780.

Boswell, R., and Collett, T.S. (2011). Current perspectives on gas hydrate resources. *Energy & environmental science* 4**,** 1206-1215.

Boswell, R., Yamamoto, K., Lee, S.-R., Collett, T., Kumar, P., and Dallimore, S. (2014). "Chapter 8 - Methane Hydrates," in *Future Energy (Second Edition),* ed. T.M. Letcher. (Boston: Elsevier), 159-178.

Boudreau, B.P., Luo, Y., Meysman, F.J., Middelburg, J.J., and Dickens, G.R. (2015). Gas hydrate dissociation prolongs acidification of the Anthropocene oceans. *Geophysical Research Letters* 42**,** 9337-9344A.

Bowles, M.W., Mogollón, J.M., Kasten, S., Zabel, M., and Hinrichs, K.-U. (2014). Global rates of marine sulfate reduction and implications for sub–sea-floor metabolic activities. *Science* 344**,** 889-891.

Bowles, M.W., Samarkin, V.A., Bowles, K.M., and Joye, S.B. (2011). Weak coupling between sulfate reduction and the anaerobic oxidation of methane in methane-rich seafloor sediments during ex situ incubation. *Geochimica et Cosmochimica Acta* 75**,** 500-519.

Bradbury, H.J., and Turchyn, A.V. (2019). Reevaluating the carbon sink due to sedimentary carbonate formation in modern marine sediments. *Earth and Planetary Science Letters* 519**,** 40-49.

Brenner, H., Braeckman, U., Le Guitton, M., and Meysman, F.J. (2016). The impact of sedimentary alkalinity release on the water column CO 2 system in the North Sea. *Biogeosciences* 13**,** 841-863.

Bristow, T.F., and Grotzinger, J.P. (2013). Sulfate availability and the geological record of cold-seep deposits. *Geology* 41**,** 811-814.

Brooks, J.M., Wiesenburg, D.A., Roberts, H., Carney, R.S., Macdonald, I.R., Fisher, C.R., Guinasso Jr, N.L., Sager, W.W., Mcdonald, S.J., and Burke Jr, R.A. (1990). Salt, seeps and symbiosis in the Gulf of Mexico. *Eos, Transactions American Geophysical Union* 71**,** 1772-1773.

Brüning, M., Sahling, H., Macdonald, I.R., Ding, F., and Bohrmann, G. (2010). Origin, distribution, and alteration of asphalts at Chapopote Knoll, Southern Gulf of Mexico. *Marine and petroleum geology* 27**,** 1093-1106.

Bryant, W.R., Lugo, J., Córdova, C., and Salvador, A. (1991). Physiography and bathymetry. *The Gulf of Mexico Basin: Boulder, Geological Society of America, Decade of North American Geology, v. J***,** 13-30.

Burdige, D.J. (2007). Preservation of organic matter in marine sediments: controls, mechanisms, and an imbalance in sediment organic carbon budgets? *Chem Rev* 107**,** 467-485.

Burdige, D.J., and Komada, T. (2011). Anaerobic oxidation of methane and the stoichiometry of remineralization processes in continental margin sediments. *Limnology and Oceanography* 56**,** 1781-1796.

Burkett, A.M., Rathburn, A.E., Pérez, M.E., Levin, L.A., Cha, H., and Rouse, G.W. (2015). Phylogenetic placement of Cibicidoides wuellerstorfi (Schwager, 1866) from methane seeps and non-seep habitats on the Pacific margin. *Geobiology* 13**,** 44-52.

Burton, E.A. (1993). Controls on marine carbonate cement mineralogy: review and reassessment. *Chemical Geology* 105**,** 163-179.

Burton, E.A., and Walter, L.M. (1990). The role of pH in phosphate inhibition of calcite and aragonite precipitation rates in seawater. *Geochimica et Cosmochimica Acta* 54**,** 797-808.

Caesar, K.H., Kyle, J.R., Lyons, T.W., Tripati, A., and Loyd, S.J. (2019). Carbonate formation in salt dome cap rocks by microbial anaerobic oxidation of methane. *Nat Commun* 10**,** 808.

Campbell, K.A. (2006). Hydrocarbon seep and hydrothermal vent paleoenvironments and paleontology: past developments and future research directions. *Palaeogeography, Palaeoclimatology, Palaeoecology* 232**,** 362-407.

Canet, C., Prol-Ledesma, R.M., Escobar-Briones, E., Mortera-Gutiérrez, C., Lozano-Santa Cruz, R., Linares, C., Cienfuegos, E., and Morales-Puente, P. (2006). Mineralogical and geochemical characterization of hydrocarbon seep sediments from the Gulf of Mexico. *Marine and Petroleum Geology* 23**,** 605-619.

Canfield, D. (2001). Biogeochemistry of sulfur isotopes. *Reviews in Mineralogy and Geochemistry* 43**,** 607-636.

Canfield, D.E., and Kump, L.R. (2013). Carbon cycle makeover. *Science* 339**,** 533-534.

Canfield, D.E., Raiswell, R., Westrich, J.T., Reaves, C.M., and Berner, R.A. (1986). The use of chromium reduction in the analysis of reduced inorganic sulfur in sediments and shales. *Chemical geology* 54**,** 149-155.

Canfield, D.E., and Teske, A. (1996). Late Proterozoic rise in atmospheric oxygen concentration inferred from phylogenetic and sulphur-isotope studies. *Nature* 382**,** 127-132.

Chambers, L.A., Trudinger, P.A., Smith, J.W., and Burns, M.S. (1975). Fractionation of sulfur isotopes by continuous cultures of Desulfovibrio desulfuricans. *Canadian Journal of Microbiology* 21**,** 1602-1607.

Chatterjee, S., Dickens, G.R., Bhatnagar, G., Chapman, W.G., Dugan, B., Snyder, G.T., and Hirasaki, G.J. (2011). Pore water sulfate, alkalinity, and carbon isotope profiles in shallow sediment above marine gas hydrate systems: A numerical modeling perspective. *Journal of Geophysical Research: Solid Earth* 116 (B9).

Chen, C.-T.A. (2002). Shelf-vs. dissolution-generated alkalinity above the chemical lysocline. *Deep Sea Research Part II: Topical Studies in Oceanography* 49**,** 5365-5375.

Chen, C.T.A., and Wang, S.L. (1999). Carbon, alkalinity and nutrient budgets on the East China Sea continental shelf. *Journal of Geophysical Research: Oceans* 104**,** 20675-20686.

Chen, F., Wang, X., Li, N., Cao, J., Bayon, G., Peckmann, J., Hu, Y., Gong, S., Cheng, H., and Edwards, R.L. (2019). Gas hydrate dissociation during sea-level highstand inferred from U/Th dating of seep carbonate from the South China Sea. *Geophysical Research Letters* 46**,** 13928-13938.

Cheng, H., Edwards, R.L., Shen, C.-C., Polyak, V.J., Asmerom, Y., Woodhead, J., Hellstrom, J., Wang, Y., Kong, X., and Spötl, C. (2013). Improvements in 230Th dating, 230Th and 234U half-life values, and U–Th isotopic measurements by multi-collector inductively coupled plasma mass spectrometry. *Earth and Planetary Science Letters* 371**,** 82-91.

Chuang, P.-C., Yang, T.F., Wallmann, K., Matsumoto, R., Hu, C.-Y., Chen, H.-W., Lin, S., Sun, C.-H., Li, H.-C., and Wang, Y. (2019). Carbon isotope exchange during anaerobic oxidation of methane (AOM) in sediments of the northeastern South China Sea. *Geochimica et Cosmochimica Acta* 246**,** 138-155.

Claypool, G.E., and Kaplan, I. (1974). "The origin and distribution of methane in marine sediments," in *Natural gases in marine sediments*. Springer), 99-139.

Coffin, R., Hamdan, L., Plummer, R., Smith, J., Gardner, J., Hagen, R., and Wood, W. (2008). Analysis of methane and sulfate flux in methane-charged sediments from the Mississippi Canyon, Gulf of Mexico. *Marine and Petroleum Geology* 25**,** 977-987.

Coffin, R., Hamdan, L., Smith, J., Rose, P., Plummer, R., Yoza, B., Pecher, I., and Montgomery, M. (2014). Contribution of vertical methane flux to shallow sediment carbon pools across Porangahau Ridge, New Zealand. *Energies* 7**,** 5332-5356.

Coffin, R.B., Osburn, C.L., Plummer, R.E., Smith, J.P., Rose, P.S., and Grabowski, K.S. (2015). Deep sediment-sourced methane contribution to shallow sediment organic carbon: atwater valley, texas-louisiana shelf, gulf of mexico. *Energies* 8**,** 1561-1583.

Colangelo-Lillis, J., Pelikan, C., Herbold, C.W., Altshuler, I., Loy, A., Whyte, L.G., and Wing, B.A. (2019). Diversity decoupled from sulfur isotope fractionation in a sulfate-reducing microbial community. *Geobiology* 17**,** 660-675.

Collett, T.S., and Kuuskraa, V.A. (1998). Hydrates contain vast store of world gas resources. *Oil and Gas Journal* 96**,** 90-94.

Contreras, S., Meister, P., Liu, B., Prieto-Mollar, X., Hinrichs, K.-U., Khalili, A., Ferdelman, T.G., Kuypers, M.M., and Jørgensen, B.B. (2013). Cyclic 100-ka (glacial-interglacial) migration of subseafloor redox zonation on the Peruvian shelf. *Proceedings of the National Academy of Sciences* 110**,** 18098-18103.

National Research Council (2003). *Oil in the sea III: inputs, fates, and effects.* National Academies Press (US).

Cremiere, A. (2015). "Cold seep carbonates along the Norwegian margin, insights into U-Th geochronology and S geochemistry", in: *2015 AGU Fall Meeting*: Agu).

Crémière, A., Lepland, A., Chand, S., Sahy, D., Condon, D.J., Noble, S.R., Martma, T., Thorsnes, T., Sauer, S., and Brunstad, H. (2016). Timescales of methane seepage on the Norwegian margin following collapse of the Scandinavian Ice Sheet. *Nature communications* 7.

Crémière, A., Pellerin, A., Wing, B.A., and Lepland, A. (2020). Multiple sulfur isotopes in methane seep carbonates track unsteady sulfur cycling during anaerobic methane oxidation. *Earth and Planetary Science Letters* 532**,** 115994.

Crémière, A., Pierre, C., Blanc-Valleron, M.-M., Zitter, T., Çağatay, M.N., and Henry, P. (2012). Methane-derived authigenic carbonates along the North Anatolian fault system in the Sea

of Marmara (Turkey). *Deep Sea Research Part I: Oceanographic Research Papers* 66**,** 114-130.

Cressot, C., Pison, I., Rayner, P.J., Bousquet, P., Fortems-Cheiney, A., and Chevallier, F. Can we detect regional methane anomalies? A comparison between three observing systems.

Cui, H., Kaufman, A.J., Xiao, S., Zhou, C., and Liu, X.-M. (2017). Was the Ediacaran Shuram Excursion a globally synchronized early diagenetic event? Insights from methane-derived authigenic carbonates in the uppermost Doushantuo Formation, South China. *Chemical Geology* 450**,** 59-80.

Cui, M., Ma, A., Qi, H., Zhuang, X., and Zhuang, G. (2015). Anaerobic oxidation of methane: an "active" microbial process. *MicrobiologyOpen* 4**,** 1-11.

D'hondt, S., Jørgensen, B., Miller, D., Aiello, I., Bekins, B., and Blake, R. (2003). "Leg 201 Initial Report–controls on microbial communities in deeply buried sediments, Eastern Equatorial Pacific and Peru Margin", in: *Proc. ODP, Init. Repts.*).

D'souza, N., Subramaniam, A., Juhl, A.R., Hafez, M., Chekalyuk, A., Phan, S., Yan, B., Macdonald, I., Weber, S., and Montoya, J. (2016). Elevated surface chlorophyll associated with natural oil seeps in the Gulf of Mexico. *Nature Geoscience*.

Damm, E., Helmke, E., Thoms, S., Schauer, U., Nöthig, E., Bakker, K., and Kiene, R.P. (2010). Methane production in aerobic oligotrophic surface water in the central Arctic Ocean. *Biogeosciences* 7**,** 1099-1108.

Damsté, J.S.S., Rijpstra, W.I.C., Hopmans, E.C., Prahl, F.G., Wakeham, S.G., and Schouten, S. (2002). Distribution of membrane lipids of planktonic Crenarchaeota in the Arabian Sea. *Appl. Environ. Microbiol.* 68**,** 2997-3002.

Davidson, D.W., Leaist, D.G., and Hesse, R. (1983). Oxygen-18 enrichment in the water of a clathrate hydrate. *Geochimica et Cosmochimica Acta* 47**,** 2293-2295.

Davis Barnes, B., Husson, J.M., and Peters, S.E. (2019). Authigenic Carbonate Burial in the Late Devonian–Early Mississippian Bakken Formation (Williston Basin, USA). *Sedimentology* 67, 2065-2094 .

De Garidel-Thoron, T., Beaufort, L., Bassinot, F., and Henry, P. (2004). Evidence for large methane releases to the atmosphere from deep-sea gas-hydrate dissociation during the last glacial episode. *Proceedings of the National Academy of Sciences of the United States of America* 101**,** 9187-9192.

Dean, J.F. (2020). Old methane and modern climate change. *Science* 367**,** 846.

Dean, J.F., Middelburg, J.J., Röckmann, T., Aerts, R., Blauw, L.G., Egger, M., Jetten, M.S., Jong, A.E., Meisel, O.H., and Rasigraf, O. (2018). Methane feedbacks to the global climate system in a warmer world. *Reviews of Geophysics* 56, 207-250

Derry, L. (2014). Organic carbon cycling and the lithosphere. *Treatise on Geochemistry 2nd Edition*, 239-249

Detmers, J., Brüchert, V., Habicht, K.S., and Kuever, J. (2001). Diversity of sulfur isotope fractionations by sulfate-reducing prokaryotes. *Applied and Environmental Microbiology* 67**,** 888-894.

Dickens, G.R. (2001). Sulfate profiles and barium fronts in sediment on the Blake Ridge: present and past methane fluxes through a large gas hydrate reservoir. *Geochimica et Cosmochimica Acta* 65**,** 529-543.

Dickens, G.R. (2003). Rethinking the global carbon cycle with a large, dynamic and microbially mediated gas hydrate capacitor. *Earth and Planetary Science Letters* 213**,** 169-183.

Dickens, G.R. (2011). Down the rabbit hole: Toward appropriate discussion of methane release from gas hydrate systems during the Paleocene-Eocene thermal maximum and other past hyperthermal events. *Climate of the Past* 7**,** 831-846.

Dickens, G.R., O'neil, J.R., Rea, D.K., and Owen, R.M. (1995). Dissociation of oceanic methane hydrate as a cause of the carbon isotope excursion at the end of the Paleocene. *Paleoceanography* 10**,** 965-971.

Dickens, G.R., and Snyder, G.T. (2009). Interpreting upward methane flux from marine pore water profiles. *Fire in the Ice, winter***,** 7-10.

Ding, F., Spiess, V., Brüning, M., Fekete, N., Keil, H., and Bohrmann, G. (2008). A conceptual model for hydrocarbon accumulation and seepage processes around Chapopote asphalt site, southern Gulf of Mexico: from high resolution seismic point of view. *Journal of Geophysical Research: Solid Earth* 113.

Ding, F., Spiess, V., Macdonald, I.R., Brüning, M., Fekete, N., and Bohrmann, G. (2010). Shallow sediment deformation styles in north-western Campeche Knolls, Gulf of Mexico and their controls on the occurrence of hydrocarbon seepage. *Marine and petroleum geology* 27**,** 959-972.

Dlugokencky, E.J., Nisbet, E.G., Fisher, R., and Lowry, D. (2011). Global atmospheric methane: budget, changes and dangers. *Philosophical Transactions of the Royal Society A: Mathematical, Physical and Engineering Sciences* 369**,** 2058-2072.

Doney, S.C., Fabry, V.J., Feely, R.A., and Kleypas, J.A. (2009). Ocean acidification: the other CO2 problem. *Ann Rev Mar Sci* 1**,** 169-192.

Dong, L., Li, Z., and Jia, G. (2019). Archaeal ammonia oxidation plays a part in late Quaternary nitrogen cycling in the South China Sea. *Earth and Planetary Science Letters* 509**,** 38-46.

Edwards, R.L., Chen, J., and Wasserburg, G. (1987). 238U234U230Th232Th systematics and the precise measurement of time over the past 500,000 years. *Earth and Planetary Science Letters* 81**,** 175-192.

Egger, M., Jilbert, T., Behrends, T., Rivard, C., and Slomp, C.P. (2015). Vivianite is a major sink for phosphorus in methanogenic coastal surface sediments. *Geochimica et Cosmochimica Acta* 169**,** 217-235.

Egger, M., Riedinger, N., Mogollón, J.M., and Jørgensen, B.B. (2018). Global diffusive fluxes of methane in marine sediments. *Nature Geoscience* 11**,** 421.

Elvert, M., Hopmans, E., Treude, T., Boetius, A., and Suess, E. (2005). Spatial variations of methanotrophic consortia at cold methane seeps: implications from a high-resolution molecular and isotopic approach. *Geobiology* 3**,** 195-209.

Elvert, M., Suess, E., Greinert, J., and Whiticar, M.J. (2000). Archaea mediating anaerobic methane oxidation in deep-sea sediments at cold seeps of the eastern Aleutian subduction zone. *Organic Geochemistry* 31**,** 1175-1187.

Escobar-Briones, E., and García-Villalobos, F.J. (2009). Distribution of total organic carbon and total nitrogen in deep-sea sediments from the southwestern Gulf of Mexico. *Boletín de la Sociedad Geológica Mexicana* 61**,** 73-86.

Etiope, G. (2012). Climate science: Methane uncovered. *Nature Geoscience* 5**,** 373.

Etiope, G. (2017). Natural Gas. *Encyclopedia of Geochemistry: A Comprehensive Reference Source on the Chemistry of the Earth***,** 1-5.

Etiope, G., and Sherwood Lollar, B. (2013). Abiotic methane on Earth. *Reviews of Geophysics* 51**,** 276-299.

Etiope, G., and Whiticar, M. (2019). Abiotic methane in continental ultramafic rock systems: Towards a genetic model. *Applied Geochemistry* 102, 139-152

Etminan, M., Myhre, G., Highwood, E., and Shine, K. (2016). Radiative forcing of carbon dioxide, methane, and nitrous oxide: A significant revision of the methane radiative forcing. *Geophysical Research Letters* 43(24), 12-614.

Ettwig, K.F., Butler, M.K., Le Paslier, D., Pelletier, E., Mangenot, S., Kuypers, M.M., Schreiber, F., Dutilh, B.E., Zedelius, J., De Beer, D., Gloerich, J., Wessels, H.J., Van Alen, T., Luesken, F., Wu, M.L., Van De Pas-Schoonen, K.T., Op Den Camp, H.J., Janssen-Megens, E.M., Francoijs, K.J., Stunnenberg, H., Weissenbach, J., Jetten, M.S., and Strous, M. (2010). Nitrite-driven anaerobic methane oxidation by oxygenic bacteria. *Nature* 464**,** 543-548.

Ettwig, K.F., Zhu, B., Speth, D., Keltjens, J.T., Jetten, M.S.M., and Kartal, B. (2016). Archaea catalyze iron-dependent anaerobic oxidation of methane. *Proc Natl Acad Sci U S A* 113**,** 12792-12796.

Evans, P.N., Boyd, J.A., Leu, A.O., Woodcroft, B.J., Parks, D.H., Hugenholtz, P., and Tyson, G.W. (2019). An evolving view of methane metabolism in the Archaea. *Nat Rev Microbiol* 17**,** 219-232.

Evans, P.N., Parks, D.H., Chadwick, G.L., Robbins, S.J., Orphan, V.J., Golding, S.D., and Tyson, G.W. (2015). Methane metabolism in the archaeal phylum Bathyarchaeota revealed by genome-centric metagenomics. *Science* 350**,** 434-438.

Falkowski, P., Scholes, R., Boyle, E., Canadell, J., Canfield, D., Elser, J., Gruber, N., Hibbard, K., Högberg, P., and Linder, S. (2000). The global carbon cycle: a test of our knowledge of earth as a system. *science* 290**,** 291-296.

Fan, L.-F., Lin, S., Hsu, C.-W., Tseng, Y.-T., Yang, T.F., and Huang, K.-M. (2018). Formation and preservation of authigenic pyrite in the methane dominated environment. *Deep Sea Research Part I: Oceanographic Research Papers* 138**,** 60-71.

Feely, R.A., Doney, S.C., and Cooley, S.R. (2009). Ocean acidification: Present conditions and future changes in a high-CO_2 world. *Oceanography* 22**,** 36-47.

Feng, D., Birgel, D., Peckmann, J., Roberts, H.H., Joye, S.B., Sassen, R., Liu, X.-L., Hinrichs, K.-U., and Chen, D. (2014). Time integrated variation of sources of fluids and seepage dynamics archived in authigenic carbonates from Gulf of Mexico Gas Hydrate Seafloor Observatory. *Chemical Geology* 385**,** 129-139.

Feng, D., Chen, D., Peckmann, J., and Bohrmann, G. (2010a). Authigenic carbonates from methane seeps of the northern Congo fan: microbial formation mechanism. *Marine and Petroleum Geology* 27**,** 748-756.

Feng, D., Chen, D., and Roberts, H.H. (2009). Petrographic and geochemical characterization of seep carbonate from Bush Hill (GC 185) gas vent and hydrate site of the Gulf of Mexico. *Marine and Petroleum Geology* 26**,** 1190-1198.

Feng, D., Peng, Y., Bao, H., Peckmann, J., Roberts, H.H., and Chen, D. (2016). A carbonate-based proxy for sulfate-driven anaerobic oxidation of methane. *Geology***,** G38233. 38231.

Feng, D., and Roberts, H.H. (2011). Geochemical characteristics of the barite deposits at cold seeps from the northern Gulf of Mexico continental slope. *Earth and Planetary Science Letters* 309**,** 89-99.

Feng, D., Roberts, H.H., Cheng, H., Peckmann, J., Bohrmann, G., Edwards, R.L., and Chen, D. (2010b). U/Th dating of cold-seep carbonates: an initial comparison. *Deep Sea Research Part II: Topical Studies in Oceanography* 57**,** 2055-2060.

Ferretti, D.F., Miller, J., White, J., Etheridge, D., Lassey, K., Lowe, D., Meure, C.M., Dreier, M., Trudinger, C., and Van Ommen, T. (2005). Unexpected changes to the global methane budget over the past 2000 years. *science* 309**,** 1714-1717.

Fike, D.A., Bradley, A.S., and Rose, C.V. (2015). Rethinking the Ancient Sulfur Cycle. *Annual Review of Earth and Planetary Sciences* 43**,** 593-622.

Fisher, C., Roberts, H., Cordes, E., and Bernard, B. (2007). Cold seeps and associated communities of the Gulf of Mexico. *Oceanography* 20**,** 118-129.

Florez-Leiva, L., Damm, E., and Farías, L. (2013). Methane production induced by dimethylsulfide in surface water of an upwelling ecosystem. *Progress in Oceanography* 112-113**,** 38-48.

Flügel, E. (2004). *Microfacies of carbonate rocks: analysis, interpretation and application.* Springer Science & Business Media.

Formolo, M.J., and Lyons, T.W. (2013). Sulfur biogeochemistry of cold seeps in the Green Canyon region of the Gulf of Mexico. *Geochimica et Cosmochimica Acta* 119**,** 264-285.

Formolo, M.J., Lyons, T.W., Zhang, C., Kelley, C., Sassen, R., Horita, J., and Cole, D.R. (2004). Quantifying carbon sources in the formation of authigenic carbonates at gas hydrate sites in the Gulf of Mexico. *Chemical Geology* 205**,** 253-264.

Foustoukos, D.I., and Seyfried, W.E. (2004). Hydrocarbons in hydrothermal vent fluids: the role of chromium-bearing catalysts. *Science* 304**,** 1002-1005.

Gallagher, K.L., Kading, T.J., Braissant, O., Dupraz, C., and Visscher, P.T. (2012). Inside the alkalinity engine: the role of electron donors in the organomineralization potential of sulfate-reducing bacteria. *Geobiology* 10**,** 518-530.

Gamo, T., Tsunogai, U., Hirota, A., Nakayama, N., Kang, D.-J., and Kim, K.-R. (2012). First measurements of methane and its carbon isotope ratio in the Japan Sea (East Sea). *Marine Chemistry* 128**,** 92-99.

Ganqing, J., Xiaoying, S., and Shihong, Z. (2006). Methane seeps, methane hydrate destabilization, and the late Neoproterozoic postglacial cap carbonates. *Chinese Science Bulletin* 51**,** 1152-1173.

Garrison, L., and Martin, R.J. (1973). Geologic Structures in the Gulf of Mexico Basin. Geological Survey Professional Paper 773. US Government Printing Office, Washington, DC

Gautam, S.B. (2018). "Anaerobic Methane Oxidizing Microbial Community in a Coastal Marine Sediment: Anaerobic Methanotrophy Dominated by ANME-3," in *Performance Assessment and Enrichment of Anaerobic Methane Oxidizing Microbial Communities from Marine Sediments in Bioreactors*. CRC Press), 107-144.

Gong, S., Peng, Y., Bao, H., Feng, D., Cao, X., Crockford, P.W., and Chen, D. (2018). Triple sulfur isotope relationships during sulfate-driven anaerobic oxidation of methane. *Earth and Planetary Science Letters* 504**,** 13-20.

Greinert, J., Bohrmann, G., and Suess, E. (2001). Gas hydrate-associated carbonates and methane-venting at Hydrate Ridge: classification, distribution, and origin of authigenic lithologies. *Natural gas hydrates: Occurrence, distribution, and detection***,** 99-113.

Guan, H., Birgel, D., Peckmann, J., Liang, Q., Feng, D., Yang, S., Liang, J., Tao, J., Wu, N., and Chen, D. (2018). Lipid biomarker patterns of authigenic carbonates reveal fluid composition and seepage intensity at Haima cold seeps, South China Sea. *Journal of Asian Earth Sciences,* 168, 163-172..

Guo, Q., Strauss, H., Kaufman, A.J., Schröder, S., Gutzmer, J., Wing, B., Baker, M.A., Bekker, A., Jin, Q., and Kim, S.-T. (2009). Reconstructing Earth's surface oxidation across the Archean-Proterozoic transition. *Geology* 37**,** 399-402.

Haas, A., Peckmann, J., Elvert, M., Sahling, H., and Bohrmann, G. (2010). Patterns of carbonate authigenesis at the Kouilou pockmarks on the Congo deep-sea fan. *Marine Geology* 268**,** 129-136.

Hagemann, A., Leefmann, T., Peckmann, J., Hoffmann, V.E., and Thiel, V. (2013). Biomarkers from individual carbonate phases of an Oligocene cold-seep deposit, Washington State, USA. *Lethaia* 46**,** 7-18.

Hancock, L.G. (2018). *Proxy Applications for Reconstructing Carbon and Sulfur Cycling in Ancient Marine Environments.* eScholarship, University of California.

Hanson, R.S., and Hanson, T.E. (1996). Methanotrophic bacteria. *Microbiol. Mol. Biol. Rev.* 60**,** 439-471.

Haroon, M.F., Hu, S., Shi, Y., Imelfort, M., Keller, J., Hugenholtz, P., Yuan, Z., and Tyson, G.W. (2013). Anaerobic oxidation of methane coupled to nitrate reduction in a novel archaeal lineage. *Nature* 500**,** 567-570.

Hayes, J.M., Strauss, H., and Kaufman, A.J. (1999). The abundance of 13C in marine organic matter and isotopic fractionation in the global biogeochemical cycle of carbon during the past 800 Ma. *Chemical Geology* 161**,** 103-125.

Henrichs, S.M., and Reeburgh, W.S. (1987). Anaerobic mineralization of marine sediment organic matter: rates and the role of anaerobic processes in the oceanic carbon economy. *Geomicrobiology Journal* 5**,** 191-237.

Hensen, C., Zabel, M., Pfeifer, K., Schwenk, T., Kasten, S., Riedinger, N., Schulz, H.D., and Boetius, A. (2003). Control of sulfate pore-water profiles by sedimentary events and the significance of anaerobic oxidation of methane for the burial of sulfur in marine sediments. *Geochimica et Cosmochimica Acta* 67**,** 2631-2647.

Hesselbo, S.P., Grocke, D.R., Jenkyns, H.C., Bjerrum, C.J., Farrimond, P., Morgans Bell, H.S., and Green, O.R. (2000). Massive dissociation of gas hydrate during a Jurassic oceanic anoxic event. *Nature* 406**,** 392-395.

Heydari, E., and Hassanzadeh, J. (2003). Deev Jahi model of the Permian–Triassic boundary mass extinction: a case for gas hydrates as the main cause of biological crisis on Earth. *Sedimentary Geology* 163**,** 147-163.

Higgins, J.A., Fischer, W., and Schrag, D. (2009). Oxygenation of the ocean and sediments: consequences for the seafloor carbonate factory. *Earth and Planetary Science Letters* 284**,** 25-33.

Hill, T.M., Kennett, J.P., and Spero, H.J. (2003). Foraminifera as indicators of methane-rich environments: A study of modern methane seeps in Santa Barbara Channel, California. *Marine Micropaleontology* 49**,** 123-138.

Himmler, T., Birgel, D., Bayon, G., Pape, T., Ge, L., Bohrmann, G., and Peckmann, J. (2015). Formation of seep carbonates along the Makran convergent margin, northern Arabian Sea and a molecular and isotopic approach to constrain the carbon isotopic composition of parent methane. *Chemical Geology* 415**,** 102-117.

Himmler, T., Brinkmann, F., Bohrmann, G., and Peckmann, J. (2011). Corrosion patterns of seep-carbonates from the eastern Mediterranean Sea. *Terra Nova* 23**,** 206-212.

Himmler, T., Sahy, D., Martma, T., Bohrmann, G., Plaza-Faverola, A., Bünz, S., Condon, D.J., Knies, J., and Lepland, A. (2019). A 160,000-year-old history of tectonically controlled methane seepage in the Arctic. *Science advances* 5**,** eaaw1450.

Hinrichs, K.-U., and Boetius, A. (2002). "The anaerobic oxidation of methane: new insights in microbial ecology and biogeochemistry," in *Ocean Margin Systems*. Springer), 457-477.

Hinrichs, K.-U., Hmelo, L.R., and Sylva, S.P. (2003). Molecular fossil record of elevated methane levels in late Pleistocene coastal waters. *Science* 299**,** 1214-1217.

Hollis, C.J., Dunkley Jones, T., Anagnostou, E., Bijl, P.K., Cramwinckel, M.J., Cui, Y., Dickens, G.R., Edgar, K.M., Eley, Y., Evans, D., Foster, G.L., Frieling, J., Inglis, G.N., Kennedy, E.M., Kozdon, R., Lauretano, V., Lear, C.H., Littler, K., Lourens, L., Meckler, A.N., Naafs, B.D.A., Pälike, H., Pancost, R.D., Pearson, P.N., Röhl, U., Royer, D.L., Salzmann, U., Schubert, B.A., Seebeck, H., Sluijs, A., Speijer, R.P., Stassen, P., Tierney, J., Tripati, A., Wade, B., Westerhold, T., Witkowski, C., Zachos, J.C., Zhang, Y.G., Huber, M., and Lunt, D.J. (2019). The DeepMIP contribution to PMIP4: methodologies for selection, compilation and analysis of latest Paleocene and early Eocene climate proxy data, incorporating version 0.1 of the DeepMIP database. *Geosci. Model Dev.* 12**,** 3149-3206.

Holmes, M.E. (2000). Methane production, consumption, and air-sea exchange in the open ocean: An evaluation based on carbon isotopic ratios M. Elizabeth Holmes, 1 Francis J. Sansone, Terri M. Rust, and Brian N. Popp. *Global Biogeochemical Cycles* 14**,** 1-10.

Hong, W.-L., Torres, M.E., Kim, J.-H., Choi, J., and Bahk, J.-J. (2013). Carbon cycling within the sulfate-methane-transition-zone in marine sediments from the Ulleung Basin. *Biogeochemistry* 115**,** 129-148.

Hong, W.-L., Torres, M.E., Kim, J.-H., Choi, J., and Bahk, J.-J. (2014). Towards quantifying the reaction network around the sulfate–methane-transition-zone in the Ulleung Basin, East Sea, with a kinetic modeling approach. *Geochimica et Cosmochimica Acta* 140**,** 127-141.

Hopmans, E.C., Schouten, S., and Damsté, J.S.S. (2016). The effect of improved chromatography on GDGT-based palaeoproxies. *Organic Geochemistry* 93**,** 1-6.

Hopmans, E.C., Weijers, J.W., Schefuß, E., Herfort, L., Damsté, J.S.S., and Schouten, S. (2004). A novel proxy for terrestrial organic matter in sediments based on branched and isoprenoid tetraether lipids. *Earth and Planetary Science Letters* 224**,** 107-116.

Horita, J., and Berndt, M.E. (1999). Abiogenic methane formation and isotopic fractionation under hydrothermal conditions. *Science* 285**,** 1055-1057.

Hornafius, J.S., Quigley, D., and Luyendyk, B.P. (1999). The world's most spectacular marine hydrocarbon seeps (Coal Oil Point, Santa Barbara Channel, California): Quantification of emissions. *Journal of Geophysical Research: Oceans* 104**,** 20703-20711.

Houghton, J.T., Ding, Y., Griggs, D.J., Noguer, M., Van Der Linden, P.J., Dai, X., Maskell, K., and Johnson, C. (2001). Climate change 2001: the scientific basis.

Hovland, M., Jensen, S., and Fichler, C. (2012). Methane and minor oil macro-seep systems—their complexity and environmental significance. *Marine Geology* 332**,** 163-173.

Hovland, M., Judd, A.G., and Burke Jr, R. (1993). The global flux of methane from shallow submarine sediments. *Chemosphere* 26**,** 559-578.

Hsu, T.-W., Jiang, W.-T., and Wang, Y. (2014). Authigenesis of vivianite as influenced by methane-induced sulfidization in cold-seep sediments off southwestern Taiwan. *Journal of Asian Earth Sciences* 89**,** 88-97.

Hu, C.-Y., Yang, T.F., Burr, G.S., Chuang, P.-C., Chen, H.-W., Walia, M., Chen, N.-C., Huang, Y.-C., Lin, S., and Wang, Y. (2017a). Biogeochemical cycles at the sulfate-methane transition zone (SMTZ) and geochemical characteristics of the pore fluids offshore southwestern Taiwan. *Journal of Asian Earth Sciences* 149**,** 172-183.

Hu, X., and Cai, W.J. (2011). An assessment of ocean margin anaerobic processes on oceanic alkalinity budget. *Global Biogeochemical Cycles* 25.

Hu, Y., Chen, L., Feng, D., Liang, Q., Xia, Z., and Chen, D. (2017b). Geochemical record of methane seepage in authigenic carbonates and surrounding host sediments: A case study from the South China Sea. *Journal of Asian Earth Sciences* 138**,** 51-61.

Hu, Y., Feng, D., Liang, Q., Xia, Z., Chen, L., and Chen, D. (2015). Impact of anaerobic oxidation of methane on the geochemical cycle of redox-sensitive elements at cold-seep sites of the northern South China Sea. *Deep Sea Research Part II: Topical Studies in Oceanography* 122**,** 84-94.

Hu, Y., Feng, D., Peckmann, J., Roberts, H.H., and Chen, D. (2014). New insights into cerium anomalies and mechanisms of trace metal enrichment in authigenic carbonate from hydrocarbon seeps. *Chemical Geology* 381**,** 55-66.

Hunt, J. (1996). Petroleum geology and geochemistry. *Freeman, New York*.

Iglesias-Rodriguez, M.D., Armstrong, R., Feely, R., Hood, R., Kleypas, J., Milliman, J.D., Sabine, C., and Sarmiento, J. (2002). Progress made in study of ocean's calcium carbonate budget. *Eos, Transactions American Geophysical Union* 83**,** 365-375.

Inagaki, F., Nunoura, T., Nakagawa, S., Teske, A., Lever, M., Lauer, A., Suzuki, M., Takai, K., Delwiche, M., and Colwell, F.S. (2006). Biogeographical distribution and diversity of microbes in methane hydrate-bearing deep marine sediments on the Pacific Ocean

Margin. *Proceedings of the National Academy of Sciences of the United States of America* 103**,** 2815-2820.

Jaffey, A., Flynn, K., Glendenin, L., Bentley, W.T., and Essling, A. (1971). Precision measurement of half-lives and specific activities of U 235 and U 238. *Physical review C* 4**,** 1889.

Jiang, G., Kennedy, M.J., and Christie-Blick, N. (2003). Stable isotopic evidence for methane seeps in Neoproterozoic postglacial cap carbonates. *Nature* 426**,** 822-826.

Jiang, K., Zhang, J., Sakatoku, A., Kambayashi, S., Yamanaka, T., Kanehara, T., Fujikura, K., and Pellizari, V.H. (2018). Discovery and biogeochemistry of asphalt seeps in the North São Paulo Plateau, Brazilian Margin. *Scientific reports* 8**,** 12619.

Jiang, L., Planavsky, N., Zhao, M., Liu, W., and Wang, X. (2019). Authigenic origin for a massive negative carbon isotope excursion. *Geology* 47**,** 115-118.

Jones, D.O., Walls, A., Clare, M., Fiske, M.S., Weiland, R.J., O'brien, R., and Touzel, D.F. (2014). Asphalt mounds and associated biota on the Angolan margin. *Deep Sea Research Part I: Oceanographic Research Papers* 94**,** 124-136.

Jørgensen, B., and Nelson, D. (2004). Sulfide oxidation in marine sediments: geochemistry meets microbiology. GSA Special Pap. 379, 63–81. doi: 10.1130.

Jørgensen, B.B. (1982). Mineralization of organic matter in the sea bed—the role of sulphate reduction. *Nature* 296**,** 643.

Jørgensen, B.B., Beulig, F., Egger, M., Petro, C., Scholze, C., and Røy, H. (2019a). Organoclastic sulfate reduction in the sulfate-methane transition of marine sediments. *Geochimica et Cosmochimica Acta*.

Jørgensen, B.B., Böttcher, M.E., Lüschen, H., Neretin, L.N., and Volkov, I.I. (2004). Anaerobic methane oxidation and a deep H 2 S sink generate isotopically heavy sulfides in Black Sea sediments. *Geochimica et Cosmochimica Acta* 68**,** 2095-2118.

Jørgensen, B.B., Findlay, A.J., and Pellerin, A. (2019b). The Biogeochemical Sulfur Cycle of Marine Sediments. *Frontiers in microbiology* 10.849

Jørgensen, B.B., and Kasten, S. (2006). "Sulfur cycling and methane oxidation," in *Marine geochemistry*. Springer), 271-309.

Joye, S.B., Boetius, A., Orcutt, B.N., Montoya, J.P., Schulz, H.N., Erickson, M.J., and Lugo, S.K. (2004). The anaerobic oxidation of methane and sulfate reduction in sediments from Gulf of Mexico cold seeps. *Chemical Geology* 205**,** 219-238.

Judd, A., and Hovland, M. (2009). *Seabed fluid flow: the impact on geology, biology and the marine environment.* Cambridge University Press.

Judd, A., Hovland, M., Dimitrov, L., Garcia Gil, S., and Jukes, V. (2002). The geological methane budget at continental margins and its influence on climate change. *Geofluids* 2**,** 109-126.

Judd, A., Noble-James, T., Golding, N., Eggett, A., Diesing, M., Clare, D., Silburn, B., Duncan, G., Field, L., and Milodowski, A. (2019). The Croker Carbonate Slabs: extensive methane-derived authigenic carbonate in the Irish Sea—nature, origin, longevity and environmental significance. *Geo-Marine Letters***,** 1-16.

Jung, M.-Y., Park, S.-J., Min, D., Kim, J.-S., Rijpstra, W.I.C., Damsté, J.S.S., Kim, G.-J., Madsen, E.L., and Rhee, S.-K. (2011). Enrichment and characterization of an autotrophic ammonia-oxidizing archaeon of mesophilic crenarchaeal group I. 1a from an agricultural soil. *Appl. Environ. Microbiol.* 77**,** 8635-8647.

Karaca, D., Hensen, C., and Wallmann, K. (2010). Controls on authigenic carbonate precipitation at cold seeps along the convergent margin off Costa Rica. *Geochemistry, Geophysics, Geosystems* 11.

Karl, D.M., Beversdorf, L., Björkman, K.M., Church, M.J., Martinez, A., and Delong, E.F. (2008). Aerobic production of methane in the sea. *Nature Geoscience* 1**,** 473-478.

Karl, D.M., and Tilbrook, B.D. (1994). Production and transport of methane in oceanic particulate organic matter. *Nature* 368**,** 732-734.

Kasting, J.F. (2005). Methane and climate during the Precambrian era. *Precambrian Research* 137**,** 119-129.

Kasting, J.F., Zahnle, K.J., and Walker, J.C. (1983). Photochemistry of methane in the Earth's early atmosphere. *Precambrian Research* 20**,** 121-148.

Kastner, M., Claypool, G., and Robertson, G. (2008). Geochemical constraints on the origin of the pore fluids and gas hydrate distribution at Atwater Valley and Keathley Canyon, northern Gulf of Mexico. *Marine and Petroleum Geology* 25**,** 860-872.

Katz, M.E., Wright, J.D., Miller, K.G., Cramer, B.S., Fennel, K., and Falkowski, P.G. (2005). Biological overprint of the geological carbon cycle. *Marine Geology* 217**,** 323-338.

Kemp, A.L.W., and Thode, H.G. (1968). The mechanism of the bacterial reduction of sulphate and of sulphite from isotope fractionation studies. *Geochimica et Cosmochimica Acta* 32**,** 71-91.

Kennedy, M.J., Christie-Blick, N., and Sohl, L.E. (2001). Are Proterozoic cap carbonates and isotopic excursions a record of gas hydrate destabilization following Earth's coldest intervals? *Geology* 29**,** 443-446.

Kennett, J.P., Cannariato, K.G., Hendy, I.L., and Behl, R.J. (2003). Methane hydrates in quaternary climate change: the clathrate gun hypothesi. *Methane Hydrates in Quaternary Climate Change: The Clathrate Gun Hypothesis* 54**,** 1-9.

Kennicutt, M.C. (2017). "Oil and Gas Seeps in the Gulf of Mexico," in *Habitats and Biota of the Gulf of Mexico: Before the Deepwater Horizon Oil Spill*. Springer), 275-358.

Key, R., Olsen, A., Van Heuven, S., Lauvset, S., Velo, A., Lin, X., Schirnick, C., Kozyr, A., Tanhua, T., and Hoppema, M. (2015). Global Ocean Data Analysis Project, Version 2 (GLODAPv2), ORNL/CDIAC-162, ND-P093.

Kim, J.H., Torres, M.E., Haley, B.A., Ryu, J.S., Park, M.H., Hong, W.L., and Choi, J. (2016). Marine silicate weathering in the anoxic sediment of the Ulleung Basin: Evidence and consequences. *Geochemistry, Geophysics, Geosystems* 17**,** 3437-3453.

Kim, S.-T., O'neil, J.R., Hillaire-Marcel, C., and Mucci, A. (2007). Oxygen isotope fractionation between synthetic aragonite and water: influence of temperature and Mg 2+ concentration. *Geochimica et Cosmochimica Acta* 71**,** 4704-4715.

Kinnaman, F.S., Kimball, J.B., Busso, L., Birgel, D., Ding, H., Hinrichs, K.-U., and Valentine, D.L. (2010). Gas flux and carbonate occurrence at a shallow seep of thermogenic natural gas. *Geo-Marine Letters* 30**,** 355-365.

Klapp, S.A., Bohrmann, G., Kuhs, W.F., Murshed, M.M., Pape, T., Klein, H., Techmer, K.S., Heeschen, K.U., and Abegg, F. (2010). Microstructures of structure I and II gas hydrates from the Gulf of Mexico. *Marine and Petroleum Geology* 27**,** 116-125.

Klauda, J.B., and Sandler, S.I. (2005). Global distribution of methane hydrate in ocean sediment. *Energy & Fuels* 19**,** 459-470.

Kniemeyer, O., Musat, F., Sievert, S.M., Knittel, K., Wilkes, H., Blumenberg, M., Michaelis, W., Classen, A., Bolm, C., and Joye, S.B. (2007). Anaerobic oxidation of short-chain hydrocarbons by marine sulphate-reducing bacteria. *Nature* 449**,** 898.

Knittel, K., and Boetius, A. (2009). Anaerobic oxidation of methane: progress with an unknown process. *Annu Rev Microbiol* 63**,** 311-334.

Knittel, K., Lösekann, T., Boetius, A., Kort, R., and Amann, R. (2005). Diversity and distribution of methanotrophic archaea at cold seeps. *Applied and environmental microbiology* 71**,** 467-479.

Knittel, K., Wegener, G., and Boetius, A. (2019). Anaerobic methane oxidizers. *Microbial Communities Utilizing Hydrocarbons and Lipids: Members, Metagenomics and Ecophysiology***,** 1-21.

Kocherla, M. (2013). Authigenic Gypsum in Gas-Hydrate Associated Sediments from the East Coast of India (Bay of Bengal). *Acta Geologica Sinica - English Edition* 87**,** 749-760.

Koga, Y., Morii, H., Akagawa-Matsushita, M., and Ohga, M. (1998). Correlation of Polar Lipid Composition with 16S rRNA Phylogeny in Methanogens. Further Analysis of Lipid Component Parts. *Bioscience, Biotechnology, and Biochemistry* 62**,** 230-236.

Komada, T., Burdige, D.J., Li, H.-L., Magen, C., Chanton, J.P., and Cada, A.K. (2016). Organic matter cycling across the sulfate-methane transition zone of the Santa Barbara Basin, California Borderland. *Geochimica et Cosmochimica Acta* 176**,** 259-278.

Konhauser, K.O., Pecoits, E., Lalonde, S.V., Papineau, D., Nisbet, E.G., Barley, M.E., Arndt, N.T., Zahnle, K., and Kamber, B.S. (2009). Oceanic nickel depletion and a methanogen famine before the Great Oxidation Event. *Nature* 458**,** 750.

Kopp, R.E., Kirschvink, J.L., Hilburn, I.A., and Nash, C.Z. (2005). The Paleoproterozoic snowball Earth: a climate disaster triggered by the evolution of oxygenic photosynthesis. *Proceedings of the National Academy of Sciences* 102**,** 11131-11136.

Körber, J.-H., Sahling, H., Pape, T., Dos Santos Ferreira, C., Macdonald, I., and Bohrmann, G. (2014). Natural oil seepage at kobuleti ridge, eastern Black Sea. *Marine and Petroleum Geology* 50**,** 68-82.

Kretschmer, K., Biastoch, A., Rüpke, L., and Burwicz, E. (2015). Modeling the fate of methane hydrates under global warming. *Global Biogeochemical Cycles* 29**,** 610-625.

Krull, E.S., and Retallack, G.J. (2000). δ13C depth profiles from paleosols across the Permian-Triassic boundary: Evidence for methane release. *Geological Society of America Bulletin* 112**,** 1459-1472.

Krumins, V., Gehlen, M., Arndt, S., Cappellen, P.V., and Regnier, P. (2013). Dissolved inorganic carbon and alkalinity fluxes from coastal marine sediments: model estimates for different shelf environments and sensitivity to global change. *Biogeosciences* 10**,** 371-398.

Kump, L.R. (2012). Sulfur Isotopes and the Stepwise Oxygenation of the Biosphere. *Elements* 8**,** 410-411.

Kump, L.R., and Arthur, M.A. (1999). Interpreting carbon-isotope excursions: carbonates and organic matter. *Chemical Geology* 161**,** 181-198.

Kvenvolden, K., and Cooper, C. (2003). Natural seepage of crude oil into the marine environment. *Geo-Marine Letters* 23**,** 140-146.

Kvenvolden, K.A. (1988). Methane hydrate—a major reservoir of carbon in the shallow geosphere? *Chemical Geology* 71**,** 41-51.

Kvenvolden, K.A. (2002). Methane hydrate in the global organic carbon cycle. *Terra Nova* 14**,** 302-306.

Kvenvolden, K.A., and Harbaugh, J.W. (1983). Reassessment of the rates at which oil from natural sources enters the marine environment. *Marine Environmental Research* 10**,** 223-243.

Kvenvolden, K.A., Lorenson, T.D., and Reeburgh, W.S. (2001). Attention turns to naturally occurring methane seepage. *Eos, Transactions American Geophysical Union* 82**,** 457-457.

Kvenvolden, K.A., and Rogers, B.W. (2005). Gaia's breath—global methane exhalations. *Marine and Petroleum Geology* 22**,** 579-590.

Lamontagne, R.A., Swinnerton, J.W., Linnenbom, V.J., and Smith, W.D. (1973). Methane concentrations in various marine environments. *Journal of Geophysical Research (1896-1977)* 78**,** 5317-5324.

Lapham, L., Marshall, K., Magen, C., Lyubchich, V., Cooper, L.W., and Grebmeier, J.M. (2017). Dissolved methane concentrations in the water column and surface sediments of Hanna Shoal and Barrow Canyon, Northern Chukchi Sea. *Deep Sea Research Part II: Topical Studies in Oceanography* 144. 92-103

Larowe, D.E., Burwicz, E., Arndt, S., Dale, A.W., and Amend, J.P. (2017). Temperature and volume of global marine sediments. *Geology* 45**,** 275-278.

Larrasoaña, J.C., Roberts, A.P., Musgrave, R.J., Gràcia, E., Piñero, E., Vega, M., and Martínez-Ruiz, F. (2007). Diagenetic formation of greigite and pyrrhotite in gas hydrate marine sedimentary systems. *Earth and Planetary Science Letters* 261**,** 350-366.

Laso-Pérez, R., Hahn, C., Van Vliet, D.M., Tegetmeyer, H.E., Schubotz, F., Smit, N.T., Pape, T., Sahling, H., Bohrmann, G., and Boetius, A. (2019). Anaerobic Degradation of Non-Methane Alkanes by "Candidatus Methanoliparia" in Hydrocarbon Seeps of the Gulf of Mexico. *mBio* 10**,** e01814-01819.

Lauvset, S.K., Key, R.M., Olsen, A., Van Heuven, S., Velo, A., Lin, X., Schirnick, C., Kozyr, A., Tanhua, T., and Hoppema, M. (2016). A new global interior ocean mapped climatology: The 1× 1 GLODAP version 2. *Earth System Science Data* 8**,** 325-340.

Levin, L.A., Baco, A.R., Bowden, D.A., Colaco, A., Cordes, E.E., Cunha, M.R., Demopoulos, A.W., Gobin, J., Grupe, B.M., and Le, J. (2016). Hydrothermal vents and methane seeps: rethinking the sphere of influence. *Frontiers in Marine Science* 3**,** 72.

Li, M., Peng, C., Wang, M., Xue, W., Zhang, K., Wang, K., Shi, G., and Zhu, Q. (2017a). The carbon flux of global rivers: A re-evaluation of amount and spatial patterns. *Ecological Indicators* 80**,** 40-51.

Li, N., Feng, D., Chen, L., Wang, H., and Chen, D. (2016). Using sediment geochemistry to infer temporal variation of methane flux at a cold seep in the South China Sea. *Marine and Petroleum Geology* 77**,** 835-845.

Li, N., Yang, X., Peng, J., Zhou, Q., and Chen, D. (2017b). Paleo-cold seep activity in the southern South China Sea: Evidence from the geochemical and geophysical records of sediments. *Journal of Asian Earth Sciences* 168. 106-111.

Liebetrau, V., Eisenhauer, A., and Linke, P. (2010). Cold seep carbonates and associated cold-water corals at the Hikurangi Margin, New Zealand: new insights into fluid pathways, growth structures and geochronology. *Marine Geology* 272**,** 307-318.

Lim, Y.C., Lin, S., Yang, T.F., Chen, Y.-G., and Liu, C.-S. (2011). Variations of methane induced pyrite formation in the accretionary wedge sediments offshore southwestern Taiwan. *Marine and Petroleum Geology* 28**,** 1829-1837.

Lin, Q., Wang, J., Algeo, T.J., Su, P., and Hu, G. (2016a). Formation mechanism of authigenic gypsum in marine methane hydrate settings: Evidence from the northern South China Sea. *Deep Sea Research Part I: Oceanographic Research Papers* 115**,** 210-220.

Lin, Q., Wang, J., Taladay, K., Lu, H., Hu, G., Sun, F., and Lin, R. (2016b). Coupled pyrite concentration and sulfur isotopic insight into the paleo sulfate–methane transition zone (SMTZ) in the northern South China Sea. *Journal of Asian Earth Sciences* 115**,** 547-556.

Lin, Z., Sun, X., Lu, Y., Strauss, H., Xu, L., Gong, J., Teichert, B.M., Lu, R., Lu, H., and Sun, W. (2017). The enrichment of heavy iron isotopes in authigenic pyrite as a possible indicator of sulfate-driven anaerobic oxidation of methane: Insights from the South China Sea. *Chemical Geology* 449**,** 15-29.

Lin, Z., Sun, X., Peckmann, J., Lu, Y., Xu, L., Strauss, H., Zhou, H., Gong, J., Lu, H., and Teichert, B.M. (2016c). How sulfate-driven anaerobic oxidation of methane affects the sulfur isotopic composition of pyrite: a SIMS study from the South China Sea. *Chemical Geology* 440**,** 26-41.

Lipp, J.S., Morono, Y., Inagaki, F., and Hinrichs, K.U. (2008). Significant contribution of Archaea to extant biomass in marine subsurface sediments. *Nature* 454**,** 991-994.

Liu, J., Izon, G., Wang, J., Antler, G., Wang, Z., Zhao, J., and Egger, M. (2018). Vivianite formation in methane-rich deep-sea sediments from the South China Sea. *Biogeosciences* 15**,** 6329-6348.

Liu, X., Lipp, J.S., and Hinrichs, K.-U. (2011). Distribution of intact and core GDGTs in marine sediments. *Organic Geochemistry* 42**,** 368-375.

Liu, Y., and Whitman, W.B. (2008). Metabolic, phylogenetic, and ecological diversity of the methanogenic archaea. *Annals of the New York Academy of Sciences* 1125**,** 171-189.

Lloyd, K.G., Alperin, M.J., and Teske, A. (2011). Environmental evidence for net methane production and oxidation in putative ANaerobic MEthanotrophic (ANME) archaea. *Environmental Microbiology* 13**,** 2548-2564.

Lobegeier, M.K., and Sen Gupta, B.K. (2008). FORAMINIFERA OF HYDROCARBON SEEPS, GULF OF MEXICO. *Journal of Foraminiferal Research* 38**,** 93-116.

Longman, J., Palmer, M.R., Gernon, T.M., and Manners, H.R. (2019). The role of tephra in enhancing organic carbon preservation in marine sediments. *Earth-Science Reviews*.

Loulergue, L., Schilt, A., Spahni, R., Masson-Delmotte, V., Blunier, T., Lemieux, B., Barnola, J.-M., Raynaud, D., Stocker, T.F., and Chappellaz, J. (2008). Orbital and millennial-scale features of atmospheric CH4 over the past 800,000 years. *Nature* 453**,** 383-386.

Luff, R., and Wallmann, K. (2003). Fluid flow, methane fluxes, carbonate precipitation and biogeochemical turnover in gas hydrate-bearing sediments at Hydrate Ridge, Cascadia Margin: numerical modeling and mass balances. *Geochimica et Cosmochimica Acta* 67**,** 3403-3421.

Luff, R., Wallmann, K., and Aloisi, G. (2004). Numerical modeling of carbonate crust formation at cold vent sites: significance for fluid and methane budgets and chemosynthetic biological communities. *Earth and Planetary Science Letters* 221**,** 337-353.

Lyons, T., and Gill, B. (2010). Ancient Sulfur Cycling and Oxygenation of the Early Biosphere. *Elements* 6**,** 93-99.

Lyons, T.W., Reinhard, C.T., and Planavsky, N.J. (2014). The rise of oxygen in Earth's early ocean and atmosphere. *Nature* 506**,** 307-315.

Lyons, T.W., Walter, L.M., Gellatly, A.M., Martini, A.M., and Blake, R.E. (2004). Sites of anomalous organic remineralization in the carbonate sediments of South Florida, USA: the sulfur cycle and carbonate-associated sulfate. *Geological Society of America Special Papers* 379**,** 161-176.

Macdonald, I., Bohrmann, G., Escobar, E., Abegg, F., Blanchon, P., Blinova, V., Brückmann, W., Drews, M., Eisenhauer, A., and Han, X. (2004). Asphalt volcanism and chemosynthetic life in the Campeche Knolls, Gulf of Mexico. *Science* 304**,** 999-1002.

Macdonald, I., Guinasso, N., Ackleson, S., Amos, J., Duckworth, R., Sassen, R., and Brooks, J. (1993). Natural oil slicks in the Gulf of Mexico visible from space. *Journal of Geophysical Research: Oceans* 98**,** 16351-16364.

Macdonald, I., Leifer, I., Sassen, R., Stine, P., Mitchell, R., and Guinasso Jr, N. (2002). Transfer of hydrocarbons from natural seeps to the water column and atmosphere. *Geofluids* 2**,** 95-107.

Macdonald, I.R., Garcia-Pineda, O., Beet, A., Daneshgar Asl, S., Feng, L., Graettinger, G., French-Mccay, D., Holmes, J., Hu, C., and Huffer, F. (2015). Natural and unnatural oil slicks in the G ulf of M exico. *Journal of Geophysical Research: Oceans* 120**,** 8364-8380.

Mahlstedt, N. (2018). Thermogenic Formation of Hydrocarbons in Sedimentary Basins. *Hydrocarbons, Oils and Lipids: Diversity, Origin, Chemistry and Fate***,** 1-30.

Malinverno, A., and Pohlman, J.W. (2011). Modeling sulfate reduction in methane hydrate-bearing continental margin sediments: Does a sulfate-methane transition require anaerobic oxidation of methane? *Geochemistry, Geophysics, Geosystems* 12.

Malone, M.J., Claypool, G., Martin, J.B., and Dickens, G.R. (2002). Variable methane fluxes in shallow marine systems over geologic time: The composition and origin of pore waters and authigenic carbonates on the New Jersey shelf. *Marine Geology* 189**,** 175-196.

Mansour, A.S. (2014). Hydrocarbon-derived carbonates along the upper–lower continental slope, Gulf of Mexico: a mineralogical and stable isotopic study. *Carbonates and Evaporites* 29**,** 89-105.

Mansour, A.S., and Sassen, R. (2011). Mineralogical and stable isotopic characterization of authigenic carbonate from a hydrocarbon seep site, Gulf of Mexico slope: possible relation to crude oil degradation. *Marine Geology* 281**,** 59-69.

Marcon, Y., Sahling, H., Macdonald, I.R., Wintersteller, P., Dos Santos Ferreira, C., and Bohrmann, G. (2018). Slow volcanoes: the intriguing similarities between marine asphalt and basalt lavas. *Oceanography* 31**,** 194-205.

Marlow, J., Peckmann, J., and Orphan, V. (2015). Autoendoliths: a distinct type of rock-hosted microbial life. *Geobiology* 13**,** 303-307.

Marlow, J.J., Steele, J.A., Ziebis, W., Thurber, A.R., Levin, L.A., and Orphan, V.J. (2014). Carbonate-hosted methanotrophy represents an unrecognized methane sink in the deep sea. *Nature communications* 5.

Martin, J.B., Day, S.A., Rathburn, A.E., Perez, M.E., Mahn, C., and Gieskes, J. (2004). Relationships between the stable isotopic signatures of living and fossil foraminifera in Monterey Bay, California. *Geochemistry, Geophysics, Geosystems* 5.

März, C., Riedinger, N., Sena, C., and Kasten, S. (2018). Phosphorus dynamics around the sulphate-methane transition in continental margin sediments: Authigenic apatite and Fe(II) phosphates. *Marine Geology* 404**,** 84-96.

Matsumoto, R. (1990). Vuggy carbonate crust formed by hydrocarbon seepage on the continental shelf of Baffin Island, northeast Canada. *Geochemical Journal* 24**,** 143-158.

Mazumdar, A., Dewangan, P., Joäo, H., Peketi, A., Khosla, V., Kocherla, M., Badesab, F., Joshi, R., Roxanne, P., and Ramamurty, P. (2009). Evidence of paleo–cold seep activity from the Bay of Bengal, offshore India. *Geochemistry, Geophysics, Geosystems* 10 (6).

Mazzini, A., Svensen, H.H., Forsberg, C.F., Linge, H., Lauritzen, S.-E., Haflidason, H., Hammer, Ø., Planke, S., and Tjelta, T.I. (2017). A climatic trigger for the giant Troll pockmark field in the northern North Sea. *Earth and Planetary Science Letters* 464**,** 24-34.

Mccollom, T.M. (2013). Laboratory simulations of abiotic hydrocarbon formation in Earth's deep subsurface. *Reviews in Mineralogy and Geochemistry* 75**,** 467-494.

Mccollom, T.M., and Seewald, J.S. (2007). Abiotic synthesis of organic compounds in deep-sea hydrothermal environments. *Chemical Reviews* 107**,** 382-401.

Mcginnis, D.F., Greinert, J., Artemov, Y., Beaubien, S., and Wüest, A. (2006). Fate of rising methane bubbles in stratified waters: How much methane reaches the atmosphere? *Journal of Geophysical Research: Oceans* 111.

Mcglynn, S.E., Chadwick, G.L., Kempes, C.P., and Orphan, V.J. (2015). Single cell activity reveals direct electron transfer in methanotrophic consortia. *Nature* 526**,** 531-535.

Meister, P. (2015). For the deep biosphere, the present is not always the key to the past: what we can learn from the geological record. *Terra Nova* 27**,** 400-408.

Meister, P., Brunner, B., Picard, A., Böttcher, M.E., and Jørgensen, B.B. (2019a). Sulphur and carbon isotopes as tracers of past sub-seafloor microbial activity. *Scientific reports* 9**,** 604.

Meister, P., Gutjahr, M., Frank, M., Bernasconi, S.M., Vasconcelos, C., and Mckenzie, J.A. (2011). Dolomite formation within the methanogenic zone induced by tectonically driven fluids in the Peru accretionary prism. *Geology* 39**,** 563-566.

Meister, P., Liu, B., Ferdelman, T.G., Jørgensen, B.B., and Khalili, A. (2013). Control of sulphate and methane distributions in marine sediments by organic matter reactivity. *Geochimica et Cosmochimica Acta* 104**,** 183-193.

Meister, P., Liu, B., Khalili, A., Böttcher, M.E., and Jørgensen, B.B. (2019b). Factors controlling the carbon isotope composition of dissolved inorganic carbon and methane in marine porewater: An evaluation by reaction-transport modelling. *Journal of Marine Systems* 200**,** 103227.

Meister, P., Mckenzie, J.A., Vasconcelos, C., Bernasconi, S., Frank, M., Gutjahr, M., and Schrag, D.P. (2007). Dolomite formation in the dynamic deep biosphere: results from the Peru Margin. *Sedimentology* 54**,** 1007-1032.

Meister, P., Prokopenko, M., Skilbeck, C., Watson, M., and Mckenzie, J. (2005). "8. Data Report: Compilation of Total Organic and Inorganic Carbon Data from Peru Margin and Eastern Equatorial Pacific Drill Sites; ODP Legs 112, 138, and 201", in: *Proc. ODP, Sci. Results*: published online: http://www-odp.tamu.edu/publications/201_SR/105/105_.htm

Meybeck, M. (1993). Riverine transport of atmospheric carbon: sources, global typology and budget. *Water, Air, and Soil Pollution* 70**,** 443-463.

Milkov, A.V. (2004). Global estimates of hydrate-bound gas in marine sediments: how much is really out there? *Earth-Science Reviews* 66**,** 183-197.

Milkov, A.V. (2011). Worldwide distribution and significance of secondary microbial methane formed during petroleum biodegradation in conventional reservoirs. *Organic Geochemistry* 42**,** 184-207.

Miller, C., and Dickens, G. (2017). "Data report: reanalysis of interstitial water barium, iron, and sulfur concentrations at Sites U1426 and U1427, In Tada, R., Murray, R.W., Alvarez Zarikian, C.A., and the Expedition 346 Scientists", in: *Proceedings of the Integrated Ocean Drilling Program.* (ed.) R. Tada, Murray, R.W., Alvarez Zarikian, C.A., and the Expedition 346 Scientists. vol. 346, p. 2.

Milliman, J., and Droxler, A. (1996). Neritic and pelagic carbonate sedimentation in the marine environment: ignorance is not bliss. *Geologische Rundschau* 85**,** 496-504.

Milliman, J.D. (1993). Production and accumulation of calcium carbonate in the ocean: budget of a nonsteady state. *Global Biogeochemical Cycles* 7**,** 927-957.

Milucka, J., Ferdelman, T.G., Polerecky, L., Franzke, D., Wegener, G., Schmid, M., Lieberwirth, I., Wagner, M., Widdel, F., and Kuypers, M.M. (2012). Zero-valent sulphur is a key intermediate in marine methane oxidation. *Nature* 491**,** 541-546.

Mitchell, R., Macdonald, I., and Kvenvolden, K. (1999). Estimates of total hydrocarbon seepage into the Gulf of Mexico based on satellite remote sensing images. *EOS Supplement* 80**,** OS242.

Miyajima, Y., Watanabe, Y., Goto, A.S., Jenkins, R.G., Sakai, S., Matsumoto, R., and Hasegawa, T. (2020). Archaeal lipid biomarker as a tool to constrain the origin of

methane at ancient methane seeps: Insight into subsurface fluid flow in the geological past. *Journal of Asian Earth Sciences* 189**,** 104134.

Moore, W.S. (2010). The effect of submarine groundwater discharge on the ocean. *Annual review of marine science* 2**,** 59-88.

Morales, C., Rogov, M., Wierzbowski, H., Ershova, V., Suan, G., Adatte, T., Föllmi, K.B., Tegelaar, E., Reichart, G.-J., De Lange, G.J., Middelburg, J.J., and Van De Schootbrugge, B. (2017). Glendonites track methane seepage in Mesozoic polar seas. *Geology* 45**,** 503-506.

Moran, J.J., Beal, E.J., Vrentas, J.M., Orphan, V.J., Freeman, K.H., and House, C.H. (2008). Methyl sulfides as intermediates in the anaerobic oxidation of methane. *Environmental Microbiology* 10**,** 162-173.

Murray, R.W., Brumsack, H.J., Von Breymann, M.T., Sturz, A.A., Dunbar, R.B., and Gieskes, J.M. (1991). "Diagenetic reactions in deeply buried sediments of the Japan Sea: a synthesis of interstitial-water chemistry results from Legs 127 and 128", in: *Proceedings of the Ocean Drilling Program Scientific Results*: Ocean Drilling Program College Station, TX), 128.

Myhre, G., Shindell, D., Bréon, F.-M., Collins, W., Fuglestvedt, J., Huang, J., Koch, D., Lamarque, J.-F., Lee, D., and Mendoza, B. (2013). Anthropogenic and natural radiative forcing. *Climate change* 423**,** 658-740.

Naehr, T., Rodriguez, N., Bohrmann, G., Paull, C., and Botz, R. (2000). "29. Methanederived authigenic carbonates associated with gas hydrate decomposition and fluid venting above the Blake Ridge Diapir", in: *Proceedings of the Ocean Drilling Program, Scientific Results*), 285-300.

Naehr, T.H., Birgel, D., Bohrmann, G., Macdonald, I.R., and Kasten, S. (2009). Biogeochemical controls on authigenic carbonate formation at the Chapopote “asphalt volcano”, Bay of Campeche. *Chemical Geology* 266**,** 390-402.

Naehr, T.H., Eichhubl, P., Orphan, V.J., Hovland, M., Paull, C.K., Ussler, W., Lorenson, T.D., and Greene, H.G. (2007). Authigenic carbonate formation at hydrocarbon seeps in continental margin sediments: a comparative study. *Deep Sea Research Part II: Topical Studies in Oceanography* 54**,** 1268-1291.

Naqvi, S., Bange, H.W., Farias, L., Monteiro, P., Scranton, M., and Zhang, J. (2010). Marine hypoxia/anoxia as a source of CH4 and N2O. *Biogeosciences (BG)*, *7*, 2159-2190.

Natalicchio, M., Birgel, D., Peckmann, J., Lozar, F., Carnevale, G., Liu, X., Hinrichs, K.-U., and Dela Pierre, F. (2017). An archaeal biomarker record of paleoenvironmental change across the onset of the Messinian salinity crisis in the absence of evaporites (Piedmont Basin, Italy). *Organic Geochemistry* 113**,** 242-253.

Nauhaus, K., Albrecht, M., Elvert, M., Boetius, A., and Widdel, F. (2007). In vitro cell growth of marine archaeal-bacterial consortia during anaerobic oxidation of methane with sulfate. *Environ Microbiol* 9**,** 187-196.

Nauhaus, K., Treude, T., Boetius, A., and Krüger, M. (2005). Environmental regulation of the anaerobic oxidation of methane: a comparison of ANME-I and ANME-II communities. *Environmental Microbiology* 7**,** 98-106.

Niemann, H., and Elvert, M. (2008). Diagnostic lipid biomarker and stable carbon isotope signatures of microbial communities mediating the anaerobic oxidation of methane with sulphate. *Organic Geochemistry* 39**,** 1668-1677.

Niemann, H., Lösekann, T., De Beer, D., Elvert, M., Nadalig, T., Knittel, K., Amann, R., Sauter, E.J., Schlüter, M., and Klages, M. (2006). Novel microbial communities of the Haakon Mosby mud volcano and their role as a methane sink. *Nature* 443**,** 854-858.

Noble, R., Orange, D., Decker, J., Teas, P., and Baillie, P. (2009). "Oil and gas seeps in deep marine sea floor cores as indicators of active petroleum systems in Indonesia", in: *33rd annual convention, Indonesian Petroleum Association*), 385-394.

Olsen, A., Key, R.M., Van Heuven, S., Lauvset, S., Velo, A., Lin, X., Schirnick, C., Kozyr, A., Tanhua, T., and Hoppema, M. (2016). An internally consistent data product for the world ocean: the Global Ocean Data Analysis Project, version 2 (GLODAPv2). *Earth System Science Data* 2016**,** 1-1.

Orcutt, B.N., Joye, S.B., Kleindienst, S., Knittel, K., Ramette, A., Reitz, A., Samarkin, V., Treude, T., and Boetius, A. (2010). Impact of natural oil and higher hydrocarbons on microbial diversity, distribution, and activity in Gulf of Mexico cold-seep sediments. *Deep Sea Research Part II: Topical Studies in Oceanography* 57**,** 2008-2021.

Orcutt, B.N., Sylvan, J.B., Knab, N.J., and Edwards, K.J. (2011). Microbial Ecology of the Dark Ocean above, at, and below the Seafloor. *Microbiology and Molecular Biology Reviews* 75**,** 361-422.

Orphan, V.J., House, C.H., Hinrichs, K.-U., Mckeegan, K.D., and Delong, E.F. (2002). Multiple archaeal groups mediate methane oxidation in anoxic cold seep sediments. *Proceedings of the National Academy of Sciences* 99**,** 7663-7668.

Orphan, V.J., House, C.H., Hinrichs, K.U., Mckeegan, K.D., and Delong, E.F. (2001). Methane-consuming archaea revealed by directly coupled isotopic and phylogenetic analysis. *Science* 293**,** 484-487.

Orphan, V.J., Iii, W.U., Naehr, T.H., House, C.H., Hinrichs, K.-U., and Paull, C.K. (2004). Geological, geochemical, and microbiological heterogeneity of the seafloor around methane vents in the Eel River Basin, offshore California. *Chemical Geology* 205**,** 265-289.

Ozaki, K., Tajika, E., Hong, P.K., Nakagawa, Y., and Reinhard, C.T. (2018). Effects of primitive photosynthesis on Earth's early climate system. *Nature Geoscience* 11**,** 55.

Pancost, R., Hopmans, E., Damsté, J.S., and Party, T.M.S.S. (2001). Archaeal lipids in Mediterranean cold seeps: molecular proxies for anaerobic methane oxidation. *Geochimica et Cosmochimica Acta* 65**,** 1611-1627.

Pancost, R.D., Zhang, C.L., Tavacoli, J., Talbot, H.M., Farrimond, P., Schouten, S., Sinninghe Damste, J.S., and Sassen, R. (2005). Lipid biomarkers preserved in hydrate-associated authigenic carbonate rocks of the Gulf of Mexico. *Palaeogeography, Palaeoclimatology, Palaeoecology* 227**,** 48-66.

Panieri, G., Camerlenghi, A., Cacho, I., Cervera, C.S., Canals, M., Lafuerza, S., and Herrera, G. (2012). Tracing seafloor methane emissions with benthic foraminifera: Results from the Ana submarine landslide (Eivissa Channel, Western Mediterranean Sea). *Marine Geology* 291-294**,** 97-112.

Panieri, G., Graves, C.A., and James, R.H. (2016). Paleo-methane emissions recorded in foraminifera near the landward limit of the gas hydrate stability zone offshore western Svalbard. *Geochemistry, Geophysics, Geosystems* 17**,** 521-537.

Panieri, G., James, R.H., Camerlenghi, A., Westbrook, G.K., Consolaro, C., Cacho, I., Cesari, V., and Cervera, C.S. (2014). Record of methane emissions from the West Svalbard

continental margin during the last 23.500 yrs revealed by δ13C of benthic foraminifera. *Global and Planetary Change* 122**,** 151-160.

Panieri, G., Lepland, A., Whitehouse, M.J., Wirth, R., Raanes, M.P., James, R.H., Graves, C.A., Crémière, A., and Schneider, A. (2017). Diagenetic Mg-calcite overgrowths on foraminiferal tests in the vicinity of methane seeps. *Earth and Planetary Science Letters* 458**,** 203-212.

Pape, T., Blumenberg, M., Seifert, R., Egorov, V.N., Gulin, S.B., and Michaelis, W. (2005). Lipid geochemistry of methane-seep-related Black Sea carbonates. *Palaeogeography, Palaeoclimatology, Palaeoecology* 227**,** 31-47.

Paull, C.K., Ussler, W., Iii, Borowski, W.S., and Spiess, F.N. (1995). Methane-rich plumes on the Carolina continental rise; associations with gas hydrates. *Geology* 23**,** 89-92.

Pavlov, A.A., Kasting, J.F., Brown, L.L., Rages, K.A., and Freedman, R. (2000). Greenhouse warming by CH4 in the atmosphere of early Earth. *Journal of Geophysical Research: Planets* 105**,** 11981-11990.

Pearson, A., Hurley, S.J., Walter, S.R.S., Kusch, S., Lichtin, S., and Zhang, Y.G. (2016). Stable carbon isotope ratios of intact GDGTs indicate heterogeneous sources to marine sediments. *Geochimica et Cosmochimica Acta* 181**,** 18-35.

Peckmann, J. (2017). Unleashing the potential of glendonite: A mineral archive for biogeochemical processes and paleoenvironmental conditions. *Geology* 45**,** 575-576.

Peckmann, J., Birgel, D., and Kiel, S. (2009). Molecular fossils reveal fluid composition and flow intensity at a Cretaceous seep. *Geology* 37**,** 847-850.

Peckmann, J., Goedert, J., Thiel, V., Michaelis, W., and Reitner, J. (2002). A comprehensive approach to the study of methane-seep deposits from the Lincoln Creek Formation, western Washington State, USA. *Sedimentology* 49**,** 855-873.

Peckmann, J., Reimer, A., Luth, U., Luth, C., Hansen, B., Heinicke, C., Hoefs, J., and Reitner, J. (2001). Methane-derived carbonates and authigenic pyrite from the northwestern Black Sea. *Marine geology* 177**,** 129-150.

Peckmann, J., and Thiel, V. (2004). Carbon cycling at ancient methane–seeps. *Chemical Geology* 205**,** 443-467.

Peketi, A., Mazumdar, A., Joao, H., Patil, D., Usapkar, A., and Dewangan, P. (2015). Coupled C–S–Fe geochemistry in a rapidly accumulating marine sedimentary system: Diagenetic and depositional implications. *Geochemistry, Geophysics, Geosystems* 16**,** 2865-2883.

Peketi, A., Mazumdar, A., Joshi, R., Patil, D., Srinivas, P., and Dayal, A. (2012). Tracing the Paleo sulfate-methane transition zones and H2S seepage events in marine sediments: An application of C-S-Mo systematics. *Geochemistry, Geophysics, Geosystems* 13.

Phillips, S.C., Hong, W.-L., Johnson, J.E., Fahnestock, M.F., and Bryce, J.G. (2018). Authigenic carbonate formation influenced by freshwater inputs and methanogenesis in coal-bearing strata offshore Shimokita, Japan (IODP site C0020). *Marine and Petroleum Geology* 96**,** 288-303.

Phrampus, B.J., Lee, T.R., and Wood, W.T. (2020). A Global Probabilistic Prediction of Cold Seeps and Associated SEAfloor FLuid ExpulsionAnomalies (SEAFLEAs). *Geochemistry, Geophysics, Geosystems* 21**,** e2019GC008747.

Pierre, C., Blanc-Valleron, M.-M., Caquineau, S., März, C., Ravelo, A.C., Takahashi, K., and Zarikian, C.A. (2016). Mineralogical, geochemical and isotopic characterization of

authigenic carbonates from the methane-bearing sediments of the Bering Sea continental margin (IODP Expedition 323, Sites U1343–U1345). *Deep Sea Research Part II: Topical Studies in Oceanography* 125**,** 133-144.

Pitcher, A., Hopmans, E., Mosier, A., Francis, C., Reese, S., Schouten, S., and Sinninghe Damsté, J. (2011). Distribution of core and intact polar tetraether lipids in enrichment cultures of Thaumarchaeota from marine sediments. *Appl. Environ. Microbiol* 77**,** 3468-3477.

Pitcher, A., Rychlik, N., Hopmans, E.C., Spieck, E., Rijpstra, W.I.C., Ossebaar, J., Schouten, S., Wagner, M., and Damsté, J.S.S. (2010). Crenarchaeol dominates the membrane lipids of Candidatus Nitrososphaera gargensis, a thermophilic Group I. 1b Archaeon. *The ISME Journal* 4**,** 542-552.

Price, F.T., and Shieh, Y. (1979). Fractionation of sulfur isotopes during laboratory synthesis of pyrite at low temperatures. *Chemical Geology* 27**,** 245-253.

Prouty, N.G., Sahy, D., Ruppel, C.D., Roark, E.B., Condon, D., Brooke, S., Ross, S.W., and Demopoulos, A.W. (2016). Insights into methane dynamics from analysis of authigenic carbonates and chemosynthetic mussels at newly-discovered Atlantic Margin seeps. *Earth and Planetary Science Letters* 449**,** 332-344.

Raghoebarsing, A.A., Pol, A., Van De Pas-Schoonen, K.T., Smolders, A.J., Ettwig, K.F., Rijpstra, W.I., Schouten, S., Damste, J.S., Op Den Camp, H.J., Jetten, M.S., and Strous, M. (2006). A microbial consortium couples anaerobic methane oxidation to denitrification. *Nature* 440**,** 918-921.

Raiswell, R. (1987). Non-steady state microbiological diagenesis and the origin of concretions and nodular limestones. *Geological Society, London, Special Publications* 36**,** 41-54.

Rathburn, A.E., Levin, L.A., Held, Z., and Lohmann, K.C. (2000). Benthic foraminifera associated with cold methane seeps on the northern California margin: Ecology and stable isotopic composition. *Marine Micropaleontology* 38**,** 247-266.

Reeburgh, W. (1993). The role of methylotrophy in the global methane budget. *Microbial growth on C-1 compounds***,** 1-14.

Reeburgh, W.S. (1976). Methane consumption in Cariaco Trench waters and sediments. *Earth and Planetary Science Letters* 28**,** 337-344.

Reeburgh, W.S. (2003). Global methane biogeochemistry. *Treatise on geochemistry* 4**,** 347.

Reeburgh, W.S. (2007). Oceanic methane biogeochemistry. *Chem Rev* 107**,** 486-513.

Repeta, D.J., Ferrón, S., Sosa, O.A., Johnson, C.G., Repeta, L.D., Acker, M., Delong, E.F., and Karl, D.M. (2016). Marine methane paradox explained by bacterial degradation of dissolved organic matter. *Nature Geoscience* 9**,** 884-887.

Rice, D.D., and Hotel, A.S.M. (1990). "Chemical and Isotopic Evidence of the Origins of Natural Gases in Offshore Gulf of Mexico," in *Gulf Coast Oils and Gases: Their Characteristics, Origin, Distribution, and Exploration and Production Significance*. SEPM Society for Sedimentary Geology).

Riedinger, N., Formolo, M.J., Lyons, T.W., Henkel, S., Beck, A., and Kasten, S. (2014). An inorganic geochemical argument for coupled anaerobic oxidation of methane and iron reduction in marine sediments. *Geobiology* 12**,** 172-181.

Roberts, H.H. (2001). Fluid and Gas Expulsion on the Northern Gulf of Mexico Continental Slope: Mud-Prone to Mineral-Prone Responses. *Natural gas hydrates: occurrence, distribution, and detection***,** 145-161.

Roberts, H.H., and Aharon, P. (1994). Hydrocarbon-derived carbonate buildups of the northern Gulf of Mexico continental slope: a review of submersible investigations. *Geo-Marine Letters* 14**,** 135-148.

Roberts, H.H., and Carney, R.S. (1997). Evidence of episodic fluid, gas, and sediment venting on the northern Gulf of Mexico continental slope. *Economic Geology* 92**,** 863-879.

Roberts, H.H., and Feng, D. (2013). "Carbonate Precipitation at Gulf of Mexico Hydrocarbon Seeps: An Overview," in *Hydrocarbon Seepage: From Source to Surface*. SEG and AAPG), 43-61.

Rodriguez, N., Paull, C., and Borowski, W. (2000). "30. Zonation of authigenic carbonates within gas hydrate-bearing sedimentary sections on the Blake Ridge: offshore southeastern north America", in: *Proceedings of the Ocean Drilling Program, Scientific Results*), 30.

Römer, M., Hsu, C.-W., Loher, M., Macdonald, I., Dos Santos Ferreira, C., Pape, T., Mau, S., Bohrmann, G., and Sahling, H. (2019). Amount and fate of gas and oil discharged at 3400 m water depth from a natural seep site in the Southern Gulf of Mexico. *Frontiers in Marine Science* 6**,** 700.

Rossel, P.E., Elvert, M., Ramette, A., Boetius, A., and Hinrichs, K.-U. (2011). Factors controlling the distribution of anaerobic methanotrophic communities in marine environments: evidence from intact polar membrane lipids. *Geochimica et Cosmochimica Acta* 75**,** 164-184.

Rossel, P.E., Lipp, J.S., Fredricks, H.F., Arnds, J., Boetius, A., Elvert, M., and Hinrichs, K.-U. (2008). Intact polar lipids of anaerobic methanotrophic archaea and associated bacteria. *Organic Geochemistry* 39**,** 992-999.

Ruddiman, W.F. (2003). The anthropogenic greenhouse era began thousands of years ago. *Climatic change* 61**,** 261-293.

Ruddiman, W.F., and Raymo, M.E. (2003). A methane-based time scale for Vostok ice. *Quaternary Science Reviews* 22**,** 141-155.

Ruppel, C.D., and Kessler, J.D. (2017). The interaction of climate change and methane hydrates. *Reviews of Geophysics* 55**,** 126-168.

Saffer, D.M., and Tobin, H.J. (2011). Hydrogeology and mechanics of subduction zone forearcs: Fluid flow and pore pressure. *Annual Review of Earth and Planetary Sciences* 39**,** 157-186.

Sagan, C., and Mullen, G. (1972). Earth and Mars: Evolution of atmospheres and surface temperatures. *Science* 177**,** 52-56.

Sahling, H., Borowski, C., Escobar-Briones, E., Gaytán-Caballero, A., Hsu, C.-W., Loher, M., Macdonald, I., Marcon, Y., Pape, T., and Römer, M. (2016). Massive asphalt deposits, oil seepage, and gas venting support abundant chemosynthetic communities at the Campeche Knolls, southern Gulf of Mexico. *Biogeosciences* 13**,** 4491-4512.

Sakai, S., Imachi, H., Hanada, S., Ohashi, A., Harada, H., and Kamagata, Y. (2008). Methanocella paludicola gen. nov., sp. nov., a methane-producing archaeon, the first isolate of the lineage 'Rice Cluster I', and proposal of the new archaeal order Methanocellales ord. nov. *International Journal of Systematic and Evolutionary Microbiology* 58**,** 929-936.

Salas-De-León, D.A., Monreal-Gómez, M.A., Díaz-Flores, M.A., Salas-Monreal, D., Velasco-Mendoza, H., Riverón-Enzástiga, M.L., and Ortiz-Zamora, G. (2008). Role of Near-

Bottom Currents in the Distribution of Sediments within the Southern Bay of Campeche, Gulf of Mexico. *Journal of Coastal Research* 24**,** 1487-1494.

Salvador, A. (1991). Origin and development of the Gulf of Mexico basin. *The gulf of Mexico basin***,** 389-444.

Sarmiento, J.L., and Gruber, N. (2006). "Remineralization and Burial in the Sediments," in *Ocean Biogeochemical Dynamics*. Princeton University Press), 227-269.

Sassen, R., Brooks, J.M., Macdonald, I.R., Kennicutt Ii, M.C., Guinasso Jr, N.L., and Requejo, A.G. (1993). Association of oil seeps and chemosynthetic communities with oil discoveries, upper continental slope, Gulf of Mexico. Gulf Coast Association of Geological Societies Transactions 43, 349-355

Sassen, R., Macdonald, I.R., Guinasso, N.L., Joye, S., Requejo, A.G., Sweet, S.T., Alcalá-Herrera, J., Defreitas, D.A., and Schink, D.R. (1998). Bacterial methane oxidation in sea-floor gas hydrate: significance to life in extreme environments. *Geology* 26**,** 851-854.

Sassen, R., Roberts, H.H., Carney, R., Milkov, A.V., Defreitas, D.A., Lanoil, B., and Zhang, C. (2004). Free hydrocarbon gas, gas hydrate, and authigenic minerals in chemosynthetic communities of the northern Gulf of Mexico continental slope: relation to microbial processes. *Chemical Geology* 205**,** 195-217.

Sassen, R., Sweet, S.T., Defreitas, D.A., Morelos, J.A., and Milkov, A.V. (2001). Gas hydrate and crude oil from the Mississippi Fan Foldbelt, downdip Gulf of Mexico Salt Basin: significance to petroleum system. *Organic Geochemistry* 32**,** 999-1008.

Sauer, S., Crémière, A., Knies, J., Lepland, A., Sahy, D., Martma, T., Noble, S.R., Schönenberger, J., Klug, M., and Schubert, C.J. (2017). U-Th chronology and formation

controls of methane-derived authigenic carbonates from the Hola trough seep area, northern Norway. *Chemical Geology* 470**,** 164-179.

Saunois, M., Bousquet, P., Poulter, B., Peregon, A., Ciais, P., Canadell, J.G., Dlugokencky, E.J., Etiope, G., Bastviken, D., and Houweling, S. (2016). The global methane budget 2000–2012. *Earth System Science Data* 8**,** 697-751.

Schneider, A., Panieri, G., Lepland, A., Consolaro, C., Crémière, A., Forwick, M., Johnson, J.E., Plaza-Faverola, A., Sauer, S., and Knies, J. (2018). Methane seepage at Vestnesa Ridge (NW Svalbard) since the Last Glacial Maximum. *Quaternary Science Reviews* 193**,** 98-117.

Schneider, R.R., Schulz, H.D., and Hensen, C. (2006). "Marine carbonates: their formation and destruction," in *Marine geochemistry*. Springer), 311-337.

Scholz, F., Hensen, C., Schmidt, M., and Geersen, J. (2013). Submarine weathering of silicate minerals and the extent of pore water freshening at active continental margins. *Geochimica et Cosmochimica Acta* 100**,** 200-216.

Schouten, S., Hopmans, E.C., Baas, M., Boumann, H., Standfest, S., Könneke, M., Stahl, D.A., and Damsté, J.S.S. (2008). Intact membrane lipids of "Candidatus Nitrosopumilus maritimus," a cultivated representative of the cosmopolitan mesophilic group I crenarchaeota. *Appl. Environ. Microbiol.* 74**,** 2433-2440.

Schouten, S., Hopmans, E.C., and Damsté, J.S.S. (2013). The organic geochemistry of glycerol dialkyl glycerol tetraether lipids: a review. *Organic geochemistry* 54**,** 19-61.

Schouten, S., Hopmans, E.C., Schefuß, E., and Damste, J.S.S. (2002). Distributional variations in marine crenarchaeotal membrane lipids: a new tool for reconstructing ancient sea water temperatures? *Earth and Planetary Science Letters* 204**,** 265-274.

Schrag, D.P., Higgins, J.A., Macdonald, F.A., and Johnston, D.T. (2013a). Authigenic carbonate and the history of the global carbon cycle. *Science* 339**,** 540-543.

Schrag, D.P., Higgins, J.A., Macdonald, F.A., and Johnston, D.T. (2013b). Authigenic carbonate and the history of the global carbon cycle. *science* 339**,** 540-543.

Schrenk, M.O., Brazelton, W.J., and Lang, S.Q. (2013). Serpentinization, carbon, and deep life. *Reviews in Mineralogy and Geochemistry* 75**,** 575-606.

Schubert, C.J., Nürnberg, D., Scheele, N., Pauer, F., and Kriews, M. (1997). 13C isotope depletion in ikaite crystals: evidence for methane release from the Siberian shelves ? *Geo-Marine Letters* 17**,** 169-174.

Schubotz, F., Lipp, J.S., Elvert, M., and Hinrichs, K.-U. (2011a). Stable carbon isotopic compositions of intact polar lipids reveal complex carbon flow patterns among hydrocarbon degrading microbial communities at the Chapopote asphalt volcano. *Geochimica et Cosmochimica Acta* 75**,** 4399-4415.

Schubotz, F., Lipp, J.S., Elvert, M., Kasten, S., Mollar, X.P., Zabel, M., Bohrmann, G., and Hinrichs, K.-U. (2011b). Petroleum degradation and associated microbial signatures at the Chapopote asphalt volcano, Southern Gulf of Mexico. *Geochimica et Cosmochimica Acta* 75**,** 4377-4398.

Schwalenberg, K., Wood, W., Pecher, I., Hamdan, L., Henrys, S., Jegen, M., and Coffin, R. (2010). Preliminary interpretation of electromagnetic, heat flow, seismic, and geochemical data for gas hydrate distribution across the Porangahau Ridge, New Zealand. *Marine Geology* 272**,** 89-98.

Sen Gupta, B.K., and Aharon, P. (1994). Benthic foraminifera of bathyal hydrocarbon vents of the Gulf of Mexico: Initial report on communities and stable isotopes. *Geo-Marine Letters* 14**,** 88-96.

Shackleton, N.J. (1985). Oceanic carbon isotope constraints on oxygen and carbon dioxide in the Cenozoic atmosphere. *The carbon cycle and atmospheric CO2: natural variations Archean to present* 32**,** 412-417.

Shipboard Scientific Party (1990). "Site 798", in: *Proc. ODP, Init. Repts., 128.* (ed.) J.C. Ingle, Jr., Suyehiro, K., Von Breymann, M.T., Et Al. (College Station, TX: (Ocean Drilling Program)).

Sikora, A., Detman, A., Chojnacka, A., and Błaszczyk, M.K. (2017). "Anaerobic digestion: I. A common process ensuring energy flow and the circulation of matter in ecosystems. II. A tool for the production of gaseous biofuels," in *Fermentation processes*. IntechOpen).

Sim, M.S., Ono, S., Donovan, K., Templer, S.P., and Bosak, T. (2011). Effect of electron donors on the fractionation of sulfur isotopes by a marine Desulfovibrio sp. *Geochimica et Cosmochimica Acta* 75**,** 4244-4259.

Sivan, O., Schrag, D., and Murray, R. (2007). Rates of methanogenesis and methanotrophy in deep-sea sediments. *Geobiology* 5**,** 141-151.

Skarke, A., Ruppel, C., Kodis, M., Brothers, D., and Lobecker, E. (2014). Widespread methane leakage from the sea floor on the northern US Atlantic margin. *Nature Geoscience* 7**,** 657-661.

Sloan Jr, E.D., and Koh, C. (2007). *Clathrate hydrates of natural gases.* CRC press.

Smith, J.P., and Coffin, R.B. (2014). Methane flux and authigenic carbonate in shallow sediments overlying methane hydrate bearing strata in Alaminos Canyon, Gulf of Mexico. *Energies* 7**,** 6118-6141.

Smrzka, D., Zwicker, J., Klügel, A., Monien, P., Bach, W., Bohrmann, G., and Peckmann, J. (2016). Establishing criteria to distinguish oil-seep from methane-seep carbonates. *Geology* 44**,** 667-670.

Smrzka, D., Zwicker, J., Misch, D., Walkner, C., Gier, S., Monien, P., Bohrmann, G., and Peckmann, J. (2019). Oil seepage and carbonate formation: A case study from the southern Gulf of Mexico. *Sedimentology*.

Snyder, G.T., Hiruta, A., Matsumoto, R., Dickens, G.R., Tomaru, H., Takeuchi, R., Komatsubara, J., Ishida, Y., and Yu, H. (2007). Pore water profiles and authigenic mineralization in shallow marine sediments above the methane-charged system on Umitaka Spur, Japan Sea. *Deep Sea Research Part II: Topical Studies in Oceanography* 54**,** 1216-1239.

Solomon, E.A., Kastner, M., Macdonald, I.R., and Leifer, I. (2009). Considerable methane fluxes to the atmosphere from hydrocarbon seeps in the Gulf of Mexico. *Nature Geoscience* 2**,** 561-565.

Solomon, E.A., Spivack, A.J., Kastner, M., Torres, M.E., and Robertson, G. (2014). Gas hydrate distribution and carbon sequestration through coupled microbial methanogenesis and silicate weathering in the Krishna–Godavari basin, offshore India. *Marine and Petroleum Geology* 58**,** 233-253.

Sowers, T. (2006). Late quaternary atmospheric CH4 isotope record suggests marine clathrates are stable. *Science* 311**,** 838-840.

Stadnitskaia, A., Nadezhkin, D., Abbas, B., Blinova, V., Ivanov, M., and Damsté, J.S. (2008). Carbonate formation by anaerobic oxidation of methane: evidence from lipid biomarker and fossil 16S rDNA. *Geochimica et Cosmochimica Acta* 72**,** 1824-1836.

Stawiarski, B., Otto, S., Thiel, V., Gräwe, U., Loick-Wilde, N., Wittenborn, A.K., Schloemer, S., Wäge, J., Rehder, G., Labrenz, M., Wasmund, N., and Schmale, O. (2019). Controls on zooplankton methane production in the central Baltic Sea. *Biogeosciences* 16**,** 1-16.

Stocker, T.F., Qin, D., Plattner, G.-K., Tignor, M., Allen, S.K., Boschung, J., Nauels, A., Xia, Y., Bex, V., and Midgley, P.M. (2014). "Climate change 2013: The physical science basis". Cambridge University Press Cambridge, UK, and New York).

Stott, L.D., Bunn, T., Prokopenko, M., Mahn, C., Gieskes, J., and Bernhard, J.M. (2002). Does the oxidation of methane leave an isotopic fingerprint in the geologic record? *Geochemistry, Geophysics, Geosystems* 3 (2).

Suess, E. (2010). "Marine cold seeps," in *Handbook of hydrocarbon and lipid microbiology*. Springer), 185-203.

Suess, E. (2018). Marine Cold Seeps: Background and Recent Advances. *Hydrocarbons, Oils and Lipids: Diversity, Origin, Chemistry and Fate***,** 1-21.

Suess, E., Von Huene, R., and Others, A. (1990). "Proceedings of the Ocean Drilling Program, Vol. 112, Scientific Results, Peru Continental Margin": Ocean Drilling Program).

Sun, X., and Turchyn, A.V. (2014). Significant contribution of authigenic carbonate to marine carbon burial. *Nature Geoscience* 7**,** 201-204.

Sun, Y., Gong, S., Li, N., Peckmann, J., Jin, M., Roberts, H.H., Chen, D., and Feng, D. (2020). A new approach to discern the hydrocarbon sources (oil vs methane) of authigenic carbonates forming at marine seeps. *Marine and Petroleum Geology***,** 104230.

Suresh, G. (2015). *Offshore oil seepage visible from space: A Synthetic Aperture Radar (SAR) based automatic detection, mapping and quantification system.* Universität Bremen.

Tada, R., Murray, R.W., Alvarez Zarikian, C.A., Anderson, W.T., Jr., Bassetti, M.-A., Brace, B.J., Clemens, S.C., Da Costa Gurgel, M.H., Dickens, G.R., Dunlea, A.G., Gallagher, S.J., Giosan, L., Henderson, A.C.G., Holbourn, A.E., Ikehara, K., Irino, T., Itaki, T., Karasuda, A., Kinsley, C.W., Kubota, Y., Lee, G.S., Lee, K.E., Lofi, J., Lopes, C.I.C.D., Peterson, L.C., Saavedra-Pellitero, M., Sagawa, T., Singh, R.K., Sugisaki, S., Toucanne, S., Wan, S., Xuan, C., Zheng, H., and Ziegler, M. (2015a). "Site U1427", in: *Proc. IODP*, ed. R. Tada, Murray, Rw, Alvarez Zarikian, Ca, and the Expedition 346 Scientists).

Tada, R., Murray, Rw, Alvarez Zarikian, Ca, and the Expedition 346 Scientists, Proceedings of the Integrated Ocean Drilling Program (2015b). *Expedition 346 summary.* College Station, TX (Integrated Ocean Drilling Program).

Talukder, A.R. (2012). Review of submarine cold seep plumbing systems: leakage to seepage and venting. *Terra Nova* 24**,** 255-272.

Teichert, B., Eisenhauer, A., Bohrmann, G., Haase-Schramm, A., Bock, B., and Linke, P. (2003). U/Th systematics and ages of authigenic carbonates from Hydrate Ridge, Cascadia Margin: recorders of fluid flow variations. *Geochimica et Cosmochimica Acta* 67**,** 3845-3857.

Teichert, B., Johnson, J.E., Solomon, E.A., Giosan, L., Rose, K., Kocherla, M., Connolly, E., and Torres, M.E. (2014). Composition and origin of authigenic carbonates in the Krishna–Godavari and Mahanadi Basins, eastern continental margin of India. *Marine and Petroleum Geology* 58**,** 438-460.

Teske, A. (2018). Hydrocarbon-Degrading Microbial Communities in Natural Oil Seeps. *Microbial Communities Utilizing Hydrocarbons and Lipids: Members, Metagenomics and Ecophysiology***,** 1-31.

Thauer, R.K. (1998). Biochemistry of methanogenesis: a tribute to Marjory Stephenson: 1998 Marjory Stephenson prize lecture. *Microbiology* 144**,** 2377-2406.

Thomas, H., Schiettecatte, L., Suykens, K., M Kone, Y., Shadwick, E., F Prowe, A., Bozec, Y., W De Baar, H., and Borges, A. (2008). Enhanced ocean carbon storage from anaerobic alkalinity generation in coastal sediments. *Biogeosciences Discussions*.

Thullner, M., Dale, A.W., and Regnier, P. (2009). Global-scale quantification of mineralization pathways in marine sediments: A reaction-transport modeling approach. *Geochemistry, geophysics, geosystems* 10 (10).

Tierney, J.E. (2014). "12.14 - Biomarker-Based Inferences of Past Climate: The TEX86 Paleotemperature Proxy," in *Treatise on Geochemistry (Second Edition),* eds. H.D. Holland & K.K. Turekian. (Oxford: Elsevier), 379-393.

Timmers, P., Widjaja-Greefkes, H.C., Ramiro-Garcia, J., Plugge, C., and Stams, A. (2015). Growth and activity of ANME clades with different sulfate and sulfide concentrations in the presence of methane. *Frontiers in Microbiology* 6.

Timmers, P.H., Welte, C.U., Koehorst, J.J., Plugge, C.M., Jetten, M.S., and Stams, A.J. (2017). Reverse Methanogenesis and Respiration in Methanotrophic Archaea. *Archaea* 2017**,** 1654237.

Tissot, B., and Welte, D. (1984). "Petroleum Formation and Occurrence, 2nd edn, 699 pp". Springer, Berlin).

Torres, M.E., and Bohrmann, G. (2016). "Cold Seeps," in *Encyclopedia of Marine Geosciences,* eds. J. Harff, M. Meschede, S. Petersen & J. Thiede. (Dordrecht: Springer Netherlands), 117-122.

Torres, M.E., Hong, W.-L., Solomon, E.A., Milliken, K., Kim, J.-H., Sample, J.C., Teichert, B.M., and Wallmann, K. (2020). Silicate weathering in anoxic marine sediment as a requirement for authigenic carbonate burial. *Earth-Science Reviews* 200**,** 102960.

Treude, T., Orphan, V., Knittel, K., Gieseke, A., House, C.H., and Boetius, A. (2007). Consumption of methane and CO2 by methanotrophic microbial mats from gas seeps of the anoxic Black Sea. *Appl Environ Microbiol* 73**,** 2271-2283.

Tribovillard, N., Du Châtelet, E.A., Gay, A., Barbecot, F., Sansjofre, P., and Potdevin, J.-L. (2013). Geochemistry of cold seepage-impacted sediments: per-ascensum or per-descensum trace metal enrichment? *Chemical Geology* 340**,** 1-12.

Turich, C., and Freeman, K.H. (2011). Archaeal lipids record paleosalinity in hypersaline systems. *Organic Geochemistry* 42**,** 1147-1157.

Ussler Iii, W., and Paull, C.K. (2008). Rates of anaerobic oxidation of methane and authigenic carbonate mineralization in methane-rich deep-sea sediments inferred from models and geochemical profiles. *Earth and Planetary Science Letters* 266**,** 271-287.

Valentine, D.L., Blanton, D.C., Reeburgh, W.S., and Kastner, M. (2001). Water column methane oxidation adjacent to an area of active hydrate dissociation, Eel River Basin. *Geochimica et Cosmochimica Acta* 65**,** 2633-2640.

Valentine, D.L., Reddy, C.M., Farwell, C., Hill, T.M., Pizarro, O., Yoerger, D.R., Camilli, R., Nelson, R.K., Peacock, E.E., and Bagby, S.C. (2010). Asphalt volcanoes as a potential source of methane to late Pleistocene coastal waters. *Nature Geoscience* 3**,** 345-348.

Valentine, D.L., and Reeburgh, W.S. (2000). New perspectives on anaerobic methane oxidation. *Environmental Microbiology* 2**,** 477-484.

Vanwonterghem, I., Evans, P.N., Parks, D.H., Jensen, P.D., Woodcroft, B.J., Hugenholtz, P., and Tyson, G.W. (2016). Methylotrophic methanogenesis discovered in the archaeal phylum Verstraetearchaeota. *Nature microbiology* 1**,** 16170.

Wakeham, S.G., Lewis, C.M., Hopmans, E.C., Schouten, S., and Damsté, J.S.S. (2003). Archaea mediate anaerobic oxidation of methane in deep euxinic waters of the Black Sea. *Geochimica et Cosmochimica Acta* 67**,** 1359-1374.

Wallmann, K., and Aloisi, G. (2012). The global carbon cycle: geological processes. *Fundamentals of Geobiology***,** 20-35.

Wallmann, K., Aloisi, G., Haeckel, M., Obzhirov, A., Pavlova, G., and Tishchenko, P. (2006). Kinetics of organic matter degradation, microbial methane generation, and gas hydrate formation in anoxic marine sediments. *Geochimica et Cosmochimica Acta* 70**,** 3905-3927.

Wallmann, K., Aloisi, G., Haeckel, M., Tishchenko, P., Pavlova, G., Greinert, J., Kutterolf, S., and Eisenhauer, A. (2008). Silicate weathering in anoxic marine sediments. *Geochimica et Cosmochimica Acta* 72**,** 2895-2918.

Wallmann, K., Pinero, E., Burwicz, E., Haeckel, M., Hensen, C., Dale, A., and Ruepke, L. (2012). The global inventory of methane hydrate in marine sediments: A theoretical approach. *Energies* 5**,** 2449-2498.

Wang, J., Chen, Q., Wei, Q., Wang, X., Li, Q., and Gao, Y. (Year). "Authigenic pyrites and their stable sulfur isotopes in sediments from IODP 311 on Cascadia margin, northeastern pacific", in: *6th International Conference on Gas Hydrates, Vancouver*).

Wang, S., Magalhães, V.H., Pinheiro, L.M., Liu, J., and Yan, W. (2015). Tracing the composition, fluid source and formation conditions of the methane-derived authigenic carbonates in the Gulf of Cadiz with rare earth elements and stable isotopes. *Marine and Petroleum Geology* 68**,** 192-205.

Wankel, S.D., Adams, M.M., Johnston, D.T., Hansel, C.M., Joye, S.B., and Girguis, P.R. (2012). Anaerobic methane oxidation in metalliferous hydrothermal sediments: influence on carbon flux and decoupling from sulfate reduction. *Environ Microbiol* 14**,** 2726-2740.

Wasmund, K., Mußmann, M., and Loy, A. (2017). The life sulfuric: microbial ecology of sulfur cycling in marine sediments. *Environmental microbiology reports* 9**,** 323-344.

Watanabe, Y., Nakai, S.I., Hiruta, A., Matsumoto, R., and Yoshida, K. (2008). U–Th dating of carbonate nodules from methane seeps off Joetsu, Eastern Margin of Japan Sea. *Earth and Planetary Science Letters* 272**,** 89-96.

Watson, R.T., Zinyowera, M.C., and Moss, R.H. (1996). *Climate change 1995. Impacts, adaptations and mitigation of climate change: scientific-technical analyses.*

Weber, T., Wiseman, N.A., and Kock, A. (2019). Global ocean methane emissions dominated by shallow coastal waters. *Nature communications* 10**,** 1-10.

Wegener, G., Krukenberg, V., Riedel, D., Tegetmeyer, H.E., and Boetius, A. (2015). Intercellular wiring enables electron transfer between methanotrophic archaea and bacteria. *Nature* 526**,** 587-590.

Wehrmann, L., Ockert, C., Mix, A., Gussone, N., Teichert, B., and Meister, P. (2016). Repeated occurrences of methanogenic zones, diagenetic dolomite formation and linked silicate alteration in southern Bering Sea sediments (Bowers Ridge, IODP Exp. 323 Site U1341). *Deep Sea Research Part II: Topical Studies in Oceanography* 125**,** 117-132.

Wehrmann, L.M., Risgaard-Petersen, N., Schrum, H.N., Walsh, E.A., Huh, Y., Ikehara, M., Pierre, C., D'hondt, S., Ferdelman, T.G., and Ravelo, A.C. (2011). Coupled organic and inorganic carbon cycling in the deep subseafloor sediment of the northeastern Bering Sea Slope (IODP Exp. 323). *Chemical Geology* 284**,** 251-261.

Weijers, J.W., Lim, K.L., Aquilina, A., Sinninghe Damsté, J.S., and Pancost, R.D. (2011). Biogeochemical controls on glycerol dialkyl glycerol tetraether lipid distributions in sediments characterized by diffusive methane flux. *Geochemistry, Geophysics, Geosystems* 12.

Weijers, J.W., Schouten, S., Van Den Donker, J.C., Hopmans, E.C., and Damsté, J.S.S. (2007). Environmental controls on bacterial tetraether membrane lipid distribution in soils. *Geochimica et Cosmochimica Acta* 71**,** 703-713.

Whiticar, M.J. (1999). Carbon and hydrogen isotope systematics of bacterial formation and oxidation of methane. *Chemical Geology* 161**,** 291-314.

Widdel, F., Knittel, K., and Galushko, A. (2010). Anaerobic hydrocarbon-degrading microorganisms: an overview. *Handbook of hydrocarbon and lipid microbiology***,** 1997-2021.

Widdel, F., and Rabus, R. (2001). Anaerobic biodegradation of saturated and aromatic hydrocarbons. *Current opinion in biotechnology* 12**,** 259-276.

Wilson, R., Monaghan, P., Osanik, A., Price, L., and Rogers, M. (1974). Natural marine oil seepage. *Science* 184**,** 857-865.

Wirsig, C., Kowsmann, R.O., Miller, D.J., De Oliveira Godoy, J.M., and Mangini, A. (2012). U/Th-dating and post-depositional alteration of a cold seep carbonate chimney from the Campos Basin offshore Brazil. *Marine Geology* 329**,** 24-33.

Wu, D., Sun, T., Xie, R., Pan, M., Chen, X., Ye, Y., Liu, L., and Wu, N. (2019). Characteristics of Authigenic Minerals around the Sulfate-Methane Transition Zone in the Methane-Rich Sediments of the Northern South China Sea: Inorganic Geochemical Evidence. *International journal of environmental research and public health* 16**,** 2299.

Wu, Z., Zhou, H., Ren, D., Gao, H., and Li, J. (2016). Quantifying the sources of dissolved inorganic carbon within the sulfate-methane transition zone in nearshore sediments of Qi'ao Island, Pearl River Estuary, Southern China. *Science China Earth Sciences* 59**,** 1959-1970.

Wuebbles, D.J., and Hayhoe, K. (2002). Atmospheric methane and global change. *Earth-Science Reviews* 57**,** 177-210.

Wurgaft, E., Findlay, A.J., Vigderovich, H., Herut, B., and Sivan, O. (2019). Sulfate reduction rates in the sediments of the Mediterranean continental shelf inferred from combined dissolved inorganic carbon and total alkalinity profiles. *Marine Chemistry* 211**,** 64-74.

Yamamoto, A., Yamanaka, Y., Oka, A., and Abe-Ouchi, A. (2014). Ocean oxygen depletion due to decomposition of submarine methane hydrate. *Geophysical Research Letters* 41**,** 5075-5083.

Yanagawa, K., Shiraishi, F., Tanigawa, Y., Maeda, T., Mustapha, N.A., Owari, S., Tomaru, H., Matsumoto, R., and Kano, A. (2019). Endolithic microbial habitats hosted in carbonate nodules currently forming within sediment at a high methane flux site in the sea of Japan. *Geosciences* 9**,** 463.

Yoshinaga, M.Y., Holler, T., Goldhammer, T., Wegener, G., Pohlman, J.W., Brunner, B., Kuypers, M.M., Hinrichs, K.-U., and Elvert, M. (2014). Carbon isotope equilibration during sulphate-limited anaerobic oxidation of methane. *Nature Geoscience* 7**,** 190.

You, K., Flemings, P.B., Malinverno, A., Collett, T.S., and Darnell, K. (2019). Mechanisms of Methane Hydrate Formation in Geological Systems. *Reviews of Geophysics* 57**,** 1146-1196.

Zeebe, R.E., Ridgwell, A., and Zachos, J.C. (2016). Anthropogenic carbon release rate unprecedented during the past 66 million years. *Nature Geoscience* 9**,** 325.

Zhang, C.L., Pearson, A., Li, Y.-L., Mills, G., and Wiegel, J. (2006). Thermophilic temperature optimum for crenarchaeol synthesis and its implication for archaeal evolution. *Appl. Environ. Microbiol.* 72**,** 4419-4422.

Zhang, M., Lu, H., Guan, H., Liu, L., Wu, D., and Wu, N. (2018). Methane seepage intensities traced by sulfur isotopes of pyrite and gypsum in sediment from the Shenhu area, South China Sea. *Acta Oceanologica Sinica* 37**,** 20-27.

Zhang, Y., Luo, M., Hu, Y., Wang, H., and Chen, D. (2019). An Areal Assessment of Subseafloor Carbon Cycling in Cold Seeps and Hydrate-Bearing Areas in the Northern South China Sea. *Geofluids* 2019.

Zhang, Y.G., Pagani, M., and Wang, Z. (2016). Ring Index: A new strategy to evaluate the integrity of TEX86 paleothermometry. *Paleoceanography* 31**,** 220-232.

Zhang, Y.G., Zhang, C.L., Liu, X.-L., Li, L., Hinrichs, K.-U., and Noakes, J.E. (2011). Methane Index: a tetraether archaeal lipid biomarker indicator for detecting the instability of marine gas hydrates. *Earth and Planetary Science Letters* 307**,** 525-534.

Zhao, M.-Y., Zheng, Y.-F., and Zhao, Y.-Y. (2016). Seeking a geochemical identifier for authigenic carbonate. *Nature communications* 7 (1), 1-7.

Zopfi, J., Ferdelman, T.G., Fossing, H., Amend, J.P., Edwards, K.J., and Lyons, T.W. (2004). "Distribution and fate of sulfur intermediates—sulfite, tetrathionate, thiosulfate, and

elemental sulfur—in marine sediments," in *Sulfur Biogeochemistry - Past and Present*. Geological Society of America), 97-116.